Skyrmions and the Dzyaloshinskii-Moriya Interaction

Computing the Dzyaloshinskii-Moriya interaction for small and large spin-orbit couplings

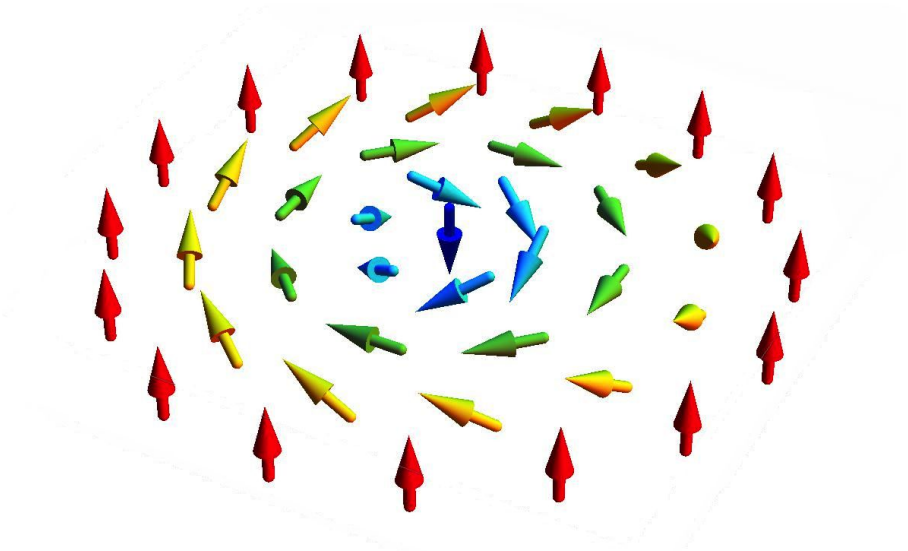

Utrecht University
Institute for Theoretical Physics

Master Thesis

Author:
Bram van Dijk

Supervisor:
Dr. Rembert Duine

December, 2014

Abstract

Chiral magnets support topologically stable spin structures that are known as magnetic skyrmions, first discovered in 2009. One of the mechanisms responsible for the formation of a skyrmion relies on the Dzyaloshinskii-Moriya (DM) interaction induced by a lack of inversion symmetry and strong spin-orbit coupling of the compound. We investigate the strength of the DM interaction in a microscopic toy model: the Rashba model coupled to a helical exchange field. We check previously-established analytical results for small Rashba couplings and use a numerical method to find the DM interaction for large Rashba couplings.

Contents

List of Figures

Preface

Topological solitons are solutions of non-linear differential equations which cannot be continuously deformed to a trivial solution. This means that they are in some way protected against small perturbations or decay. Examples of topological solitons can be found in exactly solvable models and in recently observed magnetic structures called skyrmions. Topological solitons always have received special interest from physicists and mathematicians because of their stability. A comprehensible example of such a stable solution is given by the Scottish engineer Scott Russel as early as 1834. Here he describes one of the first documented observations of a soliton wave.

> I was observing the motion of a boat which was rapidly drawn along a narrow channel by a pair of horses, when the boat suddenly stopped not so the mass of water in the channel which it had put in motion; it accumulated round the prow of the vessel in a state of violent agitation, then suddenly leaving it behind, rolled forward with great velocity, assuming the form of a large solitary elevation, a rounded, smooth and well-defined heap of water, which continued its course along the channel apparently without change of form or diminution of speed. I followed it on horseback, and overtook it still rolling on at a rate of some eight or nine miles an hour, preserving its original figure some thirty feet long and a foot to a foot and a half in height. Its height gradually diminished, and after a chase of one or two miles I lost it in the windings of the channel. Such, in the month of August 1834, was my first chance interview with that singular and beautiful phenomenon which I have called the Wave of Translation.[1]

Not only is a soliton wave an interesting and elegant observation, the stability of solitons attracts the attention of many.

In field theory for example, particles are defined as excitations of waves. It appears to be very difficult to explain the stability of these wave-excitations. This issue was under investigation by Tony Skyrme, and his hypothesis was that particles are topologically protected. In other words, a particle in field theory is a wave-excitation of the field, and this excitation cannot be undone

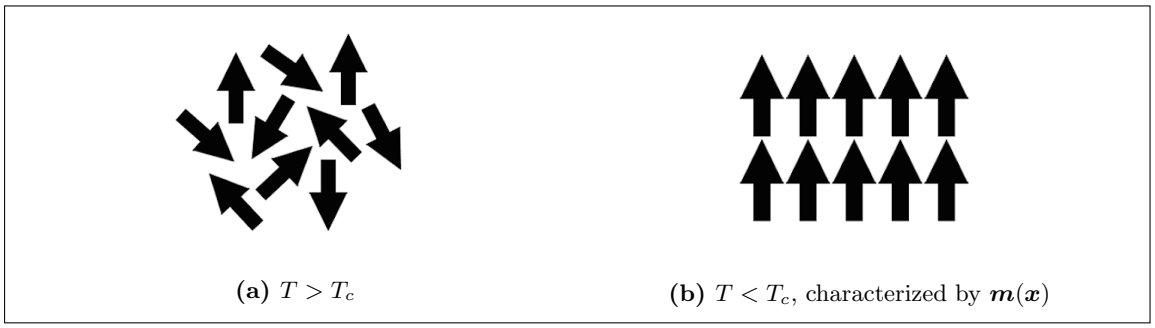

(a) $T > T_c$ **(b)** $T < T_c$, characterized by $\boldsymbol{m}(\boldsymbol{x})$

Figure 1: The magnetic spin structure of a ferromagnet for different values of T.

by any deformation of the field configuration. In mathematical terms there exists a topological integer that is unchanged. The name skyrmion thus originates from physicist Tony Skyrme, who in the sixties developed a nonlinear field theory for pions and found topologically stable field configurations behaving as particles [2]. Hereafter, in several areas of research topologically stable field configurations were named skyrmions. However, our interest lies in magnetic skyrmions appearing in chiral magnets, first discovered in 2009 [3].

Aside from being topologically protected, a magnetic skyrmion is also physically stable. This means that a skyrmion state is energetically favored by the system. So, on the one hand skyrmions are fundamentally interesting because of their stability. On the other hand skyrmions are technologically interesting. By making use of the stability of the skyrmion configuration it might be possible to use skyrmions in a new kind of information carrying device. It is hoped that more research into skyrmions will lead to a new type of data storage device.

To begin our discussion on the skyrmion structure, we consider a ferromagnet. A ferromagnet has two phases: the paramagnetic phase and the polarized phase. For temperatures above the Curie temperature the magnetization is randomly distributed in the magnet, see figure 1a. However, below the Curie temperature the magnetization vectors align in some direction, see figure 1b. The magnetization in this latter phase can be characterized by a magnetization profile, which is represented by $\boldsymbol{m}(\boldsymbol{x})$. This means that for every spatial variable $\boldsymbol{x}$ we have a vector $\boldsymbol{m}$ pointing in some direction. The polarized phase in a ferromagnet is a trivial phase where the magnetization is aligned throughout the system. Other types of magnetization profiles occur in, for example, chiral magnets. There, non-trivial magnetization profiles are formed that have a whirling structure. A skyrmion is such a structure as, see figure 2.

These whirling types of magnetization in a chiral magnet are induced by the Dzyaloshinskii-Moriya interaction. The Dzyaloshinskii-Moriya (DM) interaction is a microscopic characteristic of interacting spins that occurs in a system that lacks inversion symmetry and that has a strong spin-orbit coupling. The DM interaction creates phases which have a winding magnetic configuration.

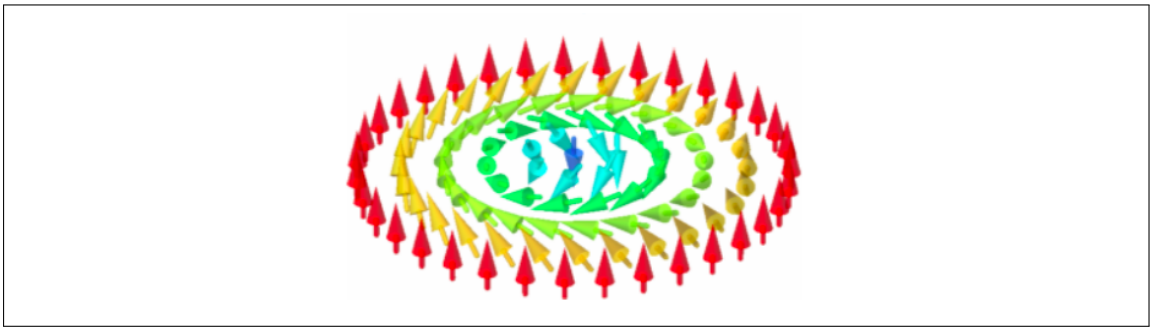

Figure 2: A skyrmion configuration. Extracted from [4].

One of these chiral configurations is identified as skyrmion structure.

The dependence of the DM interaction on spin-orbit coupling has been shown to be linear for small spin-orbit couplings in [5], which is the starting point of our research. The research in this thesis is captured with the following question: What is the full behaviour, considering both small spin-orbit coupling and large spin orbit coupling, of the Dzyalosinskii-Moriya interaction in a chiral magnet?

In order to answer this question we set up a model composed of two layers, one ferromagnetic, the other a non-magnet with strong spin-orbit coupling. We assume the surface between the two compounds is described by a Rashba model coupled to a helical exchange field. We reproduce the linear behavior of the DM interaction for small spin-orbit coupling using analytical methods and extend this behavior for large spin-orbit coupling using numerical analysis.

The first chapter introduces the most important aspects of skyrmions of relevance for this thesis. The first observation of a skyrmion lattice is explained as well as some of the dynamics of skyrmions. Also, the dependence of the formation of a skyrmion on the DM interaction is described.

In Chapter 2 we introduce the phenomenological model of a chiral magnet. We minimize the energy of this model and try to find the skyrmion magnetic footprint. We then set up our toy model: electrons coupled to a Rashba interaction and helical exchange field. We end this chapter with the previously-established dependence of the DM interaction on the Rashba coupling.

In Chapter 3 we reproduce the results of the article by Kim et al. [5]. In contrast to Kim et al., we use quantum mechanical perturbation theory. We compute the total energy of our toy model for zero spin-orbit coupling using both field theory as well as the integration of the single-particle energies over the filled Fermi sea. Subsequently, we compute the total energy of our model for small spin-orbit coupling to obtain the dependence of the DM interaction on spin-orbit coupling. All computations done in this chapter are analytical, this in comparison to the next chapter where we try to compute the DM interaction using numerics.

Chapter 4 consists of the numerical analysis of the DM interaction. The goal here is to solve the Schrödinger equation of the Rashba model with a helical exchange field without perturbation theory. We discretize the Schrödinger equation, reducing it to a matrix equation, which we numerically solve. We test our discretization method and try to find the energy spectrum of the free particle and the Rashba model. Finally, we compute the total energy of our toy model and try to plot the DM interaction against the Rashba coupling. We then have extended the behavior of the DM interaction for small spin-orbit coupling to the behavior for both small and large spin-orbit coupling.

In the final chapter we conclude the research and summarize what we have done. We discuss the assumptions we made in this thesis and question if they are reasonable. We also give an option to check whether our assumption is valid.

Chapter 1

Introducing Magnetic Skyrmions

In this chapter we describe the properties of magnetic skyrmions. We begin by mentioning the different mechanisms responsible for the formation of a skyrmion. One ingredient of the formation of skyrmions is the Dzyalosinskii-Moriya interaction. We explain this interaction and see what it does to the magnetization. Subsequently, we describe the first observation of a skyrmion structure in 2009 and its characteristic A-phase. We then briefly discuss the topological stability of a skyrmion configuration and conclude with its peculiar dynamical properties.

1.1 Formation of a Skyrmion

The formation of a skyrmion in magnetic systems consists of several mechanisms (sometimes) working together. There are four [6]:

1. Long-ranged magnetic dipolar interactions,
2. Dzyaloshinskii-Moriya interaction,
3. Frustated exchange interactions,
4. Four-spin exchange interactions.

The first mechanism is based on long-ranged dipolar interactions. In [7] they use a thin magnetic film with a perpendicular easy-axes anisotropy: the magnetization is dependent on the direction and favors some direction. A competition emerges between the dipolar interaction and the exchange energy. The exchange energy favors spins to be aligned. This competition between dipolar interactions (in-plane magnetization) and the exchange (out-of-plane magnetization) result in periodic stripes. In these stripes the magnetization rotates in the plane perpendicular to the film. Subsequently, an external magnetic field is applied perpendicular to the film, transforming the stripes into magnetic bubbles or skyrmions. This phenomenon of emergent bubbles has been studied in the seventies when people tried to use these bubbles as a new form of memory: Bubble

Memory[1].

We skip the second mechanism for the time being and discuss it in the next section. The third mechanism has been studied using Monte Carlo simulations, including nearest neighbor interactions and second neighbors interactions [11]. In this study they find several (chiral[2]) phases, including the skyrmion phase. The fourth option has been studied in [12], where they found a two dimensional square lattice of skyrmions. The short-range four-spin-interaction imposes a square symmetry on the configuration. The square symmetry in combination with the DM interaction leads to the formation of skyrmions.

The first mechanism has had a lot of attention already, however the rest of the mechanisms are currently hot topics and are being studied extensively. One of the differences between the mechanisms described above is the typical size of the skyrmion. Mechanisms (1) and (2) result in a skyrmion of 100 nm and 5 nm in diameter respectively. The other two mechanisms, (3) and (4), result in a skyrmion with a diameter of 1nm typically. Hence, since the skyrmions produced with mechanism (1) and (2) are larger than then lattice constant, the continuum approximation is justified. Also, mechanism (1) produces bubbles where the helicity, the way the magnetic structure whirls, is left unspecified. This in contrast to mechanism (2), where the helicity is specified by the direction of the DM interaction.

We are interested in the formation of skyrmions in chiral magnets due to the DM interaction, mechanism (2).

1.2 Dzyaloshinskii-Moriya Interaction

Chirality is a form of asymmetry of the system. If the atomic structure of a magnet lacks inversion symmetry we call them chiral magnets. The chirality expresses itself through the phase diagram which shows additional chiral phases. In these phases the magnetization is whirled in some way, e.g. helical. What mechanism is responsible for these additional phases?

In 1960 Dzyaloshinskii constructed a model to describe weak ferromagnetism [13]. Based on symmetries he introduced an asymmetrical term which later on was dubbed the Dzyaloshinskii-Moriya interaction. Moriya connected his name to this term when he found the mechanism behind this interaction is partly based on spin-orbit coupling [14]. Without going into details we conclude that the Dzyaloshinskii-Moriya interaction is induced by a lack of inversion symmetry of the compound and a strong spin-orbit coupling.

[1] More information on magnetic bubbles and bubble memory can be found in [8][9][10]

[2] These phases will be explained in the coming sections.

An example of a compound that lacks inversion symmetry is MnSi (manganese silicide), as depicted schematically in figure 1.1. In the figure we see that inversion symmetry is broken in a unit cell. Aside from a lack of inversion symmetry, MnSi has a strong spin- orbit coupling. This is due to several microscopic processes, which we will not go into.

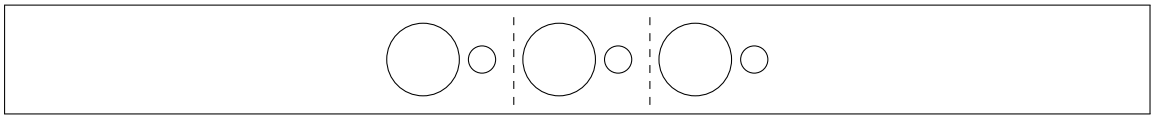

Figure 1.1: Schematic figure of the atomic structure of MnSi. The circles represent atoms and the dashed lines depict the boundaries of a unit cell. We see that this structure lacks inversion symmetry in a unit cell.

Inversion symmetry can be broken in different directions leading to a different induced DM interaction. In practice this means that the magnetization is different. We consider an example of just two spins here, however in the coming sections of this thesis we consider a bigger system. The DM interaction for two spins has the following form:

$$\mathcal{H}_{DM} = -\boldsymbol{D}_{12} \cdot (\boldsymbol{S}_1 \times \boldsymbol{S}_2). \tag{1.1}$$

In this expression $\boldsymbol{S}_1$ and $\boldsymbol{S}_2$ are the atomic spins.

In figure 1.2 there is a DM interaction emerging from the interplay of two atomic spins with a neighboring atom having a large spin-orbit coupling in a thin film. The resulting DM interaction points outwards from the plane of the atoms. The same mechanism is responsible for the interfacial DM interaction between a ferromagnetic thin layer and a non-magnetic layer with a large spin-orbit coupling. Here, at the interface between the two layers, the triangle mechanism produces a DM interaction for the interfacial spins $\boldsymbol{S}_1$ and $\boldsymbol{S}_2$. The DM interaction vector, $\boldsymbol{D}_{12}$, is perpendicular to the triangle.

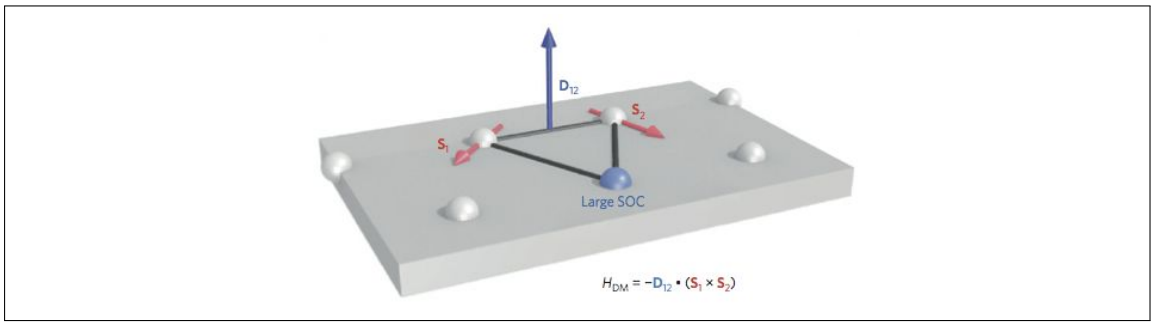

Figure 1.2: Schematic explanation of the interfacial DM interaction for two spins. Extracted from [15].

Starting with a ferromagnetic state where all spin are alligned: $\boldsymbol{S}_1 || \boldsymbol{S}_2$, we then assume a strong spin-orbit coupling present that induces a DM interaction. The resulting magnetic structure depends on the direction of the $\boldsymbol{D}$-vector, which in turn depends on the way which the symmetry

in the compound is broken. Different helicities are obtained for different DM interactions.

We call the vector joining the sites of the spins S_1 and S_2, R_{12}. The energy of the system is minimized if either $\boldsymbol{R}_{12} \perp \boldsymbol{D}_{12}$ or $\boldsymbol{R}_{12} || \boldsymbol{D}_{12}$. If $\boldsymbol{R}_{12} \perp \boldsymbol{D}_{12}$, the DM interaction tilts S_1 around D_{12}, with respect to S_2. This rotation eventually results in the configuration depicted in figure 2. If however $\boldsymbol{R}_{12} || \boldsymbol{D}_{12}$ the configuration in figure 2.2 is obtained.

In the next section we will see what the chiral phases, induced by a DM interaction, will look like using the phase diagram of MnSi.

1.3 First Observation

Skyrmion spin structures were first observed in 2009, using neutron scattering [15][3][16]. This was the first time the A-phase, as it was called [17], in a chiral magnet was identified as skyrmion phase. The A-phase is shown in figure 1.3 among two other chiral phases. In the first experiment people used neutron scattering to observe the spontaneous formation of a two-dimensional lattice of skyrmions in MnSi. Also, observations have been made in real space using microscopy techniques, see figure 1.7. Skyrmions have since been observed in many other materials, such as the doped semiconductor material $Fe_{1-x}Co_xSi$ [18], in iron and cobalt doped MnSi [19], chiral magnetic bulk materials and thin films [20]. However, to explain the skyrmion features we focus on MnSi.

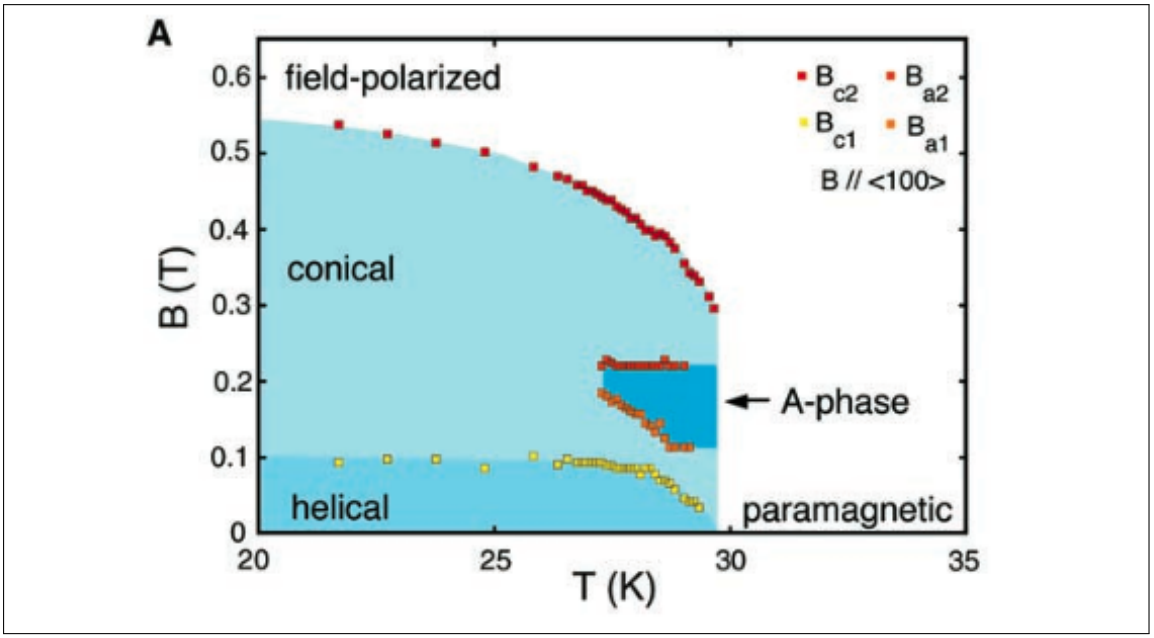

Figure 1.3: The figure shows the different magnetic phases of MnSi. Figure extracted from [3]. The phase diagram includes the A-phase which corresponds to the skyrmion phase.

The first observation of a magnetic skyrmion structure has been made in the chiral ferromagnetic

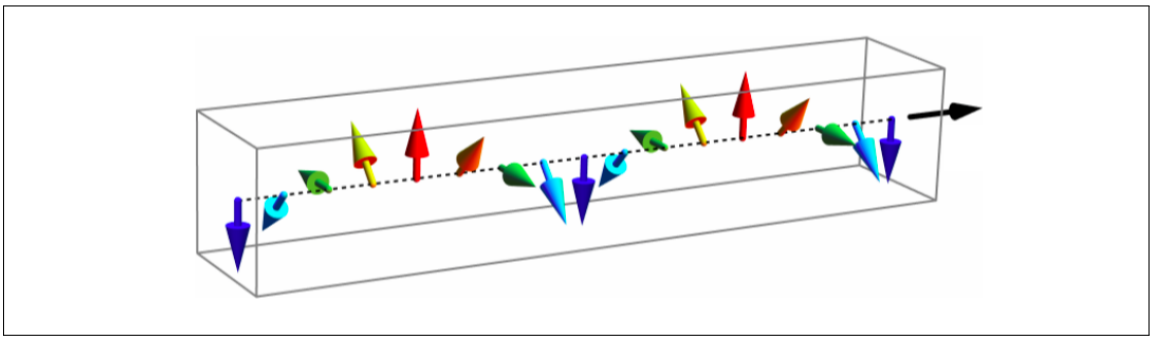

Figure 1.4: The helical phase, where the magnetization precesses around the propagation vector.

MnSi. Furthermore, MnSi crystallizes in the B20 structure that lacks inversion symmetry, recall 1.1. Due to this property it allows for non-inversion symmetric magnetic structures to appear. A skyrmion is such a structure.

In the phase diagram of a ferromagnet there are two different phases. The spins are ordered below the Curie temperature and above this temperature point the spins change direction and become disordered. We expect to see the same two phases in the phase diagram of MnSi, since this too is a ferromagnet.

We see five different phases when we look at the phase diagram of MnSi in figure 1.3. The most familiar phases are the polarized phase, which occurs for large magnetic fields and the paramagnetic phase, which appears above the Curie temperature.

Between these two phases, there are three additional phases which are not present in a basic ferromagnet. These three phases are chiral phases. These chiral phases occur due to the DM interaction, as explained in the previous section. There is a conical phase, a helical phase and an A-phase. There is a strong exchange energy present in this magnet which favors uniform magnetization. The weaker energy scale comes from the DM interaction. This interaction favors twisted spin structures, such as the three chiral phases we see in the figure. There are other interactions at play here, but they are negligible.

The helical phase appears below the critical Curie temperature at small (or zero) magnetic field. The magnetization in the helical phase precesses around an axis which is perpendicular to the external magnetic field. The helical magnetization is shown in figure 1.4. If the temperature is below the Curie temperature, and the external magnetic field is increased a crossover to the conical phase happens.

The crossover between the helical phase and the conical phase occurs at $B_{c1} > 0.1\,T$, when $T < T_c$. In the conical phase the magnetization obtains a component parallel tot the magnetic field. The angle of the cone continuously decreases to zero when the magnetic field increases to a value of

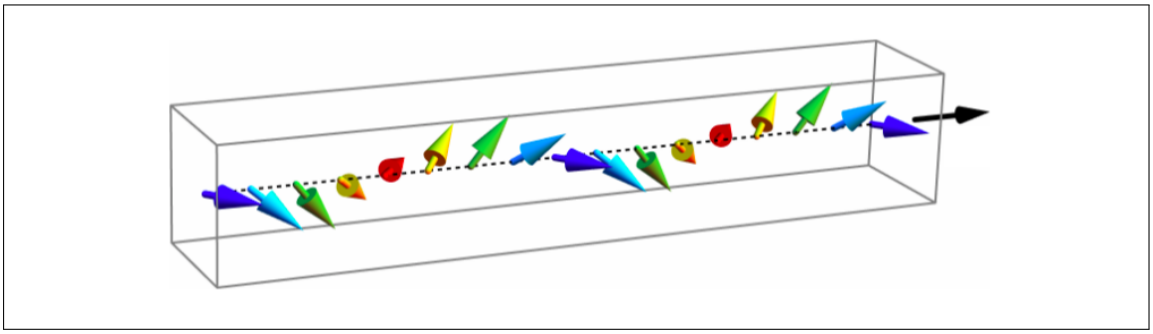

Figure 1.5: The conical phase, where the magnetization precesses around the propagation vector, and has a component parallel to the external magnetic field.

$B = 0.55T$, at which point all spins align. The magnetization profile of the conical phase is shown in figure 1.5.

It is important to see that at a magnetic field value of $B > 0.55\,T$ the effect of the DM interaction is very weak compared to the exchange energy scale. The ferromagnetic energy scale dominates the magnetization and the DM interaction is negligible. So for a stronger magnetic field we have a field polarized state as ground state.

The A-phase occurs in a small region of the phase-diagram. The region for temperatures just below T_c and for a magnetic field value around $B = 0.2\,T$. In this small area a two dimensional hexagonal lattice of (anti-) skyrmions is the stable ground state of the system. The magnetic field is perpendicular to the skyrmion lattice. As is depicted in figure 1.6b, the lattice consists of several individual skyrmion structures.

The individual skyrmion appearing in the lattice is a structure we have already seen: recall figure 2. The magnetic structure is translationally invariant along the direction of the magnetic field, which is perpendicular to the skyrmion structure. The color in the picture indicates whether the spins are parallel (blue) or anti-parallel (red) to the external magnetic field. Also, the skyrmion is rotationally symmetric if we rotate around the axes parallel to the external magnetic field. We can imagine skyrmion tubes could form if we translate the skyrmion structure along the magnetic field. These tubes could be compared to vortices in an Abrikosov vortex lattice of a type-II superconductor, as has been done in [4].

Before the discovery of the skyrmion structure in 2009, the consensus was that the A-phase was some kind of helix with a wave vector aligned perpendicular to the applied field. By using neutron scattering this hypothesis is disproven, since there it shows that the structure emerging in the A-phase is a hexagonal lattice. However, using neutron scattering alone, it is not possible to deduce the magnetic structure of the A-phase. Measurements of the topological Hall effect of the A-phase are necessary to prove that the A-phase corresponds to a skyrmion structure [16][21]. The

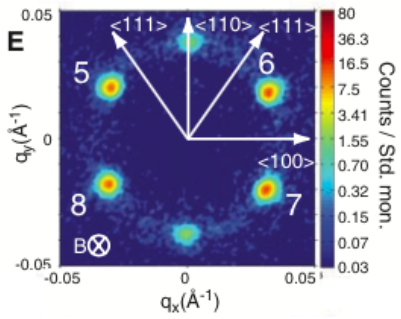

(a) Neutron scattering of the skyrmion phase. Figure extracted from [3].

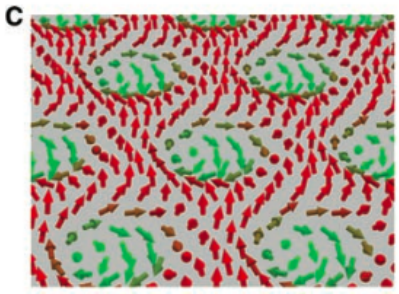

(b) Modelled skyrmion lattice in MnSi A-phase [Muhlbauer, 2009].

Figure 1.6: Left figure: neutron scattering. Right figure: skyrmion lattice modelled.

topological Hall effect is induced by the magnetic field of the skyrmions on conduction electrons. The movement of a skyrmion leads to a change in the magnetic field produced by the skyrmion and thus changes the electromagnetic induction. Then the induced electric field gives an additional contribution to the Hall effect when skyrmions move. From measurements of the topological Hall effect of the A-phase in combination with theory, the magnetic structure shown in figure 1.6b is modelled. This visualization of the A-phase is treated as a hypothesis of what a real space image of the magnetization would look like.

In 2010 real space images were produced using Lorentz transmission electron microscopy (TEM). One of the biggest advantages of using Lorentz TEM is that this technique offers a direct observation of the magnetic structure of the sample. On the other hand the sample needs to be electron-transparent, and this can only be realized if the samples are very thin. This is the reason why the study in [22] used thin films. Aside from this, another property that troubles the observations is that with Lorentz TEM one only measures the in-plane component of the magnetization. The real space image of the A-phase is shown in figure 1.7. Since at the edges and at the center of a skyrmion the magnetization is opposite or along the magnetic field, the magnetization is not specified and is black. What we do see in the figure is the winding of the magnetization around the center of the skyrmion. The hypothesis is validated and from then on the A-phase is identified as a skyrmion structure.

1.4 Classification of Skyrmions

The skyrmion configuration is physically stable. This means that the spin configuration of a skyrmion could minimize the energy of the system and therefore the system favors this configuration. Moreover, the skyrmion is topologically protected: small deformations of the system cannot

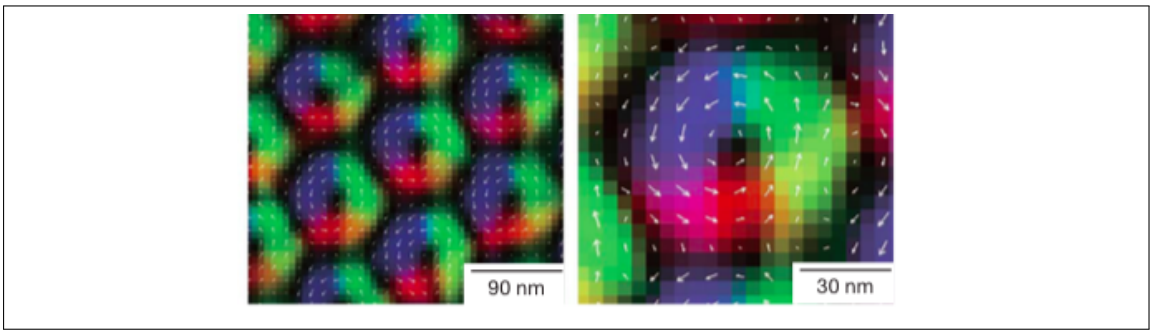

Figure 1.7: Magnified real space picture of a skyrmion at a magnetic field value of $B = 50\,mT$ using Lorentz transmission electron microscopy (TEM). Picture extracted from [22].

transform the spin structure to some trivial structure. This topological property is made explicit with a topological charge.

The topological charge, or skyrmion number, is the quantized winding number which counts how many times the configuration wraps around the unit sphere. The skyrmion number is defined, for a two dimensional system, as

$$N_{sk} = \frac{1}{4\pi} \int dx \int dy\, \hat{\mathbf{\Omega}} \cdot (\frac{\partial}{\partial x}\hat{\mathbf{\Omega}} \times \frac{\partial}{\partial y}\hat{\mathbf{\Omega}}), \tag{1.2}$$

where $\hat{\mathbf{\Omega}}$ is the normalized field configuration, the direction of spin at some spatial position. Figure 1.8 shows how the topological charge works. It shows a skyrmion magnetization from the side. If we start wrapping this structure around a unit sphere we go round once. This gives the skyrmion structure a winding number of 1. Depending on whether the center of the skyrmion is parallel or anti-parallel with the external magnetic field the skyrmion number either is $+1$ or -1.

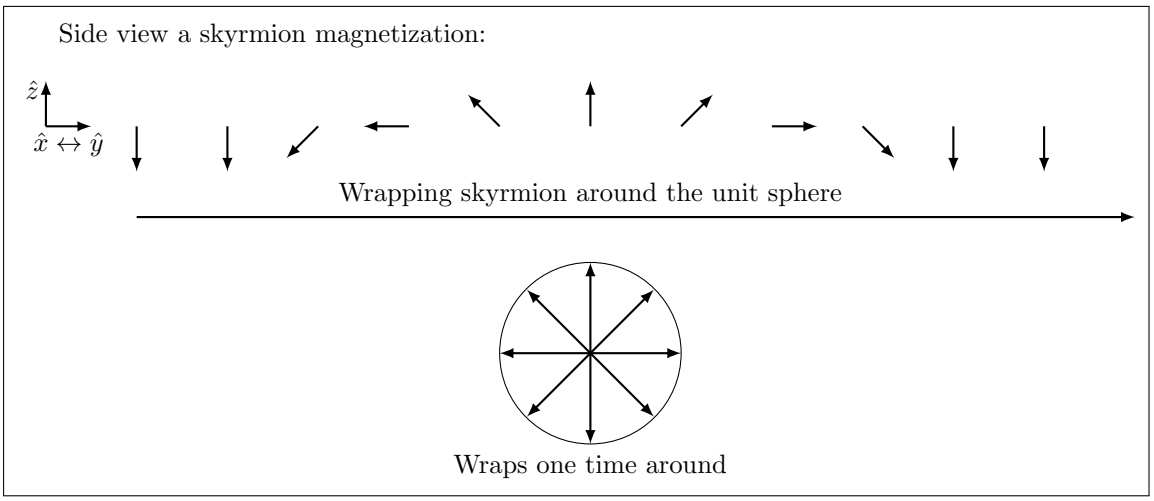

Figure 1.8: Skyrmion wrapping around a sphere.

If we would deform the skyrmion state to some trivial state we would end up with the configuration shown in figure 1.9. Based on energy considerations this state is not allowed (it costs a lot of

energy). If we were to take a different magnetization, a domain wall for example, and deform the state, we would be able to obtain a state where all spins are aligned. This means that the magnetic structure we deformed is not topologically protected.

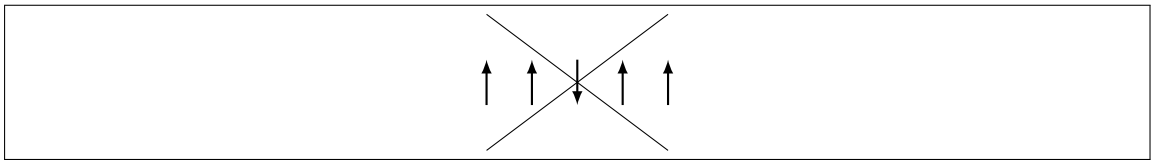

Figure 1.9: Figure depicting a state which is not allowed due to energy considerations (hence the cross).

People categorize different skyrmion structures by their helicity and value of their skyrmion number, depicted in figure 1.10. The helicity of a skyrmion depends on the DM interaction that is induced and this depends on the direction in which inversion symmetry is broken in the compound. The skyrmion structure we saw in MnSi corresponds to the top right configuration in figure 1.10, $m = 1$ and $\gamma = \frac{\pi}{2}$.

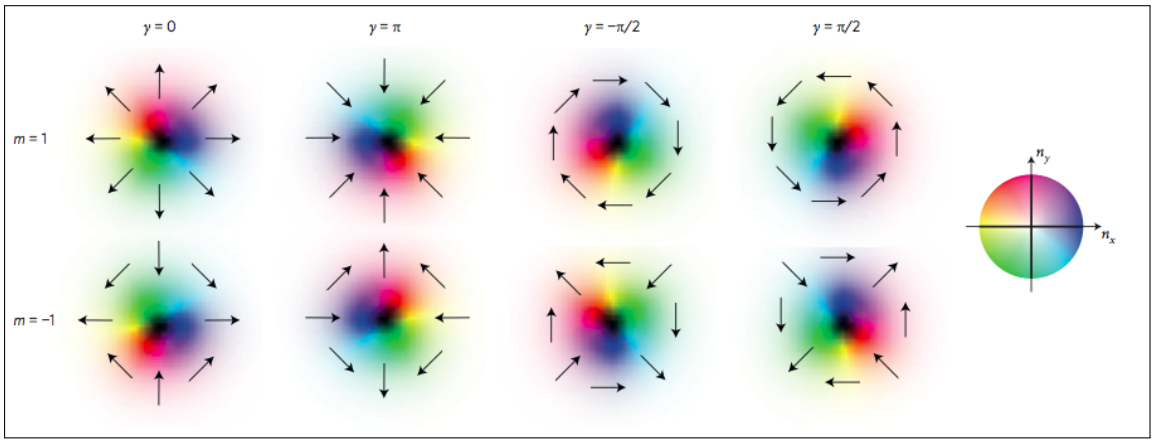

Figure 1.10: Several skyrmion structures with different skyrmion numbers m and helicity γ, where the arrows depict the direction of the (in-plane) spin component. Figure extracted from [6].

1.5 Dynamics of a Skyrmion

The interesting dynamics of skyrmions is one of their biggest advantages over other magnetic structures. Two main advantages of skyrmion dynamics are explained. First, it has been discovered that current-driven skyrmion motion happens at very low current densities of around 10^6A m^{-2} [23]. This is astonishing, since the current density necessary for the motion of domain walls in ferromagnets is substantially (by a factor of 10^6) bigger. The ultralow density required for the motion of skyrmions is very interesting with respect to the possible application as information carrier. It enables the manipulation of information with a very low power consumption per bit. On the other hand, these ultra low current density movements only occur in the slow speed regime,

the story differs in the high speed regime. In this regime skyrmions need more or less the same current density for movement as is used for the motion of domain walls.

A second interesting aspect of the dynamics of a skyrmion is the way they seem to pass impurities in the medium. In [24] they studied the current-driven motion of the skyrmion state as well as the helical state in a confined geometry including an impurity. They found a current-velocity almost independent of the impurity pinning for the skyrmion state in contrast to the helical state which showed a current-velocity similar to domain walls. This interesting property of a skyrmion to avoid impurities is traced back to the equation of motion, where the motion of skyrmions is transverse to the potential. An example is figure 1.11, where we see the movement of a skyrmion in a restricted geometry. Figure 1.12 shows a visualization of a skyrmion moving around an obstacle. This property is very useful in the transport of information through wires and thus is technologically beneficial.

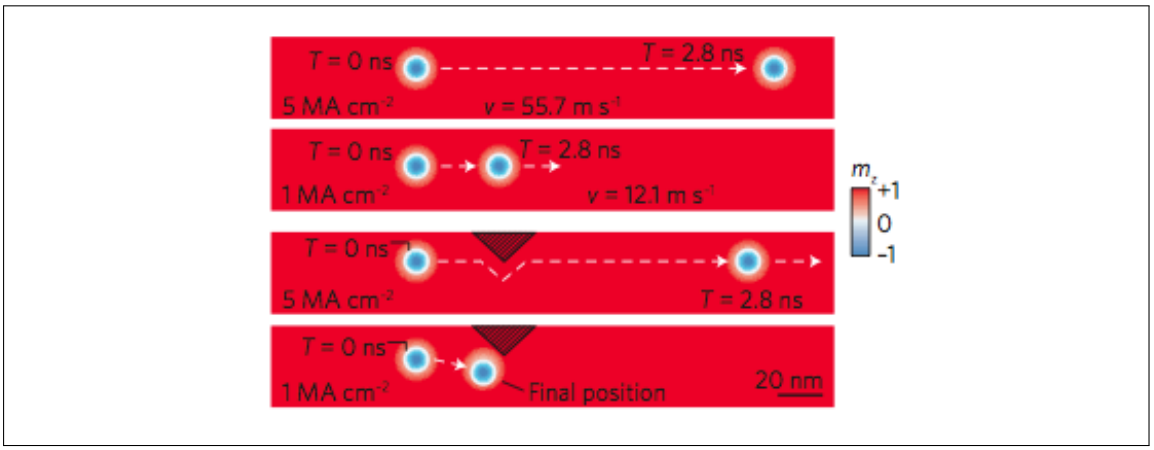

Figure 1.11: Individual skyrmions moving in perfect stripes (the first two stripes). The bottom two stripes include pinning (the dark triangles). Extracted from [15].

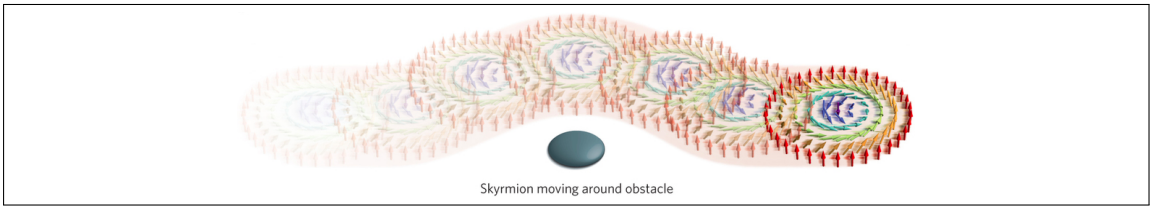

Figure 1.12: A visualization of a skyrmion moving around an obstacle. Figure extracted from [25].

An example where skyrmions could be used is in the production of so called race-track memory (domain wall memory). In 2008, in a research facility of IBM in the US, people managed to create a 3-bit memory using domain walls. Their aim was to produce a memory with a storage density and reading and writing capabilities that surpass any memory storage device we use today. However, after producing a prototype they found the memory was a thousand times slower

than they predicted it to be. They needed very high current densities to push the domain walls through the wire to obtain decent memory speeds. The reason for the slow movement of domain walls through the wire, and therefore slow memory, is that domain walls got stuck at impurities in the wire. Here skyrmions enter the stage. Since we saw skyrmions have this peculiar behavior in confined geometries, they might be the solution to the problem caused by impurities. Since the motion of skyrmions depends only slightly on the depinning force, they could offer a lot faster transport of information through the wire.

Chapter 2

Phenomenological Model of a Chiral Magnet

In this chapter the phenomenological model of a chiral magnet is given. We minimize the energy in order to find the peculiar skyrmion footprint. Lastly, we briefly describe the known behavior of the DM interaction using the article by Kim et al. [5].

A chiral magnet ows its chirality to a lack of inversion symmetry and a strong spin-orbit coupling of the compound. The direction in which the inversion symmetry in broken directly influences the DM interaction. One could write down all the allowed energy terms bases on the direction of the broken symmetry. The phenomenological energy equation of a chiral magnet where symmetry is broken in the $\hat{z}$-direction, has the following form [26]:

$$E[\boldsymbol{m}] = t_{FM} \int d\boldsymbol{x}[-\frac{J_s}{2}\boldsymbol{m} \cdot \nabla^2 \boldsymbol{m} + K(1 - \boldsymbol{m}_z^2) \\ + \frac{c}{2}\left(\hat{y} \cdot (\boldsymbol{m} \times \frac{\partial \boldsymbol{m}}{\partial x}) - \hat{x} \cdot (\boldsymbol{m} \times \frac{\partial \boldsymbol{m}}{\partial y})\right) + \mu_0 HM(1 - \boldsymbol{m}_z) - \mu_0 M \boldsymbol{m} \cdot \boldsymbol{H}_d]. \tag{2.1}$$

The first term in the formulation of the energy corresponds to the exchange energy with coupling J_s and the second term to anisotropy, where K is a constant. The Dzyalosinskii-Moriya interaction is the third term and is determined by the constant c. The last two terms correspond to an external field H and a dipolar field $\boldsymbol{H}_d$, with μ_0 the permeability of vacuum and M the saturation magnetization [26].

2.1 Minimizing the Energy

As we have seen, skyrmions in a magnetic material have a whirling spin structure. Here we explicitly show how the magnetization depends on the position in space. We give a parametrization to the magnetization vector and plug it in our energy expression 2.1. Subsequently, we minimize this expression in order to find the skyrmion structure [27]. We parametrize the magnetization as

$$\boldsymbol{m}(\boldsymbol{x}) = \sin\theta\cos\phi\hat{\rho} + \sin\theta\sin\phi\hat{\phi} + \cos\theta\hat{z}. \tag{2.2}$$

In this parametrization both ϕ and θ depend on the spatial coordinate $\boldsymbol{x} = (\rho, \phi, z)$, which we now write in cylindrical coordinates. Before plugging in our parametrization in the energy equation we already know some properties of the configuration we are looking for. First of all, we want our solution to have translational symmetry in the $\hat{z}$-direction. Second, we demand rotational symmetry in the $\hat{\phi}$-direction. Here, ϕ is the helicity of the configuration. From these statements it follows that θ depends on the radial coordinate ρ. We now express $\boldsymbol{m}\nabla^2\boldsymbol{m}$ and $\boldsymbol{m}\cdot(\nabla\times\boldsymbol{m})$ in cylindrical coordinates. We only consider a dependence of θ on ρ and ϕ we find

$$\boldsymbol{m}\cdot\nabla^2\boldsymbol{m} = -(\frac{d\theta}{d\rho})^2 - \frac{\sin^2\theta}{\rho^2}, \tag{2.3}$$

$$\boldsymbol{m}\cdot(\nabla\times\boldsymbol{m}) = \sin\phi\left(\frac{d\theta}{d\rho} + \frac{\sin\theta\cos\theta}{\rho}\right), \tag{2.4}$$

$$K(1-\boldsymbol{m}_z^2) = K\sin^2\theta, \tag{2.5}$$

and,

$$\mu_0 HM(1-\boldsymbol{m}_z) = \mu_0 HM(1-\cos\theta). \tag{2.6}$$

We are left with $-\mu_0 M\boldsymbol{m}\cdot\boldsymbol{H}_d$, which we rewrite using Maxwell's equations in a medium. These are

$$\nabla\times\boldsymbol{H}_d = 0, \tag{2.7}$$

$$\nabla\cdot\boldsymbol{H}_d = -M\nabla\cdot\boldsymbol{m}. \tag{2.8}$$

Since $\nabla\times\nabla U = 0$ for all U, we write $\boldsymbol{H}_d = \nabla U$. From the fact that $\boldsymbol{m}$ only depends on ρ, U and $\boldsymbol{H}_d$ will only depend on ρ as well. We write $\boldsymbol{H}_d(\rho) = \nabla U(\rho) = \frac{dU}{d\rho}\hat{\rho}$. If we then plug the magnetization into Maxwell equation 2.8, we find

$$M\nabla\cdot\boldsymbol{m} = M\cos\phi\left(\cos\theta\frac{d\theta}{d\rho} + \frac{\sin\theta}{\rho}\right). \tag{2.9}$$

We then compare $-\nabla\cdot\boldsymbol{H}_d = -\nabla^2 U = -\frac{d^2U}{d\rho^2} - \frac{1}{\rho}\frac{dU}{d\rho}$, where on the right side we implemented cylindrical coordinates. From equation 2.9 we deduce $\boldsymbol{H}_d$,

$$\boldsymbol{H}_d = -M\cos\phi\sin\theta\hat{\rho}, \tag{2.10}$$

such that our energy contribution becomes,

$$-M\boldsymbol{m}\cdot\boldsymbol{H}_d = M^2\cos^2\phi\sin^2\theta. \tag{2.11}$$

We want to minimize the total energy to find the skyrmion structure. A first step towards minimizing this model is to look at all the terms depending on ϕ. The energy of the dipolar field is minimized when $\cos^2\phi = 0$, such that $\phi = \pm\frac{\pi}{2}$. In the DM interaction we see that depending

on whether the constant $\frac{c}{2}$ is positive or negative, $\sin\phi = \pm 1$. This is the case for $\phi = \pm\frac{\pi}{2}$. All together we find the following expression depending on $\theta(\rho)$,

$$E[\theta(\rho)] = \int \left(\frac{J_s}{2}((\frac{d\theta}{d\rho})^2 + \frac{\sin^2\theta}{\rho^2}) + \frac{c}{2}(\frac{d\theta}{d\rho} + \frac{\sin\theta\cos\theta}{\rho}) + K\sin^2\theta + \mu_0 HM(1-\cos\theta) \right) \rho\, d\rho. \tag{2.12}$$

The next step is to minimize the above expression by varying with respect to θ and equal it to zero. For example varying the first term gives

$$E[\theta+\delta\theta] = \int \frac{J_s}{2}((\frac{d\theta + d\delta\theta}{d\rho})^2))\rho/, d\rho = \int \frac{J_s}{2}((\frac{d\theta}{d\rho})^2 + 2\frac{d\theta d\delta\theta}{d\rho} + (\frac{d\delta\theta}{d\rho})^2)\rho\, d\rho \tag{2.13}$$

$$= \int \frac{J_s}{2}(-2\frac{d^2\theta}{d\rho}\delta\theta\rho d\rho - 2\frac{d\theta}{d\rho}\delta\theta d\rho) = 0 \tag{2.14}$$

$$\rightarrow -J_s(\frac{d^2\theta}{d\rho} + \frac{1}{\rho}\frac{d\theta}{d\rho})\rho = 0. \tag{2.15}$$

When we do this for all terms we find

$$-J_s\left(\frac{d^2\theta}{d\rho} + \frac{1}{\rho}\frac{d\theta}{d\rho}\right) - C\frac{\sin^2\theta}{\rho} + 2K\sin\theta\cos\theta + \mu_0 HM\sin\theta = 0, \tag{2.16}$$

which is a differential equation we numerically solve for $\theta(\rho)$. In order to solve 2.16 numerically, we need to make the expression dimensionless by introducing $\widetilde{\rho} = \frac{C}{J_s}\rho$, such that we obtain

$$\frac{d^2\theta}{d\widetilde{\rho}} + \frac{1}{\widetilde{\rho}}\frac{d\theta}{d\widetilde{\rho}} + \frac{\sin^2\theta}{\widetilde{\rho}} - C_1\sin\theta\cos\theta - C_2\sin\theta = 0, \tag{2.17}$$

where, $C_1 = \frac{2J_sK}{C^2}$ and $C_2 = \frac{\mu_0 J_s HM}{C^2}$. We then solve the differential equation by imposing boundary conditions: $\theta(0) = \pi$ and $\theta(\infty) = 0$. The result is plotted in figure 2.1.

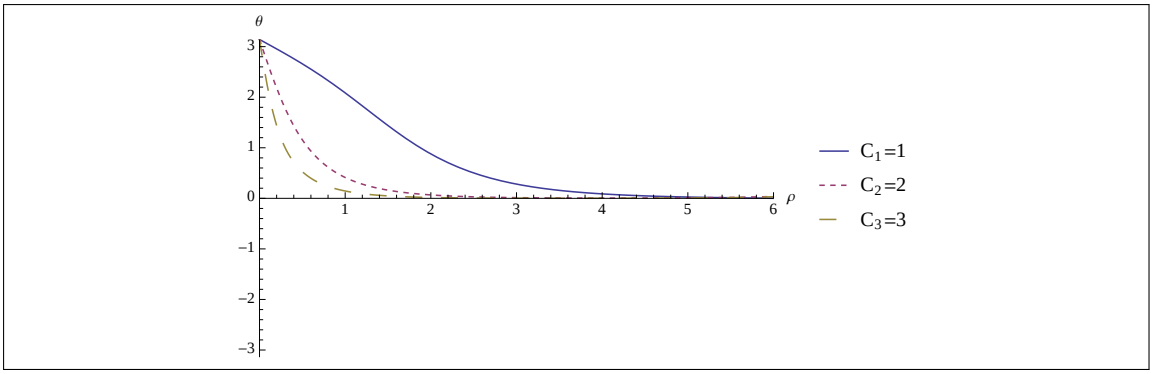

Figure 2.1: The skyrmion footprint for different values of parameters C_1 and C_2. In this figure $C_2 = 0$.

We then use the parametrization we choose to create a vector plot of the skyrmion state, shown in figure 2.2.

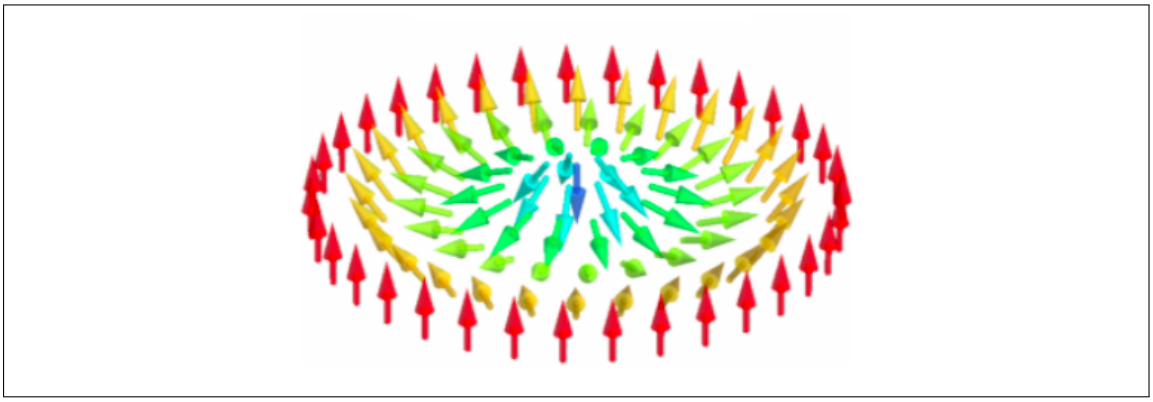

Figure 2.2: Skyrmion configuration obtained from minimizing the phenomenological model. Figure extracted from [4].

2.2 Model

In order to produce a DM interaction we need a broken inversion symmetry and a strong spin-orbit coupling. To break inversion symmetry we take two layers of different compounds. One compound is some ferromagnet, while the other is a non-magnet which has a strong spin-orbit coupling. This system is schematically shown in figure 2.3. We then assume we can describe the physics between the two layers with a Rashba model. Thus, in our model a strong spin-orbit coupling is due to a Rashba coupling. The strong Rashba coupling together with a lack of inversion symmetry then induces a DM interaction in our toy model.

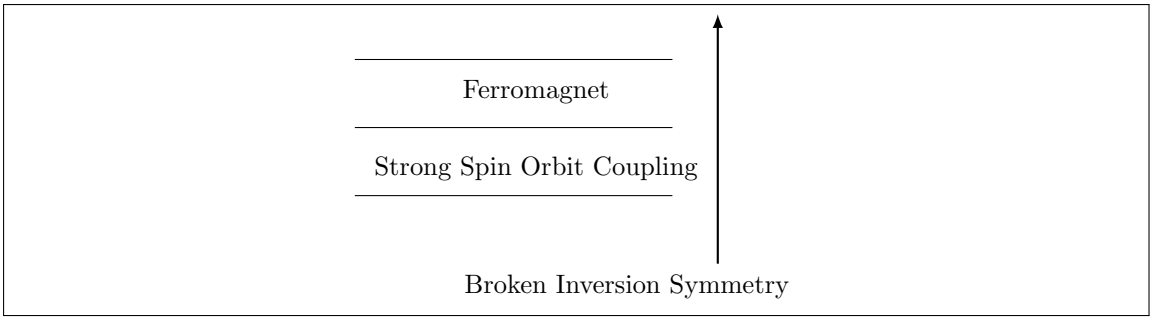

Figure 2.3: Schematic model we use in this thesis. Inversion symmetry is broken in the $\hat{z}$-direction. Between the two layers we assume a Rashba model.

The toy model we consider is a Rashba model coupled to a helical exchange field. The Hamiltonian for this model is

$$\mathcal{H} = \frac{\boldsymbol{p}^2}{2m} - \frac{\alpha_R}{\hbar}(\boldsymbol{\tau} \times \boldsymbol{p}) \cdot \hat{z} - \frac{\Delta}{2}\boldsymbol{m}(x) \cdot \boldsymbol{\tau}, \tag{2.18}$$

where the magnetization: $\boldsymbol{m}(\boldsymbol{x}) = \sin qx\hat{x} + \cos qx\hat{z}$, depicted in figure 2.4, where we see a helix precessing around the x-axes. The number of precessions is characterized by q. In the Hamiltonian, $\boldsymbol{p}$ is the electron momentum in the xy-plane, the vector $\boldsymbol{\tau}$ represents the electron spin. The Rashba

coupling, α_R, determines the strength of the spin-orbit and Δ is the strength of the exchange field. This model captures several broken symmetries. Time reversal symmetry gets broken by the implementation of an external magnetic field and the Rashba spin-orbit coupling breaks inversion symmetry. We then have all ingredients to induce a DM interaction.

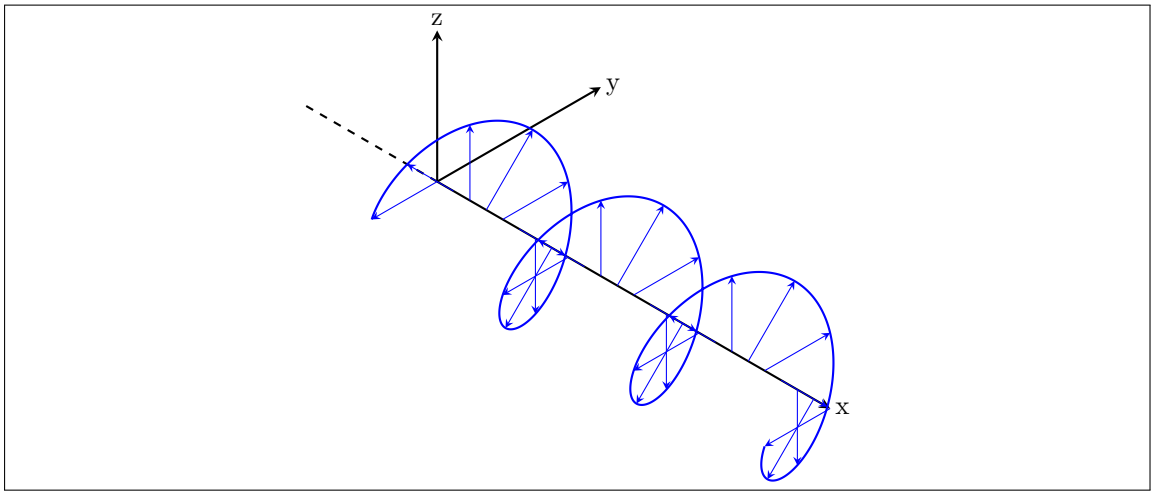

Figure 2.4: The helical configuration of the magnetization, where we see a spin helix precessing around the x-axes.

We have set up a model where a DM interaction should emerge which we can retrace in the energy density of the model. What we expect is that the energy density does not minimize for $q = 0$, but due to the DM interaction, minimizes for $q \neq 0$. More explicitly, we expect the energy density of our system to be

$$\epsilon_{tot}(q, \Delta, \epsilon_F, \alpha_R) = Dq + Aq^2, \tag{2.19}$$

where, $D = D(\alpha_R, \epsilon_F) =$ DM interaction, $A = A(\epsilon_F) =$ exchange coefficient. Both terms depend on the Fermi energy as becomes clear in the next chapter.

Another way this energy density can be obtained is to consider the following terms in the energy density of the phenomenological model.

$$\epsilon_{tot}[\boldsymbol{m}] = -\frac{J_s}{2}\boldsymbol{m} \cdot \nabla^2 \boldsymbol{m} + \frac{c}{2}\left(\hat{y} \cdot (\boldsymbol{m} \times \frac{\partial \boldsymbol{m}}{\partial x}) - \hat{x} \cdot (\boldsymbol{m} \times \frac{\partial \boldsymbol{m}}{\partial y})\right). \tag{2.20}$$

If we then plug in our helical magnetization we end up with the same structure as in expression 2.19. We want to compute both D and A in order to find the typical length scale of a chiral magnetic structure: $\frac{D}{A}$. This length scale corresponds to the size of a skyrmion. Before we compute these terms we give a brief summary of the previously established result of this ratio.

2.3 Known Analytical Behavior of the DM Interaction

The inspiration to research the Dzyaloshinkii-Moriya interaction came from an article by Kim et al. [5]. In that article the DM interaction is computed with a simple mathematical construct. This construct is a chiral derivative. The relevant part of the article for this thesis is where a derivation of the interfacial DM interaction is given. Below is a very brief summary of the computation and the results. The starting point is the two-dimensional Rashba model, using the following Hamiltonian,

$$\mathcal{H} = \mathcal{H}_{kin} + \mathcal{H}_R + \mathcal{H}_{exc} + \mathcal{H}_{imp} \tag{2.21}$$

$$= \frac{\boldsymbol{p}^2}{2m} + \frac{\alpha_R}{\hbar}\boldsymbol{\tau}\cdot(\boldsymbol{p}\times\hat{\boldsymbol{z}}) + J\boldsymbol{\tau}\cdot\hat{\boldsymbol{m}} + \mathcal{H}_{imp}. \tag{2.22}$$

In this last expression, $\mathcal{H}_{imp}$ describes scattering of impurities, the rest we have seen before. Then, a unitary transformation is introduced of the form

$$\mathcal{U} = e^{-ik_R\boldsymbol{\tau}\cdot\frac{(\boldsymbol{r}\times\hat{\boldsymbol{z}})}{2}}, \tag{2.23}$$

equation where the momentum is defined as $k_R = \frac{2\alpha_R m_e}{\hbar^2}$, and $\boldsymbol{r} = (x, y)$. Here, $\mathcal{U}$ rotates the electron spin around the $\hat{\boldsymbol{r}}\times\hat{\boldsymbol{z}}$ direction by the angle $k_R r$. Also, a $\boldsymbol{r}$-dependent rotation matrix $\mathcal{R}$ is introduced. Without giving too much details, when the unitary transformation is applied to the Hamiltonian one obtains

$$\mathcal{U}^\dagger\mathcal{H}\mathcal{U} = \mathcal{H}_{kin} + J\boldsymbol{\tau}\cdot\hat{\boldsymbol{m}}' + \mathcal{H}_{imp} + \mathcal{O}(\alpha_R^2), \tag{2.24}$$

where $\boldsymbol{m}' = \mathcal{R}^{-1}\hat{\boldsymbol{m}}$. The interest lies in small Rashba coupling, so quadratic and higher orders of α_R are neglected.

Next, the energy of the Fermi sea is computed. Without the presence of $\mathcal{H}_R$, $\boldsymbol{m}$ is homogeneous, such that the energy only depends on spatial derivatives. The energy is expressed as: $\epsilon = A(\partial_x\hat{\boldsymbol{m}}\cdot\partial_x\hat{\boldsymbol{m}} + \partial_y\hat{\boldsymbol{m}}\cdot\partial_y\hat{\boldsymbol{m}})$, where A is the interfacial exchange stiffness coefficient. In the presence of the Rashba interaction, $\mathcal{H}_R$, $\hat{\boldsymbol{m}} \to \hat{\boldsymbol{m}}$. The same is done for the energy. We have: $\epsilon = A(\partial_x\hat{\boldsymbol{m}}'\cdot\partial_x\hat{\boldsymbol{m}}' + \partial_y\hat{\boldsymbol{m}}'\cdot\partial_y\hat{\boldsymbol{m}}')$. Using the supplemental material Kim et al. have provided we write

$$\partial_i\hat{\boldsymbol{m}}' = \partial_i(\mathcal{R}^{-1}\hat{\boldsymbol{m}}) = \mathcal{R}^{-1}\tilde{\partial}_i\hat{\boldsymbol{m}}, \tag{2.25}$$

where $i \in [x, y]$, and where a *chiral derivative* $\tilde{\partial}_i$ is defined. This chiral derivative is given by

$$\tilde{\partial}_i\hat{\boldsymbol{m}} = \partial_i\hat{\boldsymbol{m}} + k_R(\hat{\boldsymbol{z}}\times\hat{\boldsymbol{u}})\times\hat{\boldsymbol{m}}, \tag{2.26}$$

where $\hat{\boldsymbol{u}}$ is the unit vector along the direction of the derivative i. The second term comes from acting with a derivative on the inverse rotation matrix $\mathcal{R}^{-1}$. Putting this together, the energy is

$$\epsilon = A(\partial_x\hat{\boldsymbol{m}}\cdot\partial_x\hat{\boldsymbol{m}} + \partial_y\hat{\boldsymbol{m}}\cdot\partial_y\hat{\boldsymbol{m}}) + D[\hat{\boldsymbol{y}}\cdot(\hat{\boldsymbol{m}}\times\partial_x\hat{\boldsymbol{m}}) - \hat{\boldsymbol{x}}(\hat{\boldsymbol{m}}\times\partial_y\hat{\boldsymbol{m}})], \tag{2.27}$$

where, $\frac{D}{A} = 2k_R = 4\frac{\alpha_R m}{\hbar^2}$. In the next chapter we try to reproduce the same result using different techniques.

Chapter 3

Analytical Computation of the DM Interaction

In this chapter we check the known behavior of the DM interaction using quantum mechanical perturbation theory and field theory. The toy model we consider is a Rashba model coupled to a helical exchange field. The Hamiltonian for this model is

$$\mathcal{H} = \frac{\boldsymbol{p}^2}{2m} - \frac{\alpha_R}{\hbar}(\boldsymbol{\tau} \times \boldsymbol{p}) \cdot \hat{z} - \frac{\Delta}{2}\boldsymbol{m}(x) \cdot \boldsymbol{\tau},$$

where the magnetization: $\boldsymbol{m}(\boldsymbol{x}) = \sin qx\hat{x} + \cos qx\hat{z}$. The expression in the previous chapter defining the behavior of the DM interaction for small spin-orbit coupling is: $\frac{D}{A} = 4\frac{\alpha_R m}{\hbar^2}$. Recall that we expect for the energy density of the system that,

$$\epsilon_{tot}(q) = Aq^2 + Dq. \tag{3.1}$$

Here A corresponds to the micro magnetic exchange energy and D to the DM interaction. We are thus trying to find in what way the electron energy density depends on q in our toy model. We then compare the coefficients of the quadratic and linear terms in q of the total energy density, such that we are able to determine the relation between A and D.

First, we consider the case $\alpha_R = 0$. This means we solve a system of electrons coupled to a helical exchange field. We compute the total energy density of this system using both field theory and integration over the filled Fermi sea. The latter can be found in Section 3.1 and the former in Section 3.2. Second, we compute the total energy for $\alpha_R \ll 1$. This computation is done using first order perturbation theory and again integration over the filled Fermi sea, this is located in Section 3.3.

3.1 Computing the Total Energy for $\alpha_R = 0$ Using Field Theory

From the phenomenological model introduced earlier we see that in order to obtain the total kinetic energy of the system with spin-orbit coupling, we need to find the term quadratic in the magnetization, and quadratic in ∇. When we are in Fourier space this ∇^2 corresponds to k^2. We use a linearized magnetization, $\boldsymbol{m} = (\delta m_x, \delta m_y, 1 - \frac{\delta m_x^2}{2} - \frac{\delta m_y^2}{2})$, and using this magnetization we first compute the eigenvalues of the relevant Hamiltonian.

3.1.1 Eigenvalues and Eigenfunctions

For the following Hamiltonian,

$$\mathcal{H} = \frac{\boldsymbol{p}^2}{2m} - \frac{\Delta}{2}\boldsymbol{m}\cdot\boldsymbol{\tau}, \tag{3.2}$$

we try to find the corresponding eigenvalues. In the computation of the eigenvalues of this hamiltonian terms of $\boldsymbol{m}$ depending on δm are omitted in the self-energy. We are only interested in 1 in the τ^z component. Note that $p_{x_i} = -i\hbar\frac{\partial}{\partial x_i}$, we obtain

$$\mathcal{H} = \begin{pmatrix} \frac{\hbar^2}{2m}\boldsymbol{k}^2 - \frac{\Delta}{2} & 0 \\ 0 & \frac{\hbar^2}{2m}\boldsymbol{k}^2 + \frac{\Delta}{2} \end{pmatrix}. \tag{3.3}$$

In this last equation we expressed the Hamiltonian in the wave numbers k_x, k_y, this is allowed since the Hamiltonian commutes with the momentum operator. From the Hamiltonian we find the energy spectrum, by computing its eigenvalues. This gives two eigenvalues: $E_{k,\sigma} = \frac{\hbar^2\boldsymbol{k}^2}{2m} + \sigma\frac{\Delta}{2}$, where $\sigma \in [\pm]$. In the next section the eigenvalues are of use in the computation of the Greens function.

3.1.2 Field Theory

The partition is given by

$$\mathcal{Z} = \int d[\phi_\sigma^*]d[\phi_{\sigma'}]d[\boldsymbol{m}]e^{\frac{-1}{\hbar}S[\phi_\sigma^*,\phi_{\sigma'},\boldsymbol{m}]}, \tag{3.4}$$

where S is given by the following expression

$$S = \int_0^{\hbar\beta} d\tau \int d\boldsymbol{x} \sum_{\sigma,\sigma'} \phi_\sigma(\boldsymbol{x},\tau)^* \left[(\hbar\frac{\partial}{\partial\tau} - \frac{\hbar^2\nabla^2}{2m} - \mu)\delta_{\sigma,\sigma'} - \frac{\Delta}{2}\boldsymbol{\tau}_{\sigma,\sigma'}\cdot\boldsymbol{m}(\boldsymbol{x},\tau) \right] \phi_{\sigma'}(\boldsymbol{x},\tau). \tag{3.5}$$

The $\boldsymbol{\tau}$ are the well known Pauli matrices. We investigate the terms quadratic in the magnetization as mentioned before. We consider the system to be below the transition temperature. We rewrite

the previous equation using the Green's function

$$S = \int_0^{\hbar\beta} d\tau \int_0^{\hbar\beta} d\tau' \int d\boldsymbol{x} \int \boldsymbol{x}' \sum_{\sigma,\sigma'} \phi^*(\boldsymbol{x},\tau) \left[-\hbar G^{-1}_{\sigma,\sigma'}(\boldsymbol{x},\tau;\boldsymbol{x}',\tau')\right] \phi_{\sigma'}(\boldsymbol{x},\tau), \tag{3.6}$$

with

$$G^{-1}_{\sigma,\sigma'}(\boldsymbol{x},\tau;\boldsymbol{x'},\tau') = \frac{-1}{\hbar}\left[(\hbar\frac{\partial}{\partial\tau} - \frac{\hbar^2\nabla^2}{2m} - \mu)\delta_{\sigma,\sigma'} - \frac{\Delta}{2}\boldsymbol{\tau}_{\sigma,\sigma'}\cdot\boldsymbol{m}(\boldsymbol{x},\tau)\right]\delta(\boldsymbol{x}-\boldsymbol{x'})\delta(\tau-\tau'). \tag{3.7}$$

The inverse Green's function is defined as: $G^{-1}_{\sigma,\sigma'}(\boldsymbol{x},\tau;\boldsymbol{x'},\tau') = G_0^{-1}(\boldsymbol{x},\tau;\boldsymbol{x'},\tau) - \Sigma_{\sigma,\sigma'}(\boldsymbol{x},\tau;\boldsymbol{x'},\tau)$. Next, we want to integrate out the fermionic fields from equation (3.4) and find the effective action

$$\mathcal{Z} = \int d[\boldsymbol{m}] e^{\frac{-1}{\hbar}S^{eff}[\boldsymbol{m}]}. \tag{3.8}$$

In the equation above, the fields have been integrated out using $\int d[\phi^*]d[\phi]\exp(-\phi^* M\phi) = \exp(\mathrm{Tr}\ln M)$ resulting in

$$S^{eff}[\boldsymbol{m}] = \int_0^{\hbar\beta} d\tau \int d\boldsymbol{x}\left[-\hbar\,\mathrm{Tr}\ln(-G^{-1})\right]. \tag{3.9}$$

Subsequently, we perform a Taylor series of the trace and find for the effective action

$$S_{eff}[\boldsymbol{m}] = \int_0^{\hbar\beta} d\tau \int d\boldsymbol{x}(-\hbar\,\mathrm{Tr}\ln(G_0^{-1}) + \hbar\,\mathrm{Tr}(G_0\Sigma) + \frac{\hbar}{2}\,\mathrm{Tr}(G_0\Sigma G_0\Sigma) + ...), \tag{3.10}$$

with the following self energy,

$$\hbar\Sigma(\boldsymbol{x},\tau;\boldsymbol{x}',\tau')_{\sigma,\sigma'} = -\frac{\Delta}{2}(\delta m_x, \delta m_y, -\frac{\delta m_x^2}{2} - \frac{\delta m_y^2}{2})\boldsymbol{\tau}_{\sigma,\sigma'}\delta(\tau-\tau')\delta(\boldsymbol{x}-\boldsymbol{x}'). \tag{3.11}$$

Here, the 1 in the z-direction of the magnetization has been excluded, since this contribution is already captured in the energy, E_σ. We are only interested in the terms quadratic in the magnetization and these are found in both $\hbar\,\mathrm{Tr}(G_0\Sigma)$, by considering the τ^z component of the magnetization, and in $\frac{\hbar}{2}\,\mathrm{Tr}(G_0\Sigma G_0\Sigma)$, by taking the x and y components of the Pauli matrices. However, before we compute this trace, we have to compute the Green's function from the equation

$$\left[\hbar\frac{\partial}{\partial\tau} - \frac{\hbar^2\nabla^2}{2m} - \mu - \frac{\Delta}{2}\tau^z m^z\right](G_0)_{\sigma,\sigma'}(\boldsymbol{x},\tau;\boldsymbol{x'},\tau') = -\hbar\delta(\boldsymbol{x}-\boldsymbol{x'})\delta(\tau-\tau'). \tag{3.12}$$

The solution to this equation is given as

$$(G_0)_{\sigma,\sigma'} = \frac{1}{\hbar\beta V}\sum_{\boldsymbol{k},n}\frac{\hbar\delta_{\sigma,\sigma'}}{-i\hbar\omega_n + \epsilon_k - \mu - \sigma\frac{\Delta}{2}}e^{ik(\boldsymbol{x}-\boldsymbol{x'})}e^{-\omega_n(\tau-\tau')}. \tag{3.13}$$

Here, ϵ_k is the one-particle free electron dispersion. We rewrite the effective action using the expansion of the trace and noting that in the definition of the self energy a $\hbar$ is included, we find

$$\begin{aligned} S^{eff}[\boldsymbol{m}] = \int_0^{\hbar\beta} d\tau \int d\boldsymbol{x} \sum_{a\in[x,y]} (&\frac{\Delta}{4}\,\mathrm{Tr}[G_0(\boldsymbol{x},\tau;\boldsymbol{x},\tau^+)\tau^z](m_a)^2 \\ &+ \frac{\Delta^2}{8\hbar}\int_0^{\hbar\beta} d\tau' \int d\boldsymbol{x}' \sum_{b\in[x,y]} m_a\,\mathrm{Tr}[\tau^a G_0(\boldsymbol{x},\tau;\boldsymbol{x}',\tau')\tau^b G_0(\boldsymbol{x}',\tau';\boldsymbol{x},\tau))m_b]). \end{aligned}$$

As seen from the expression above, only quadratic terms in magnetization m are present. The next step is to perform a Fourier transform and introduce a new function such that we write the effective action as

$$S^{eff}(\boldsymbol{m}) = \hbar\beta V \sum_{n,\boldsymbol{k}} \sum_{a,b\in x,y} m^a_{\boldsymbol{k},n}\Pi^{a,b}(\boldsymbol{k}, i\omega_n)m^b_{-\boldsymbol{k},-n}. \tag{3.14}$$

Lets consider each computation of the traces separately,

$$\int_0^{\hbar\beta} d\tau \int d\boldsymbol{x}\, \mathrm{Tr}(G_0\tau^z)m_a(\boldsymbol{x},\tau)^2 =$$

$$\int_0^{\hbar\beta} d\tau \int d\boldsymbol{x}\, \mathrm{Tr}\left[\sum_{\sigma,\sigma'}\sum_{\boldsymbol{k},n} \frac{-\hbar\delta_{\sigma,\sigma'}}{-i\hbar\omega_n + \epsilon_{\boldsymbol{k}} - \mu - \sigma\frac{\Delta}{2}} e^{ik(\boldsymbol{x}-\boldsymbol{x'})}\frac{e^{-\omega_n(\tau-\tau')}}{\hbar\beta V}\tau^z\delta(\boldsymbol{x}-\boldsymbol{x'})\delta(\tau-\tau')\right] m_a^2(\boldsymbol{x},\tau).$$

The trace in the expression is taken over spin-space, space and time. Next we transform $\boldsymbol{m}(\boldsymbol{x},\tau)$ to Fourier space, which will be helpful in the computation.

$$\int d\boldsymbol{x}\int d\boldsymbol{x'}\int d\tau\int d\tau' \sum_{k,k',k''}\sum_{n,n',n''} \mathrm{Tr}[\sum_{\sigma,\sigma'} \frac{-\hbar\delta_{\sigma,\sigma'}}{-i\hbar\omega_n + \epsilon_{\boldsymbol{k}} - \mu - \sigma\frac{\Delta}{2}}$$
$$e^{ik'(\boldsymbol{x}-\boldsymbol{x'})}\frac{e^{-\omega_n(\tau-\tau')}}{\hbar\beta V}e^{ik(\boldsymbol{x}-\boldsymbol{x'})}\frac{e^{-i\omega_{n'}(\tau-\tau')}}{\hbar\beta V}e^{ik''\boldsymbol{x}}e^{-i\omega_{n''}}\tau^z m^2_{n''}(k'')].$$

This leads to several delta functions, implying $k''=0$ and $n''=0$, leaving us with a trace over spin space.

Then performing both the sum over spins and the sum over Matsubara frequencies we find[1]

$$\sum_k \frac{\Delta}{4}(n_+ - n_-)\delta_{a,b}. \tag{3.15}$$

The next quantity we need to compute is, $\mathrm{Tr}[G_0\Sigma G_0\Sigma] =$

$$\int_0^{\hbar\beta} d\tau\int d\boldsymbol{x}\int_0^{\hbar\beta} d\tau'\int d\boldsymbol{x'}\frac{\Delta^2}{8}m_a(\boldsymbol{x},\tau)\,\mathrm{Tr}[G_0\Sigma G_0\Sigma]m_b(\boldsymbol{x},\tau) =$$
$$\int d\boldsymbol{x}\int d\boldsymbol{x'}\int d\boldsymbol{x''}\int d\boldsymbol{x'''}\int d\tau\int d\tau'\int d\tau''\int d\tau'''$$
$$\times\,\mathrm{Tr}[\sum_{\sigma,\sigma'}\sum_{n,\boldsymbol{k}}\frac{-\hbar\delta_{\sigma,\sigma'}}{-i\omega_n\hbar+\epsilon_{\boldsymbol{k}}-\mu-\sigma\frac{\Delta}{2}}e^{ik(\boldsymbol{x}-\boldsymbol{x'})}\frac{e^{-i\omega_n(\tau-\tau')}}{\hbar\beta}m_a(\boldsymbol{x'},\tau')\tau^a\delta(\boldsymbol{x}-\boldsymbol{x'})\delta(\tau-\tau')$$
$$\times\sum_{n',k'}\frac{-\hbar\delta_{\sigma,\sigma'}}{-i\omega'_n\hbar+\epsilon_{\boldsymbol{k'}}-\mu-\sigma'\frac{\Delta}{2}}e^{ik'(\boldsymbol{x''}-\boldsymbol{x'''})}\frac{e^{-i\omega_{n'}(\tau''-\tau''')}}{\hbar\beta}m_b(\boldsymbol{x'''},\tau''')\tau^b\delta(\boldsymbol{x'''}-\boldsymbol{x})\delta(\tau'''-\tau)].$$

We immediately integrate over $\boldsymbol{x''}$, $\boldsymbol{x'''}$, τ'' and τ''', implying the following: $\boldsymbol{x'''}\to\boldsymbol{x}$, $\boldsymbol{x''}\to\boldsymbol{x'}$, $\tau'''\to\tau$ and $\tau''\to\tau$,

$$\frac{\Delta^2}{8}\int d\boldsymbol{x}\int d\boldsymbol{x'}\int d\tau\int d\tau'\,\mathrm{Tr}[\sum_{\sigma,\sigma'}\sum_{n,k}\frac{-\hbar\delta_{\sigma,\sigma'}}{-i\omega_n\hbar+\epsilon_{\boldsymbol{k}}-\mu-\sigma\frac{\Delta}{2}}e^{ik(\boldsymbol{x}-\boldsymbol{x'})}\frac{e^{-i\omega_n(\tau-\tau')}}{\hbar\beta}m_a(\boldsymbol{x'},\tau')\tau^a$$
$$\times\sum_{k',n'}\frac{-\hbar\delta_{\sigma,\sigma'}}{-i\omega_{n'}\hbar+\epsilon_{\boldsymbol{k'}}-\mu-\sigma'\frac{\Delta}{2}}e^{ik'(\boldsymbol{x'}-\boldsymbol{x})}\frac{e^{-i\omega_{n'}(\tau'-\tau)}}{\hbar\beta}m_b(\boldsymbol{x},\tau)\tau^b].$$

[1]The same line of thought is followed in the computation of $\mathrm{Tr}[G_0\Sigma G_0\Sigma]$, where more details are given.

Just as before we Fourier transform the magnetization, resulting in

$$\frac{\Delta^2}{8}\int d\boldsymbol{x}\int d\boldsymbol{x}'\int d\tau\int d\tau'\,\mathrm{Tr}[\sum_{\sigma,\sigma'}\sum_{n,k}\frac{-\hbar\delta_{\sigma,\sigma'}}{-i\omega_n\hbar+\epsilon_{\boldsymbol{k}}-\mu-\sigma\frac{\Delta}{2}}e^{ik(\boldsymbol{x}-\boldsymbol{x}')}\frac{e^{-i\omega_n(\tau-\tau')}}{\hbar\beta}$$
$$\times\sum_{n',k'}m_{n'}(\boldsymbol{k'})e^{i\boldsymbol{k}'\boldsymbol{x}'}e^{i\omega_{n'}\tau'}\tau^a$$
$$\sum_{n'',k''}\frac{-\hbar\delta_{\sigma,\sigma'}}{-i\omega_{n''}\hbar+\epsilon_{\boldsymbol{k}''}-\mu-\sigma'\frac{\Delta}{2}}e^{ik''(\boldsymbol{x}'-\boldsymbol{x})}\frac{e^{-i\omega_{n''}(\tau'-\tau)}}{\hbar\beta}$$
$$\times\sum_{n''',k'''}m_{n'''}(\boldsymbol{k'''})e^{i\boldsymbol{k}'''\boldsymbol{x}}e^{-i\omega_{n'''}\tau}\tau^b].$$

By integrating over $\boldsymbol{x}$, $\boldsymbol{x}'$, τ and τ', we find four delta functions in our expression

$$\frac{\Delta^2}{8}\sum_{k,k',k'',k'''}\sum_{n,n',n'',n''''}\mathrm{Tr}[\sum_{\sigma,\sigma'}\frac{-\hbar\delta_{\sigma,\sigma'}}{-i\omega_n\hbar+\epsilon_{\boldsymbol{k}}-\mu-\sigma\frac{\Delta}{2}}\tau^a m^a_{n'}(\boldsymbol{k'})$$
$$\times\frac{-\hbar\delta_{\sigma,\sigma'}}{-i\omega_{n''}\hbar+\epsilon_{\boldsymbol{k}''}-\mu-\sigma'\frac{\Delta}{2}}\tau^b m^b_{n'''}(\boldsymbol{k'''})$$
$$\times\delta(\boldsymbol{k}-\boldsymbol{k}''+\boldsymbol{k}''')\delta(-\boldsymbol{k}+\boldsymbol{k}'+\boldsymbol{k}'')\delta(-\omega_n+\omega_{n''}-\omega_{n'''})\delta(\omega_n-\omega_{n'}-\omega_{n''})],$$

which reduces the equation to the following if we sum over $\boldsymbol{k}'$, $\boldsymbol{k}''$, $\omega_{n'}$ and $\omega_{n'''}$:

$$\frac{\Delta^2}{8}\sum_{k,k''}\sum_{n,n'}\mathrm{Tr}[\sum_{\sigma,\sigma'}\frac{-\hbar\delta_{\sigma,\sigma'}}{-i\omega_n\hbar+\epsilon_{\boldsymbol{k}}-\mu-\sigma\frac{\Delta}{2}}m^a_{n-n''}(\boldsymbol{k}-\boldsymbol{k}'')\tau^a$$
$$\times\frac{-\hbar\delta_{\sigma,\sigma'}}{-i\omega_{n''}\hbar+\epsilon_{\boldsymbol{k}''}-\mu-\sigma'\frac{\Delta}{2}}m^b_{n''-n}(\boldsymbol{k}''-\boldsymbol{k})\tau^b].$$

Next, we make the integral symmetric by letting $\boldsymbol{k}\to\boldsymbol{k}+\boldsymbol{k}''$ and $\omega_n\to\omega_n+\omega_{n''}$, such that we find

$$\frac{\Delta^2}{8}\sum_{k,k''}\sum_{n,n'}\mathrm{Tr}[\frac{-\hbar\delta_{\sigma,\sigma'}}{-i\omega_{n+n''}\hbar+\epsilon_{\boldsymbol{k}+\boldsymbol{k}''}-\mu-\sigma\frac{\Delta}{2}}m^a_n(\boldsymbol{k})\tau^a$$
$$\times\frac{-\hbar\delta_{\sigma,\sigma'}}{-i\omega_{n''}\hbar+\epsilon_{\boldsymbol{k}''}-\mu-\sigma'\frac{\Delta}{2}}m^b_{-n}(-\boldsymbol{k})\tau^b].$$

We then set $\boldsymbol{k}''=\boldsymbol{q}$, $n''\to n$ and rewrite our result as

$$\sum_{n,k}\sum_{a,b\in x,y}m^a_n(\boldsymbol{k})\Pi_{a,b}(\boldsymbol{k},\omega_n)m^b_{-n}(-\boldsymbol{k}). \tag{3.16}$$

In this equation $\Pi_{a,b}$ is

$$\Pi^{a,b}=\frac{\Delta}{4}(n_+-n_-)\delta_{a,b}+\frac{\Delta^2}{8}\int\frac{d\boldsymbol{q}}{(2\pi)^3}\sum_{n'}\mathrm{Tr}[\sum_{\sigma,\sigma'}\frac{-\hbar\delta_{\sigma,\sigma'}}{-i\omega_n\hbar+\epsilon_{\boldsymbol{k}+\boldsymbol{q}}-\mu-\sigma\frac{\Delta}{2}}\tau_a\frac{-\hbar\delta_{\sigma,\sigma'}}{-i\omega_n\hbar+\epsilon_{\boldsymbol{k}}-\mu-\sigma'\frac{\Delta}{2}}\tau_b],$$

where we included the term we previously found. We also wrote:$\sum_q\to\int\frac{d\boldsymbol{q}}{(2\pi)^3}$. The next step is to compute $\Pi_{a,b}$ by splitting the fraction in the second term and performing the Matsubara sum,

such that we obtain

$$\Pi^{a,b}(\boldsymbol{k},\omega_n) = \frac{\Delta}{4}(n_+ - n_-)\delta_{a,b} + \frac{\Delta^2}{8}\sum_{\sigma,\sigma'}\tau^a_{\sigma,\sigma'}\tau^b_{\sigma',\sigma}\int\frac{d\boldsymbol{q}}{(2\pi)^3}\frac{N_{FD}(\epsilon_{\boldsymbol{q})-\boldsymbol{k}/2}-\mu-\sigma'\frac{\Delta}{2}) - N_{FD}(\epsilon_{\boldsymbol{q}+\boldsymbol{k}/2}-\mu-\sigma\frac{\Delta}{2})}{\epsilon_{\boldsymbol{q}-\boldsymbol{k}/2}-\epsilon_{\boldsymbol{q}+\boldsymbol{k}/2}+i\omega_n\hbar}], \tag{3.17}$$

where we pulled the trace over the Pauli matrices out. In this last equation we also symmetrized the integral by letting $\boldsymbol{q}\to\boldsymbol{q}-\boldsymbol{k}/2$.

3.1.3 Computing the Diagonal Elements of $\Pi^{a,b}$

In this section we calculate the Π-function, and find its matrix elements at zero temperature. As can be seen from the sum over the spin indices, $\Pi^{xx}=\Pi^{yy}$. To find the total exchange energy of the system we are interested in the terms that go as k^2, which appear in Π^{xx} and Π^{yy}. Also, from $\sum_{\sigma,\sigma'}\tau^a_{\sigma,\sigma'}\tau^b_{\sigma,\sigma'}$ we find $\sigma\neq\sigma'$ for the expression to be non-zero. Below we compute the Π^{xx} where we first sum over the six indices.

$$\Pi_{a,b}(\boldsymbol{k},\omega_n) = \frac{\Delta}{4}(n_+ - n_-)\delta_{a,b} +$$
$$\frac{\Delta^2}{8}\int\frac{d\boldsymbol{q}}{(2\pi)^3}\frac{N_{FD}(\epsilon_{\boldsymbol{q}}-\mu+\frac{\Delta}{2}) - N_{FD}(\epsilon_{\boldsymbol{q}+\boldsymbol{k}}-\mu-\frac{\Delta}{2})}{\epsilon_{\boldsymbol{q}}-\epsilon_{\boldsymbol{k}+\boldsymbol{q}}-i\omega_n\hbar+\Delta} + \frac{N_{FD}(\epsilon_{\boldsymbol{q}}-\mu-\frac{\Delta}{2}) - N_{FD}(\epsilon_{\boldsymbol{q}+\boldsymbol{k}}-\mu+\frac{\Delta}{2})}{\epsilon_{\boldsymbol{q}}-\epsilon_{\boldsymbol{k}+\boldsymbol{q}}-i\omega_n\hbar-\Delta}.$$

We take the limit where $\omega\to 0$ and $k\ll 1$, such that we are able to make the following approximation

$$\epsilon_{\boldsymbol{k}+\boldsymbol{q}} \simeq \epsilon_{\boldsymbol{q}} + \frac{\partial\epsilon_{\boldsymbol{q}}}{\partial q}\cdot\boldsymbol{k} = \epsilon_{\boldsymbol{q}} + \frac{\hbar^2}{m}\boldsymbol{q}\cdot\boldsymbol{k}. \tag{3.18}$$

Using this approximation we find for the denominator of the first term

$$\frac{1}{\epsilon_{\boldsymbol{q}}-\epsilon_{\boldsymbol{k}+\boldsymbol{q}}+\Delta} = \frac{1}{\Delta(1+\frac{\hbar^2}{m\Delta}\boldsymbol{q}\cdot\boldsymbol{k})} = \frac{1}{\Delta}(1-\frac{\hbar^2}{m\Delta}\boldsymbol{q}\cdot\boldsymbol{k}). \tag{3.19}$$

Next, we continue the computation at zero temperature, such that we expand the Fermi distribution as follows

$$N_{FD}(\epsilon_{\boldsymbol{q}+\boldsymbol{k}}-\mu\pm\frac{\Delta}{2}) \simeq N_{FD}(\epsilon_{\boldsymbol{q}}-\mu\pm\frac{\Delta}{2}) + \frac{\hbar^2}{m}\boldsymbol{k}\cdot\boldsymbol{q}\frac{\partial N_{FD}(\epsilon_{\boldsymbol{q}+\boldsymbol{k}}-\mu\pm\frac{\Delta}{2})}{\partial\epsilon}. \tag{3.20}$$

Combining these results we find[2]

$$\frac{\Delta^2}{8}\int\frac{d\boldsymbol{q}}{(2\pi)^2}\left[N_{FD}(\epsilon_q-\mu+\frac{\Delta}{2}) - N_{FD}(\epsilon_q-\mu-\frac{\Delta}{2}) + \frac{\hbar^2}{m}\frac{\partial}{\partial\epsilon}N_{FD}(\epsilon_q-\mu-\frac{\Delta}{2})\boldsymbol{q}\cdot\boldsymbol{k}\right]\frac{1}{\Delta}(1-\frac{\hbar^2}{m\Delta}\boldsymbol{q}\cdot\boldsymbol{k})$$
$$+\left[N_{FD}(\epsilon_q-\mu-\frac{\Delta}{2}) - N_{FD}(\epsilon_q-\mu+\frac{\Delta}{2}) + \frac{\hbar^2}{m}\frac{\partial}{\partial\epsilon}N_{FD}(\epsilon_q-\mu+\frac{\Delta}{2})\boldsymbol{q}\cdot\boldsymbol{k}\right]\frac{-1}{\Delta}(1+\frac{\hbar^2}{m\Delta}\boldsymbol{q}\cdot\boldsymbol{k}).$$

[2] I choose a two dimensional integral here, because eventually we want to compare this result with a previous result which also is obtained in two dimensions.

Note that the integral linear in $\boldsymbol{k}\cdot\boldsymbol{q}$ is anti-symmetric. We thus take terms of zeroth order and quadratic order in $\boldsymbol{k}\cdot\boldsymbol{q}$,

$$\frac{\Delta^2}{8}\int\frac{d\boldsymbol{q}}{(2\pi)^2}\left[\frac{N_{FD}(\epsilon_q-\mu+\frac{\Delta}{2})-N_{FD}(\epsilon_q-\mu-\frac{\Delta}{2})}{\Delta}+\frac{\hbar^4}{m^2\Delta^2}\frac{\partial}{\partial\epsilon}N_{FD}(\epsilon_q-\mu-\frac{\Delta}{2})(\boldsymbol{q}\cdot\boldsymbol{k})^2\right]$$
$$-\left[\frac{N_{FD}(\epsilon_q-\mu+\frac{\Delta}{2})+N_{FD}(\epsilon_q-\mu-\frac{\Delta}{2})}{\Delta}+\frac{\hbar^4}{m^2\Delta^2}\frac{\partial}{\partial\epsilon}N_{FD}(\epsilon_q-\mu+\frac{\Delta}{2})(\boldsymbol{q}\cdot\boldsymbol{k})^2\right].$$

Recall the term coming from $Tr[G_0\Sigma]$: $\frac{\Delta}{4}(n_+-n_-)\delta_{a,b}$. This term exactly cancels against the two Fermi Dirac distributions without a derivative to the energy on them. This leaves us with the following

$$\frac{\Delta^2}{8}\frac{\hbar^4}{m^2\Delta^2}\int\frac{d\boldsymbol{q}}{(2\pi)^2}(\boldsymbol{k}\cdot\boldsymbol{q})\left[\frac{\partial N_{FD}(\epsilon_{\boldsymbol{q}}-\mu+\frac{\Delta}{2})}{\partial\epsilon}+\frac{\partial N_{FD}(\epsilon_{\boldsymbol{q}}-\mu-\frac{\Delta}{2})}{\partial\epsilon}\right]. \tag{3.21}$$

At zero temperature the derivative of the Fermi distribution is peaked at the chemical potential such that we have

$$\frac{\partial N_{FD}(\epsilon_{\boldsymbol{q}+\boldsymbol{k}}-\mu\pm\frac{\Delta}{2})}{\partial\epsilon}\simeq-\delta(\epsilon_{\boldsymbol{q}}-\mu\pm\frac{\Delta}{2}). \tag{3.22}$$

Plugging this result in our expression, going to cylindrical coordinates and noting $\boldsymbol{k}\cdot\boldsymbol{q}=\cos(\theta)kq$, we end up with

$$\frac{\Delta^2}{8}\frac{\hbar^4k^2}{m^2\Delta^2}\int\frac{dq}{(2\pi)^2}\int_0^{2\pi}d\theta q^3\cos^2(\theta)[-\delta(\epsilon_{\boldsymbol{q}}-\mu+\frac{\Delta}{2})-\delta(\epsilon_{\boldsymbol{q}}-\mu-\frac{\Delta}{2}]. \tag{3.23}$$

We rewrite the delta functions using:

$$\delta(g(x))=\sum_i\frac{\delta(x-x_i)}{|g'(x_i)|}, \tag{3.24}$$

where x_i are the roots of g. For example,

$$\delta(\epsilon_q-\mu+\frac{\Delta}{2})=\frac{1}{\frac{\hbar^2}{m}\sqrt{\frac{2m}{\hbar^2}(\mu-\frac{\Delta}{2})}}\delta(q+\sqrt{\frac{2m}{\hbar^2}(\mu+\frac{\Delta}{2})})+\frac{1}{\frac{\hbar^2}{m}\sqrt{\frac{2m}{\hbar^2}(\mu-\frac{\Delta}{2})}}\delta(q-\sqrt{\frac{2m}{\hbar^2}(\mu+\frac{\Delta}{2})}). \tag{3.25}$$

Using these expressions, we perform the integral and find:

$$\Pi^{xx}=\frac{-\mu k^2}{4\pi}=\frac{-\epsilon_F k^2}{4\pi}=\Pi^{yy}. \tag{3.26}$$

Where at low temperature the chemical potential equals the Fermi energy. We simply read of the total exchange energy of this system. The k^2 term becomes a ∇^2 if we would transform back to real space. The energy term then corresponds to the micro magnetic exchange energy and is:

$$A=\frac{\epsilon_F}{2\pi}. \tag{3.27}$$

In the next section we try to obtain the same result, but then we use an integration of all one-particle energies over the Fermi sea.

3.2 Computing the Total Energy for $\alpha_R = 0$ by Integrating Over the Fermi Sea

This is a model for non-interacting electrons in a helical exchange field. The single particle hamiltonian is given by

$$\mathcal{H} = -\frac{\hbar^2\nabla^2}{2m} - \frac{\Delta}{2}\boldsymbol{m}(x)\cdot\boldsymbol{\tau}. \tag{3.28}$$

In this expression $\boldsymbol{m}(x) = \sin(qx)\hat{x} + \cos(qx)\hat{z}$ and we take the exchange constant $\Delta > 0$. We compute the eigenfunctions and eigenvalues using the same procedure used by Miguel Calvo in [28].

3.2.1 Eigenvectors and Eigenvalues of the Helimagnet

The equation we solve is

$$H\psi(\boldsymbol{x}) = E\psi(\boldsymbol{x}) \to \left(-\frac{\hbar^2\nabla^2}{2m} - \frac{\Delta}{2}(\sin(xq)\tau_x + \cos(xq)\tau_z)\right)\psi(\boldsymbol{x}) = E\psi(\boldsymbol{x}). \tag{3.29}$$

Notice that the hamiltonian does not depend on y nor z, thus we are allowed to write

$$\psi(\boldsymbol{x}) = \phi(x)e^{i(k_y y + k_z z)}. \tag{3.30}$$

Subsequently, we plug the wave ansatz in equation (3.29), to find

$$(E - \frac{\hbar^2\boldsymbol{k}^2}{2m})\phi(x) = \left(-\frac{\hbar^2}{2m}\frac{d^2}{dx^2} - \frac{\Delta}{2}(\sin(xq)\tau^x + \cos(xq)\tau^z)\right)\phi(x). \tag{3.31}$$

Where in the last expression $\boldsymbol{k} = (0, k_y, k_z)$. Next, we rewrite the equation such that we have

$$\epsilon\phi(x) = \left(-\frac{d^2}{dx^2} + A(\sin(xq)\tau^x + \cos(xq)\tau^z\right)\phi(x), \tag{3.32}$$

where $\epsilon = \frac{2m}{\hbar^2}(E - \frac{\hbar^2}{2m}\boldsymbol{k}^2)$ and $A = -\frac{2m}{\hbar^2}\frac{\Delta}{2}$. We then apply a linear unitary transformation to the rotating frame: $\phi(x) = Re^{-i\tau^y q\frac{x}{2}}\hat{\phi}(x)$. It is important to note the following equalities. We split up the sum in even and odd terms to retrieve sine and cosine functions.

$$e^{-iq\tau_x x/2} = \sum_{l=0}^{\infty}\frac{1}{(2l)!}(-iqx/2)^{2l}\mathbb{I} + \sum_{l=0}^{\infty}\frac{1}{2l+1}(-iqx/2)^{2l+1}\tau_y = \cos(qx/2)\mathbb{I} - i\sin(qx/2)\tau_y. \tag{3.33}$$

We then plug our linear transformation in (3.32) such that we find

$$\epsilon\hat{\phi}(x) = \left[-\frac{d^2}{dx^2} + (\frac{q}{2})^2 + iq\frac{d}{dx} + A(\tau^z)\right]\hat{\phi}(x). \tag{3.34}$$

The last term in this expression comes from the following computation, using the decomposition in sine and cosine functions of the unitary transformation

$$e^{-i\tau_y q\frac{y}{2}}[\sin(qx)\tau_x + \cos(qx)\tau_z]e^{-i\tau_y q\frac{y}{2}} = \tag{3.35}$$

$$= (\cos(q\frac{x}{2})\mathbb{I} + i\sin(q\frac{x}{2})\tau_y)[\sin(qx)\tau_x + \cos(qx)\tau_z](\cos(q\frac{x}{2})\mathbb{I} - i\sin(q\frac{x}{2})\tau_y)$$

$$= \tau_z.$$

Since $\frac{d}{dx}$ commutes with $iq\frac{d}{dx}$, we decompose the eigenfunction as follows,

$$\hat{\phi}(x) = e^{ik_x x}\chi(k_x). \tag{3.36}$$

Here, $\chi(k_x)$ is a undetermined spinor. Plugging this decomposition into eq. (3.34), we find

$$\epsilon\chi(k_x) = \left[k_x^2 + (\frac{q}{2})^2 - qk_x\tau_y + A\tau_z\right]\chi(k)x). \tag{3.37}$$

We are now able to compute the eigenvalues and eigenvectors of the previous equation. The eigenvalues, or one-particle-energies, are

$$\epsilon_\pm = \left[k_x^2 + (\frac{q}{2})^2 \pm \sqrt{(qk_x)^2 + A^2}\right]. \tag{3.38}$$

Or, after plugging in our definitions for A and ϵ we find

$$E_\pm = \frac{\hbar^2}{2m}\left[k_x^2 + k_y^2 + k_z^2 + (\frac{q}{2})^2 \pm \sqrt{(qk_x)^2 + (\frac{m\Delta}{\hbar^2})^2}\right]. \tag{3.39}$$

The eigenvectors $\chi(p)$ for eq. (3.37) are

$$\chi(p)_\pm = e^{-i\tau_x\frac{\theta_{k_x}}{2}}\eta_\pm, \tag{3.40}$$

where $\eta_\pm = \begin{pmatrix}1\\0\end{pmatrix}, \begin{pmatrix}0\\1\end{pmatrix}$, the eigenvectors of τ_z. The angle θ_{k_x} is given by

$$\theta_{k_x} = 2\arctan\frac{(\frac{m\Delta}{\hbar^2}) + \sqrt{k_x^2q^2 + (\frac{m\Delta}{\hbar^2})^2}}{(k_xq)}. \tag{3.41}$$

In conclusion, we combine everything to find for the wave function of our model for $\alpha_R = 0$

$$\psi_{\boldsymbol{k},\pm}(\boldsymbol{x}) = \frac{1}{\sqrt{V}}e^{i\boldsymbol{k}\cdot\boldsymbol{x}}e^{-iqx\frac{\tau^y}{2}}e^{-i\theta_{k_x}\frac{\tau^x}{2}}\eta_\pm, \tag{3.42}$$

To be complete, the dimensions of $q = [\frac{1}{m}]$ and $\Delta = [J]$, this will be useful when we check the dimension of the final expression. In the figures below the one-particle energies are plotted.

3.2.2 Computation of the Total Energy

Now we have found the one particle energy of the system for $\alpha_R = 0$, we are able to compute the energy of the system as follows

$$E[q]_{tot} = \sum_k N_{FD}(\epsilon_F - \epsilon_{\boldsymbol{k},\pm})\epsilon_{\boldsymbol{k},\pm}. \tag{3.43}$$

The procedure to compute the total energy goes as follows. First, we rewrite the sum over k to an integral over k and go to cylindrical coordinates. This amounts to $\sum_{\boldsymbol{k}} \to \int S\frac{d\boldsymbol{k}}{(2\pi)^2} \to \int_0^{2\pi}\frac{d\phi}{(2\pi)^2}\int dk\, k$. In this last expression S is the surface.

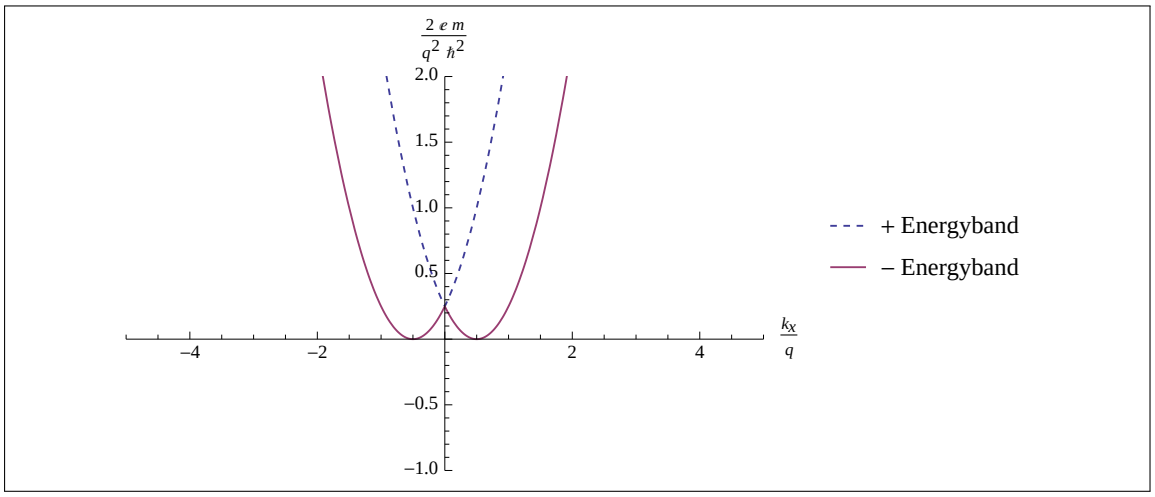

Figure 3.1: Energy Bands for $\frac{m\Delta}{q^2\hbar^2} = 0.0$. We still see a separation between both states but it actually is the same state, with the same minimum. The dispersion comes from the fact that k is not the physical momentum, since we made the expression dimensionless by using $k \to kq$.

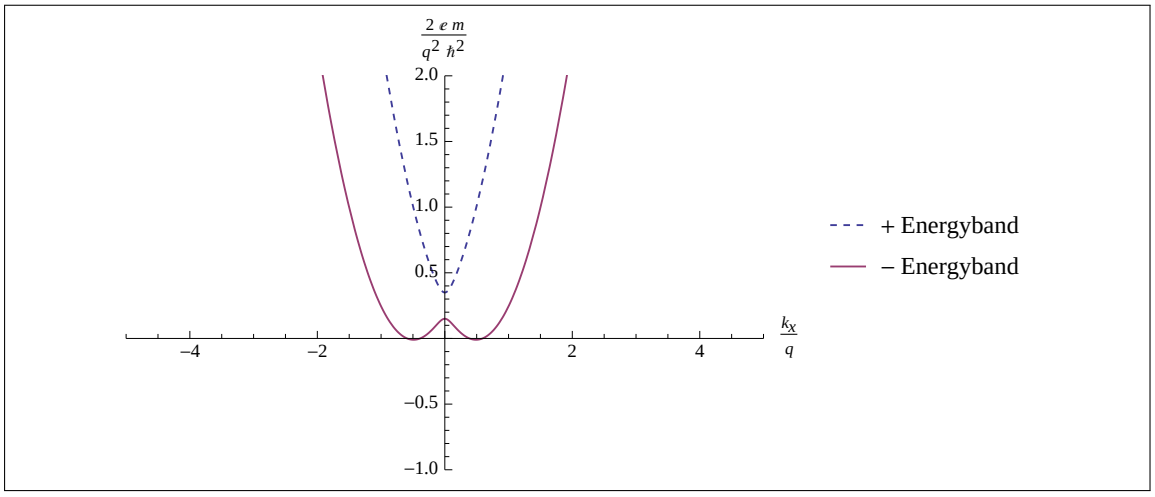

Figure 3.2: Energy Bands for $\frac{m\Delta}{q^2\hbar^2} = 0.1$. There is a gap appearing between the two energy bands.

We then perform the k-integral from 0 to k_{F+}, where k_{F+} is computed from the distribution function taken at zero temperature. Moreover, all computations in this chapter are taken at zero temperature. Subsequently, we perform the integral over the angle ϕ and make a series expansion in q of the resulting expression. We then expect to find a zero order term and a quadratic term, because of the vector structure in the phenomenological model.

The one particle energy depends on k_x, which we rewrite this as $k_x = k\cos(\phi)$ using cylindrical coordinates. Also, the temperature is set to zero, such that the distribution function becomes a Θ-function. As aforementioned, from the distribution function, $\Theta(\epsilon_F - \epsilon_{k,\pm})$, we find the different values of k_F we use as our integration boundaries. Depending on where we put our chemical potential, we use different boundaries 3.4.

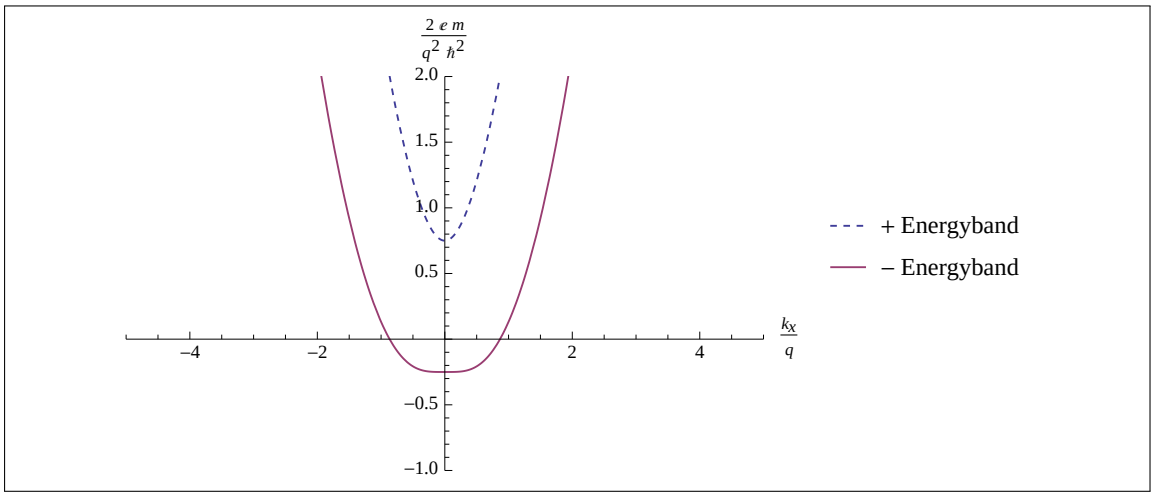

Figure 3.3: Energy Bands for $\frac{m\Delta}{q^2\hbar^2} = 0.5$. The gap increases between the energy bands.

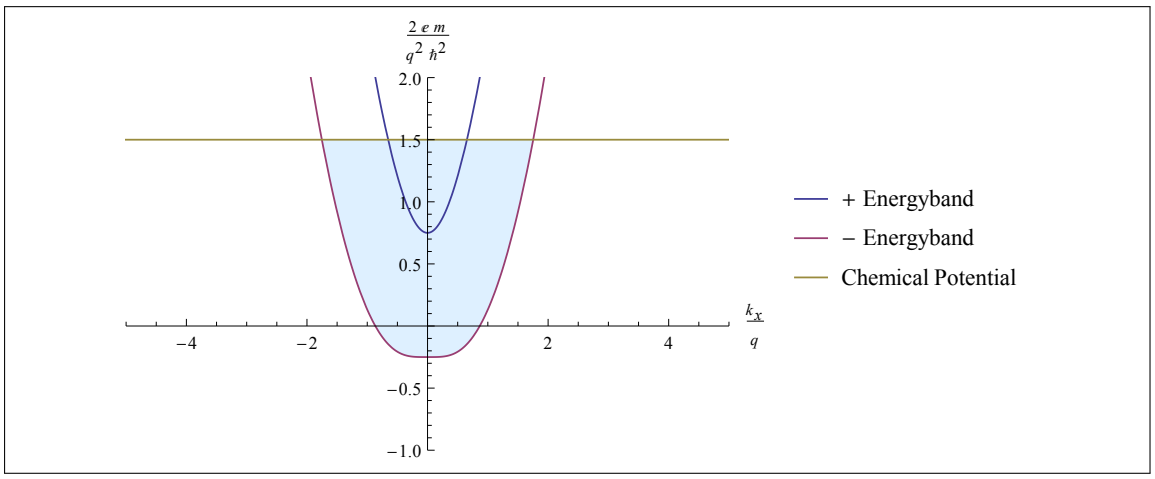

Figure 3.4: This picture shows the chemical potential, placed at a positive point, intersecting both energy bands. We fill the bands to the chemical potential, hence the coloring, and then compute the total energy.

The total energy equation then is given by

$$E[q]_{tot} = \sum_{\delta\in[\pm]} \frac{S}{(2\pi)^2} \int_0^{2\pi} d\phi \int_0^{k_{F,\delta}} dk\, k\, \epsilon_{\boldsymbol{k},\delta}. \tag{3.44}$$

We compute the total energy for both spins ($\pm$) and add them at the end

$$E[q]_{tot} = \sum_{\delta\in[\pm]} \frac{S}{(2\pi)^2} \int_0^{2\pi} d\phi \int_0^{k_F,\delta} dkk \frac{\hbar^2}{2m} \left[k^2 + (\frac{q}{2})^2 + \delta\sqrt{(kq\cos\phi)^2 + (\frac{m\Delta}{\hbar^2})^2} \right] \tag{3.45}$$

.

From the Θ-function we find

$$\Theta(\epsilon_F - \epsilon_k) = \begin{cases} 1, & \text{if } \epsilon_k < \epsilon_F \\ 0, & \text{if } \epsilon_k > \epsilon_F \end{cases}$$

We then set up the following equation,

$$\epsilon_F = \frac{\hbar^2}{2m}[k_F^2 + (\frac{q}{2})^2 \pm \sqrt{(k_F q\cos\phi)^2 + (\frac{m\Delta}{\hbar^2})^2}, \tag{3.46}$$

such that we find four solutions for k_F. We find four solutions because we have not specified the values of the various parameters. We have to choose what our upper boundary is, such that we are able to perform the integral (3.45).

The next few steps are trivial and thus expressions are not written out. We plug in our result for k_F, and make a series expansion in q. We do this for both spins and combine the result to find the total energy

$$E[q]_{tot} = \frac{Sq^2\epsilon_F}{2\pi}, \tag{3.47}$$

such that,

$$A = \frac{\epsilon_F}{2\pi}. \tag{3.48}$$

It is worth mentioning that we only find a zeroth order term and a quadratic term, this therefore confirms the vector structure of the phenomenological model. Also, looking at the dimension of the expression, we find $[m^2][\frac{1}{m^2}][J] \to [J]$, which is what we aimed for.

3.3 Computing the Total Energy for $\alpha_R \ll 1$ Using Perturbation Theory

The Rashba model is a two dimensional model that induces the splitting of energy bands, as shown in figures (3.5 and 3.6). When the spin-orbit coupling vanishes we retrieve the energy band of the free particle (3.5). This model is based on the hamiltonian given by

$$\mathcal{H} = \frac{p_x^2 + p_y^2}{2m} - \frac{\alpha_R}{\hbar}(\boldsymbol{\tau}\times\boldsymbol{p})\cdot\hat{z} = \begin{pmatrix} \frac{\hbar^2}{2m}(k_x^2+k_y^2) & \alpha_R(k_y + ik_x) \\ \alpha_R(k_y - ik_x) & \frac{\hbar^2}{2m}(k_x^2+k_y^2) \end{pmatrix}. \tag{3.49}$$

Here, α_R is the Rashba coupling, $\boldsymbol{p}$ is the momentum and $\boldsymbol{\tau}$ is the Pauli matrix vector. The solutions to the equation $\mathcal{H}|\psi\rangle = E_0|\psi\rangle$ are in this case known to be

$$\psi_\delta(\boldsymbol{k}) = \frac{1}{\sqrt{2V}} e^{i\boldsymbol{x}\cdot\boldsymbol{k}} \begin{pmatrix} 1 \\ -\delta i e^{i\theta_{\boldsymbol{k}}} \end{pmatrix}, \tag{3.50}$$

as the eigenfunctions, where $\delta \in [+,-]$ and $\theta_{\boldsymbol{k}} = \tan^{-1}(\frac{k_x}{k_y})$. The eigenvalues, or one particle energies are given by

$$E_\delta(\boldsymbol{k}) = \frac{\hbar^2 k^2}{2m} + \delta\alpha_R\boldsymbol{k}. \tag{3.51}$$

The dimension of $\alpha_R = [\frac{kg\cdot m^3}{s^2}]$.

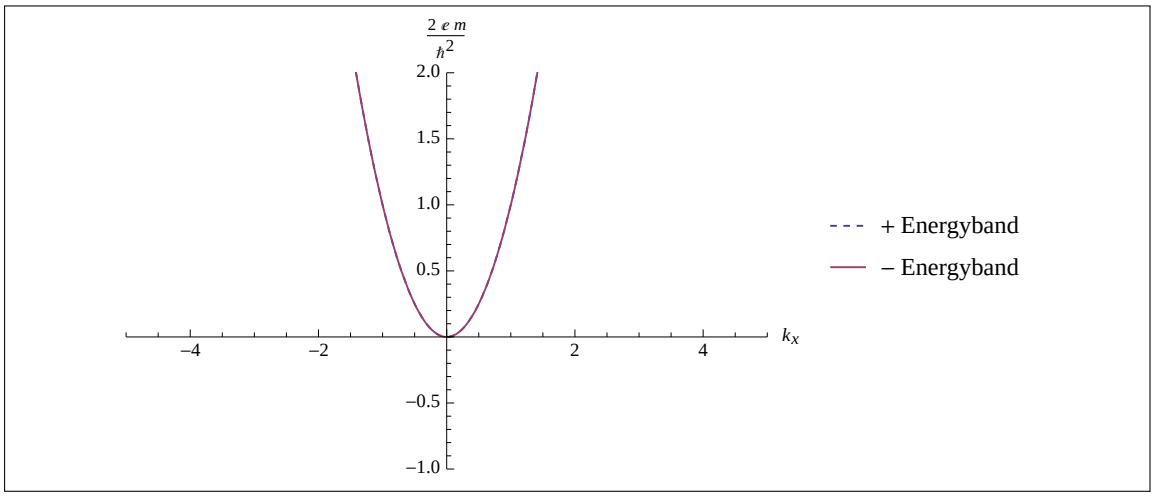

Figure 3.5: Energy Bands for $\frac{2m\alpha_R}{\hbar^2} = 0.0$. For $\alpha_R = 0$ we retrieve the free particle dispersion.

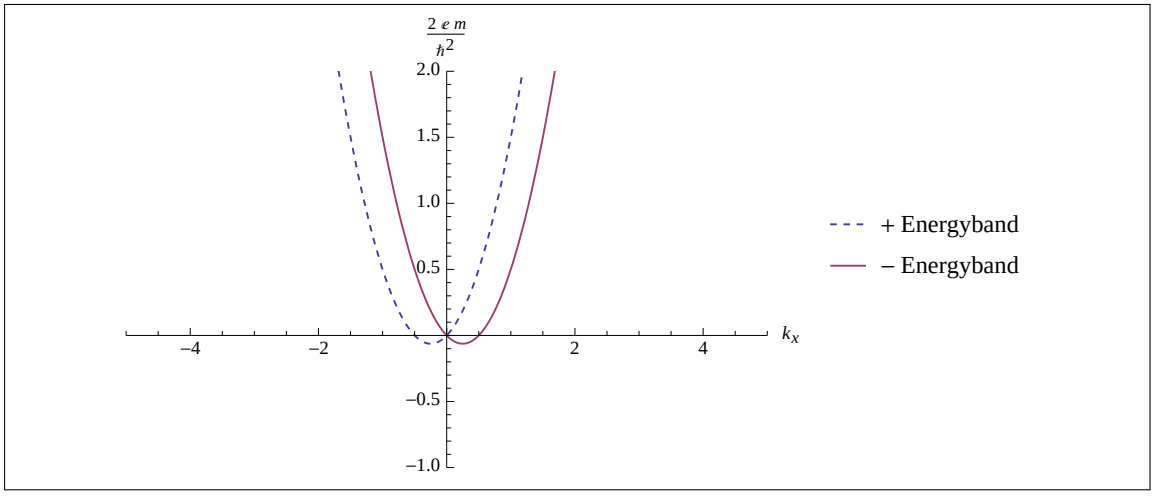

Figure 3.6: Energy Bands for $\frac{2m\alpha_R}{\hbar^2} = 0.5$. A splitting of energy bands occurs here.

3.3.1 Perturbation Theory

In this section we apply perturbation theory to our model for $\alpha_R \ll 1$, to compute D. The set-up is as follows

$$\mathcal{H} = H_0 + V, \tag{3.52}$$

where H_0 is the part of the Hamiltonian that can be solved exact and V is the perturbation.

$$H_0 = -\frac{\hbar^2\nabla^2}{2m} - \frac{\Delta}{2}\boldsymbol{m}(x)\cdot\boldsymbol{\tau}, \tag{3.53}$$

and the perturbation is

$$V = -\frac{\alpha_R}{\hbar}(\boldsymbol{\tau}\times\boldsymbol{p})\cdot\hat{z}. \tag{3.54}$$

In Section 3.2 we already computed the eigenvalues and eigenfunctions corresponding to H_0. Recall, the eigenfunctions are

$$\psi_{\boldsymbol{k},\pm}(\boldsymbol{x}) = \frac{1}{\sqrt{V}} e^{i\boldsymbol{k}\cdot\boldsymbol{x}} e^{-iqx\frac{\tau^y}{2}} e^{-i\theta_{k_x}\frac{\tau^x}{2}} \eta_{\pm}, \tag{3.55}$$

where $\eta_{\pm} = \begin{pmatrix} 1 \\ 0 \end{pmatrix}, \begin{pmatrix} 0 \\ 1 \end{pmatrix}$. The angle θ_{k_x} is given by

$$\theta_{k_x} = 2\arctan \frac{(\frac{m\Delta}{\hbar^2}) + \sqrt{k_x^2 q^2 + (\frac{m\Delta}{\hbar^2})^2}}{(k_x q)}. \tag{3.56}$$

The eigenvalues are

$$\epsilon_{\boldsymbol{k},\pm} = \frac{\hbar^2}{2m}\left[\boldsymbol{k}^2 + (\frac{q}{2})^2 \pm \sqrt{(k_x q)^2 + (\frac{m\Delta}{\hbar^2})^2}\right]. \tag{3.57}$$

Perturbing the energy then gives

$$E_{\pm}(\boldsymbol{k}) \approx E^0_{\pm}(\boldsymbol{k}) + \langle\psi^0_{\pm}(\boldsymbol{k})|\, V\, |\psi^0_{\pm}(\boldsymbol{k})\rangle + \sum_k \frac{|\,\langle\psi^0_{\pm}(\boldsymbol{k})|\, V\, |\psi^0_{\pm}(\boldsymbol{n})\rangle\,|^2}{E^0_{\pm}(\boldsymbol{n}) - E^0_{\pm}(\boldsymbol{k})} + \text{higher order}. \tag{3.58}$$

The zero in the superscript refers to the energy or eigenfunctions of the unperturbed hamiltonian. The second term is computed as follows, as shown below for spin +.

$$\langle\psi^0_{+}(\boldsymbol{k})|\, V\, |\psi^0_{+}(\boldsymbol{k})\rangle = \int d\boldsymbol{x}\, \frac{1}{V}(1,0) e^{i\theta_k\tau_x/2} e^{iqx\tau_y/2} e^{-i\boldsymbol{k}\boldsymbol{x}} \frac{\alpha_R}{\hbar}(\tau_x p_y - \tau_y p_x) e^{i\boldsymbol{k}\boldsymbol{x}} e^{-iqx\tau_y/2} e^{-i\theta_k\tau_x/2} \begin{pmatrix} 1 \\ 0 \end{pmatrix}. \tag{3.59}$$

Writing $p_i = -i\hbar\frac{\partial}{\partial x_i}$, we find

$$\langle\psi^0_{+}(\boldsymbol{k})|\, V\, |\psi^0_{+}(\boldsymbol{k})\rangle = \int d\boldsymbol{x}\, \frac{1}{V}(1,0) e^{i\theta_k\tau_x/2} e^{iqx\tau_y/2} e^{-i\boldsymbol{k}\boldsymbol{x}} \alpha_R(\tau_x k_y - \tau_y k_x + \frac{q}{2}\mathbb{I}) e^{i\boldsymbol{k}\boldsymbol{x}} e^{-iqx\tau_y/2} e^{-i\theta_k\tau_x/2} \begin{pmatrix} 1 \\ 0 \end{pmatrix}. \tag{3.60}$$

Using the same decomposition of the exponents of Pauli matrices used before, we are able to compute the various matrix multiplications.

$$\begin{aligned}\langle\psi^0_{+}(\boldsymbol{k})|\, V\, |\psi^0_{+}(\boldsymbol{k})\rangle = \alpha_R \int d\boldsymbol{x}\, \frac{1}{V}(1,0)(\cos(\theta_k/2)\mathbb{I} - i\sin(\theta_k)\tau_x)(\cos(qx/2)\mathbb{I} - i\sin(qx/2)\tau_y) \\ \times(\tau_x k_y - \tau_y k_x + \frac{q}{2}\mathbb{I})(\cos(qx/2)\mathbb{I} + i\sin(qx/2)\tau_y)(\cos(\theta_k/2)\mathbb{I} + i\sin(\theta_k)\tau_x) \begin{pmatrix} 1 \\ 0 \end{pmatrix}.\end{aligned}$$

After writing out all the matrix multiplications, we find as first order in perturbation theory,

$$\alpha_R \int d\boldsymbol{x} \frac{1}{V}\left(k_x \sin(\theta_k) k_y \cos(\theta_k)\sin(qx) + \frac{q}{2}\right). \tag{3.61}$$

The integration over $\sin(qx)$ gives zero, such that

$$E^1_{\pm}(\boldsymbol{k}) = (\frac{q}{2} \pm k_x \sin(\theta_k))\alpha_R, \tag{3.62}$$

Using this result we find our perturbed energy to be

$$\epsilon_{\boldsymbol{k},\pm} = \frac{\hbar^2}{2m}\left[\boldsymbol{k}^2 + (\frac{q}{2})^2 + \pm\sqrt{k_z q + (\frac{m\Delta}{\hbar^2})^2}\right] + (\frac{q}{2} \pm \sin(\theta_k))\alpha_R. \tag{3.63}$$

The one-particle perturbed energies are plotted in the figure below.

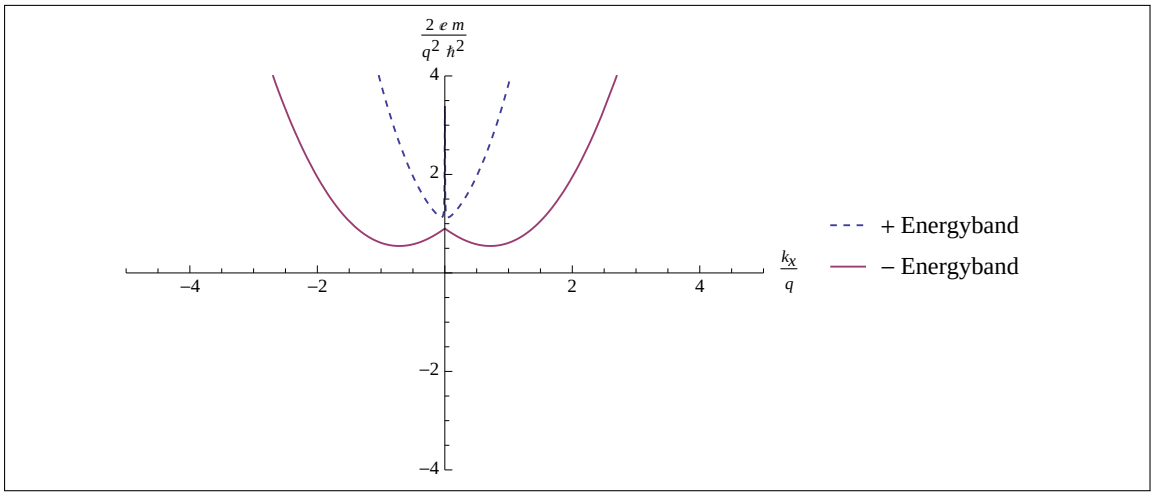

Figure 3.7: Energy Bands of the perturbed helimagnet for $\frac{m\Delta}{q^2\hbar^3} = 0.05$, $\frac{m\alpha_R}{\hbar^3 q^2} = 0.7$. We see both a gap, due to the helical exchange field, as well as splitting of the energy bands, due to the spin-orbit coupling.

3.3.2 Computation of the Total Energy of the Perturbed Model

Now that we have found the perturbed one-particle energy, we again want to compute the total energy.

$$E[q]_{tot} = \sum_k N_{FD}(\epsilon_F - (\epsilon^0_{\boldsymbol{k},\pm} + \epsilon^1_{\boldsymbol{k},\pm}))(\epsilon^0_{\boldsymbol{k},\pm} + \epsilon^1_{\boldsymbol{k},\pm}). \tag{3.64}$$

However, we discard terms of quadratic and higher order in α_R. We follow the same procedure as before, we begin by turning the sum into a two dimensional integral, perform the k-integral, and use the k_F found from the Θ-function as boundaries. Subsequently, we make a series expansion, up to linear order in q, and lastly, perform the integral over the angle. Below is the computation for spin $+$, the computation for spin $-$ is similar.

$$E[q]_{tot} = \frac{S}{(2\pi)^2}\int_0^{2\pi} d\phi \int_0^{k_F} dk k \left(\frac{\hbar^2}{2m}[k^2 + (\frac{q}{2})^2 + \sqrt{(kq\cos\phi)^2 + (\frac{m\Delta}{\hbar^2})^2}] + \alpha_R(\frac{q}{2} + k\cos(\phi)\sin(\theta_k)\right). \tag{3.65}$$

The boundaries of the integral are chosen to go from 0 to a k_F, the same as in the previous model. The first part of the integral we already computed, and we found no linear order in q.

First, we compute the part that goes linear in q, which is easy, because it has no extra dependence on k

$$\frac{S}{(2\pi)^2}\int_0^{2\pi} d\phi \int_0^{k_F} dk k \alpha_R \frac{q}{2} = \frac{S}{2\pi}\frac{q}{4}(k^2_{F+} + k^2_{F-}). \tag{3.66}$$

Plugging both $k_{F,\pm}$ we obtain

$$\frac{S\Delta m\alpha_R q}{4\pi\hbar^2}, \tag{3.67}$$

which dimensionally goes as $[J]$. We then consider the second part of perturbation and write out the full expression of the angle θ_k[3], such that we have

$$\begin{aligned} E[q]_{tot} &= \frac{S}{(2\pi)^2}\int_0^{2\pi} d\phi \int_0^{k_F} dk k(\alpha_R k\cos(\phi)\sin(\theta_k)) \\ &= \frac{S}{(2\pi)^2}\int_0^{2\pi} d\phi \int_0^{k_F} dk k(\alpha_R k\cos(\phi))2\left(\frac{\frac{\frac{m\Delta}{\hbar^2}+\sqrt{k^2\cos(\phi)^2q^2+(\frac{m\Delta}{\hbar^2})^2}}{k\cos(\phi)q}}{1+(\frac{\frac{m\Delta}{\hbar^2}+\sqrt{k^2\cos(\phi)^2q^2+(\frac{m\Delta}{\hbar^2})^2}}{k\cos(\phi)q})^2}\right). \end{aligned}$$

We then name $\frac{m\Delta}{\hbar^2\cos(\phi)q} = w$, and rewrite the integral to make the computation more comprehensible. We have

$$\begin{aligned} E[q]_{tot} &= \frac{S}{(2\pi)^2}\int_0^{2\pi} d\phi \int_0^{k_F} dk k(2\alpha_R k\cos(\phi)\left(\frac{\frac{w+\sqrt{k^2+w^2}}{k}}{1+(\frac{w+\sqrt{k^2+w^2}}{k})^2}\right) \\ &= \frac{S}{(2\pi)^2}\int_0^{2\pi} d\phi \int_0^{k_F} dk 2\alpha_R k^3\cos(\phi)\left(\frac{w+\sqrt{k^2+w^2}}{k^2+(w+\sqrt{k^2+w^2})^2}\right). \end{aligned}$$

After computing this integral the next steps are trivial. We make a series expansion up to linear order in q and perform the integral over the angle ϕ and add the result of both spin + and spin −, such that we find

$$E[q]_{tot} = \frac{\epsilon_F m q S\alpha_R}{2\pi\hbar^2}. \tag{3.68}$$

The last step to find the total energy of the perturbed system for $\alpha_R \ll 1$ is to add the contribution of $\alpha_R\frac{q}{2}$ we found before. This results in

$$E[q]_{tot} = \frac{\epsilon_F m q S\alpha_R}{2\pi\hbar^2} + \frac{mS\alpha\Delta}{4\pi\hbar^2}. \tag{3.69}$$

The dimension of this last expression is again that of Joule. Now we are able to compute the ratio between D and A.

$$\frac{D}{A} = \frac{m\alpha_R}{\hbar^2} + \frac{m\alpha_R\Delta}{2\epsilon_F\hbar^2}. \tag{3.70}$$

The first term is in perfect agreement with [5], and the second term is a remnant of our computational method. By setting a limit of $\frac{\Delta}{\epsilon_F}$ to zero, we find the original expression represented in the paper. This limit is justified by experimental data where $\Delta \ll \epsilon_F$.

3.3.3 The One Dimensional Result

We have just reproduced the behavior of the DM interaction for small spin orbit couplings in two dimensions. In the next section we use numerical methods to compute the DM interaction

[3]Using the fact that $\sin(2\arctan(x)) = \frac{2x}{1+x^2}$.

for small and large spin orbit couplings, however that computation is done in 1 dimension. So, in order to compare results between the numerical computation and the analytical one, we need to give the behavior of the DM interaction in 1 dimension. We just need to solve the following integrals in 1 dimension and take the limit of $\frac{\Delta}{\epsilon_F} \to 0$. We have the two integrals again:

$$E[q]_{tot} = \sum_{\delta\in[\pm]} \frac{L}{(2\pi)} \int_0^{k_F,\delta} dk k \frac{\hbar^2}{2m} \left[k^2 + (\frac{q}{2})^2 + \delta\sqrt{(kq\cos\phi)^2 + (\frac{m\Delta}{\hbar^2})^2} \right], \tag{3.71}$$

and,

$$E[q]_{tot} = \frac{L}{(2\pi)} \int_0^{k_F} dk \left(\alpha_R (\frac{q}{2} + k\cos(\phi)\sin(\theta_k)) \right). \tag{3.72}$$

Such that the DMI in 1 dimension becomes:

$$\frac{D}{A} = \frac{32}{29} \frac{m\alpha_R}{\hbar^2}. \tag{3.73}$$

We conclude that the behavior of the DM interaction is the same in both 1 dimension as 2 dimensions, except for an additional pre-factor in the one-dimensional case.

Chapter 4

Numerical Computation of the DM interaction

In the previous chapter we reproduced the result of [5], the DM interaction for small Rashba coupling. In this chapter, however, we compute the DM interaction for $\alpha_R \neq 0$, up to any order. First, the discretization method is explained and validated by comparing the analytical results of the free particle and the Rashba model to our numerical results. Subsequently, we introduce Bloch's theorem, look at the model for $\alpha_R = 0$, find the total energy of this system and see if it corresponds to our analytical result. The next step is set $\alpha_R \neq 0$ and again compute the total energy. Using these results we can find the DM interaction as a function of the Rashba coupling.

4.1 Discretization Method

The goal is to solve the Schrödinger equation, $\mathcal{H}\psi(\boldsymbol{x}) = \epsilon\psi(\boldsymbol{x})$. The way we proceed is to turn the differential equation into a matrix equation. However, before going into the procedure of solving the Schrödinger equation we discretize the Hamiltonian of the free particle and the Rashba model and see if their energy spectrum corresponds to the analytical computation.

4.1.1 The Free Particle

The one-dimensional free particle hamiltonian is given by

$$\mathcal{H} = -\frac{\hbar^2\nabla^2}{2m}. \tag{4.1}$$

If we want to discretize this equation, we proceed as follows:

1. $x = n \cdot a$, where n runs from $-N, N+1, ..., N$ and a is the discretization step.
2. $\psi(\boldsymbol{x}) = \psi(\boldsymbol{x_n}) = \psi_n$.

3. Turning differentials into difference equations, e.g. $\nabla^2\psi_n = \frac{\psi_{n+1}+\psi_{n-1}-2\psi_n}{a^2}$, note that this difference equation is symmetric in order to keep the Hamiltonian hermitian.

4. We add periodic boundary conditions: $\psi_{N+1} = \psi_{-N}$.

Using these steps to discretize the Hamiltonian and wave functions of a free particle, we end up with the following Schrödinger equation

$$\mathcal{H}_{free}\psi_n = \frac{\hbar^2}{2ma^2}(2\psi_n - (\psi_{n+1} + \psi_{n-1})) \tag{4.2}$$

$$\Rightarrow \begin{pmatrix} 2J & 0 & -J & 0 & \cdots & 0 & -J & 0 \\ 0 & 2J & 0 & -J & 0 & \cdots & 0 & -J \\ -J & 0 & \ddots & \ddots & \ddots & 0 & \vdots & 0 \\ 0 & -J & \ddots & \ddots & \ddots & \ddots & 0 & \vdots \\ \vdots & 0 & \ddots & \ddots & \ddots & \ddots & -J & 0 \\ 0 & \vdots & 0 & \ddots & \ddots & \ddots & 0 & -J \\ -J & 0 & \cdots & 0 & -J & 0 & 2J & 0 \\ 0 & -J & 0 & \cdots & 0 & -J & 0 & 2J \end{pmatrix} \begin{pmatrix} \psi_{1,+} \\ \psi_{1,-} \\ \vdots \\ \vdots \\ \vdots \\ \vdots \\ \psi_{n,+} \\ \psi_{n,-} \end{pmatrix} = \epsilon_{k,n} \begin{pmatrix} \psi_{1,+} \\ \psi_{1,-} \\ \vdots \\ \vdots \\ \vdots \\ \vdots \\ \psi_{n,+} \\ \psi_{n,-} \end{pmatrix}, \tag{4.3}$$

where J is the hopping parameter defined as $J = \frac{\hbar^2}{2ma^2}$. The two blocks in the upper right and lower left corner are due to the implemented boundary conditions. If we consider the Tight Binding Hamiltonian of a free particle written in matrix form, it corresponds to our discretized matrix,

$$\mathcal{H} = \sum_{j,s} \epsilon_0 \hat{c}^\dagger_{j,s}\hat{c}_{j,s} - J\sum_{i,j,s} \hat{c}^\dagger_{i,j+1,s}\hat{c}_{i,j,s}, \tag{4.4}$$

where, in order to correspond to our model, $\epsilon_0 = 2J$.

Now we want to check whether our discretization method is correct. We do this by means of introducing a discretized wave ansatz and solve the Schrödinger equation analytically. We will obtain a function of the energy which we compare with the eigenvalues of our discretized Hamiltonian. We start again from the continuum Hamiltonian

$$\frac{-\hbar^2\nabla^2}{2m}\psi = \epsilon\psi, \tag{4.5}$$

$$\frac{-\hbar^2}{2ma^2}(\psi_{n+1} + \psi_{n-1} - 2\psi_n) = \epsilon_k\psi_n. \tag{4.6}$$

$$\tag{4.7}$$

We then introduce a discretized complex wave ansatz $\psi = \frac{1}{\sqrt{N}} \sum_i^N e^{ikna} \psi_n$, and plug it in the Schrödinger equation to find an expresion for the energy ϵ.

$$2Je^{ikna} - J(e^{ika(n+1)} + e^{ika(n-1)}) = \epsilon_k e^{ikna} \tag{4.8}$$

$$2J - 2J\cos(ka) = \epsilon_k \tag{4.9}$$

$$\epsilon_k = 2J(1 - \cos(ka)). \tag{4.10}$$

We make a Taylor approximation of this result for small $k \cdot a$, to check if it corresponds to the well known continuum dispersion relation of the free particle, we find

$$\epsilon_k = \frac{\hbar^2}{m}(\frac{k^2}{2} - \frac{1}{24}a^2k^4 + ...). \tag{4.11}$$

This result agrees with the continuum result and this shows that our discretization method is correct.

Next, we check if the obtained energies from equation 4.10, match the eigenvalues of the discretized Hamiltonian. The results are shown in figure 4.1. We made a table of the energies of equation 4.10 for different values of momentum: $k \cdot a \in -\frac{m}{N}\pi, ..., \frac{m}{N}\pi$, where $m \in 1, ..., 100$ for $N = 100$. Also, we devided by J, to obtain dimensionless parameters. As shown in the figure, the eigenvalues of the Hamiltonian are degenerate, this happens because we implemented boundary conditions and spin structure to the Hamiltonian. Other from that, the numerical result matches the analytical result, thus our discretization method is valid.

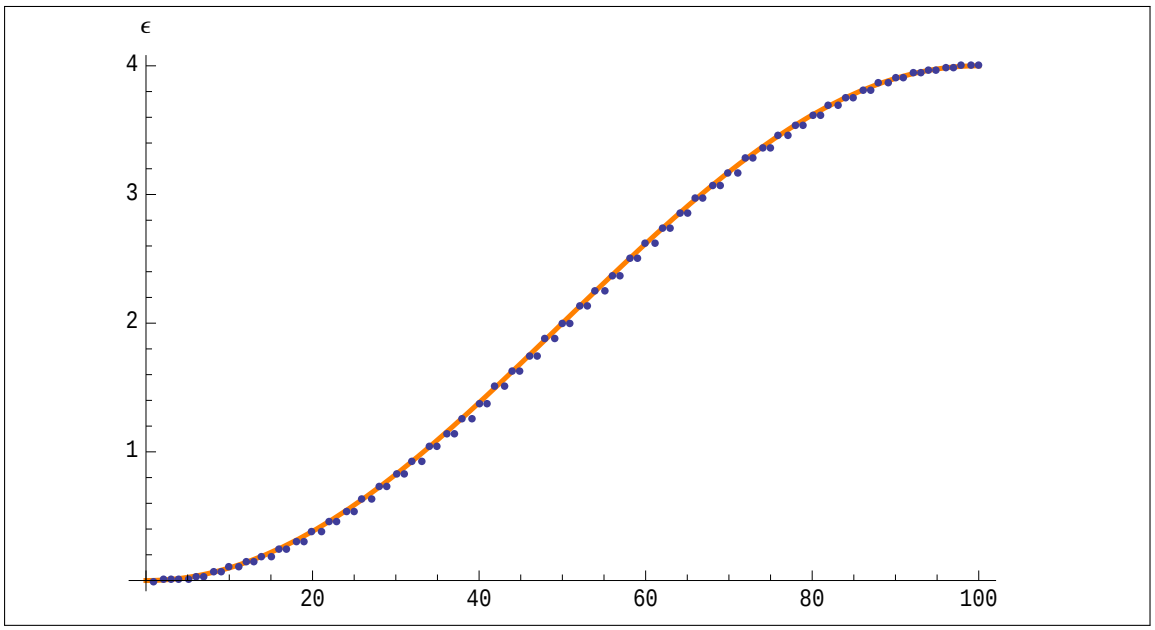

Figure 4.1: The eigenvalues of the free particle Hamiltonian, blue dots, are plotted in ascending order combined with the analytical result, displayed with an orange interpolated curve.

4.1.2 The Rashba Model

Just as for the free particle we discretize the Hamiltonian of the Rashba model and check whether or not our discretization is correct and corresponds to analytical computations. Again starting from the continuum Hamiltonian we have

$$\mathcal{H}_R = -\frac{\hbar^2\nabla^2}{2m} - \frac{\alpha_R}{\hbar}(\boldsymbol{\tau}\times\boldsymbol{p})\cdot\hat{\boldsymbol{z}}. \tag{4.12}$$

Discretizing along the same lines as before gives us the following discretized matrix,

$$\mathcal{H}_R\psi_n = (2J\psi_n - J(\psi_{n+1}+\psi_{n-1})) + \alpha_R \begin{pmatrix} 0 & \frac{-(\psi_{n+1}-\psi_{n-1})}{a} \\ \frac{\psi_{n+1}-\psi_{n-1}}{a} & 0 \end{pmatrix}, \tag{4.13}$$

$$\Rightarrow \begin{pmatrix} A & B & 0 & \cdots & 0 & B^T \\ B^T & A & \ddots & 0 & 0 & 0 \\ 0 & \ddots & \ddots & \ddots & 0 & \vdots \\ \vdots & 0 & \ddots & \ddots & \ddots & 0 \\ 0 & 0 & 0 & \ddots & A & B \\ B & 0 & \cdots & 0 & B^T & A \end{pmatrix} \begin{pmatrix} \psi_{1,\pm} \\ \vdots \\ \vdots \\ \vdots \\ \vdots \\ \psi_{n,\pm} \end{pmatrix} = \epsilon_{n,k} \begin{pmatrix} \psi_{1,\pm} \\ \vdots \\ \vdots \\ \vdots \\ \vdots \\ \psi_{n,\pm} \end{pmatrix}, \tag{4.14}$$

the 2×2 block matrices A and B have the following form,

$$A = \begin{pmatrix} 2 & 0 \\ 0 & 2 \end{pmatrix}, \tag{4.15}$$

$$B = \begin{pmatrix} -1 & -\frac{\alpha_R}{2aJ} \\ \frac{\alpha_R}{2aJ} & -1 \end{pmatrix}, \tag{4.16}$$

where we devided by J, to end up with one dimensionless parameter: $\frac{\alpha_R}{aJ}$. This corresponds to the Tight Binding model if it was written in matrix form,

$$\mathcal{H}_{free} + \mathcal{H}_{Rashba} = \sum_{j,s}\epsilon_0\hat{c}^\dagger_{j,s}\hat{c}_{j,s} - J\sum_{i,j,s}\hat{c}^\dagger_{i,j+1,s}\hat{c}_{i,j,s} - \frac{\alpha_R}{2a}\sum_{i,j,s,s'}(-i\hat{c}^\dagger_{i,j+1,s}(\tau_y)_{s,s'}\hat{c}_{i,j,s} + \text{h.c.}), \tag{4.17}$$

where, $\epsilon_0 = 2J$.

We explicitly check our discretization method, similarly as we did for the free particle case. We introduce a wave function ansatz with spin dependence: $\psi = \frac{1}{\sqrt{2N}}\sum_{n=0}^{N} e^{ikna}\begin{pmatrix} 1 \\ -\delta i e^{i\theta_k} \end{pmatrix}\psi_n$, with

$\delta \in [\pm]$. Subsequently, plugging this ansatz in our expression, we find for spin +

$$
\begin{aligned}
&- J\sum_{n=0}^{N}\frac{1}{\sqrt{2N}}(e^{ika(n+1)}\begin{pmatrix}1\\-ie^{i\theta_k}\end{pmatrix}+e^{ika(n-1)}\begin{pmatrix}1\\-ie^{i\theta_k}\end{pmatrix}-2e^{ikna}\begin{pmatrix}1\\-ie^{i\theta_k}\end{pmatrix}) \qquad (4.18)\\
&-\sum_{n=0}^{N}\frac{1}{\sqrt{2N}}\frac{i\alpha_R}{2a}\tau_y(e^{ika(n+1)}\begin{pmatrix}1\\-ie^{i\theta_k}\end{pmatrix}-e^{ika(n-1)}\begin{pmatrix}1\\-ie^{i\theta_k}\end{pmatrix})=\epsilon_k\sum_{n=0}^{N}\frac{1}{\sqrt{2N}}e^{ikna}\begin{pmatrix}1\\-ie^{i\theta_k}\end{pmatrix}.
\end{aligned}
$$

Plugging in $\tau_y=\begin{pmatrix}0&-i\\i&0\end{pmatrix}$, we end up with

$$
\begin{aligned}
&- J\sum_{n=0}^{N}\frac{1}{\sqrt{2N}}(e^{ika(n+1)}+e^{ika(n-1)}-2e^{ikan})\begin{pmatrix}1\\-\delta ie^{i\theta_k}\end{pmatrix} \qquad (4.19)\\
&-\sum_{n=0}^{N}\frac{1}{\sqrt{2N}}\frac{i\alpha_R}{2a}(e^{ika(n+1)}-e^{ika(n-1)})\begin{pmatrix}-e^{i\theta_k}\\i\end{pmatrix}=\epsilon_k\sum_{n=0}^{N}\frac{1}{\sqrt{2N}}e^{ikna}\begin{pmatrix}1\\-ie^{i\theta_k}\end{pmatrix}.
\end{aligned}
$$

The next thing is to multiply both sides with the complex conjugate transpose of the wave function resulting in

$$
\begin{aligned}
&- J(e^{ika}+e^{-ika}-2)-\frac{i\alpha_R}{2a}(e^{ika}-e^{-ika})(-\frac{e^{i\theta_k}+e^{-i\theta_k}}{2})=\epsilon_k \qquad (4.20)\\
&\epsilon_k=2J(1-\cos ka)-\frac{\alpha_R}{a}\cos\theta_k\sin ka.
\end{aligned}
$$

When we also consider spin $-$, and set the angle $\theta_k=1$, we find

$$\epsilon_{k,\pm}=2J(1-\cos ka)\pm\frac{\alpha_R}{a}\sin ka. \qquad (4.21)$$

Again we check if this result matches our analytical result obtained in Chapter 3. We make a Taylor approximation for $k\cdot a << 1$ such that we find

$$
\begin{aligned}
\epsilon_{k,\pm}&=\frac{\hbar^2}{m}(\frac{k^2}{2}-\frac{1}{24}a^2k^4+...)\pm\alpha_R(k-\frac{1}{6}k^3a^2+...) \qquad (4.22)\\
&=\frac{\hbar^2k^2}{2m}\pm\alpha_Rk. \qquad (4.23)
\end{aligned}
$$

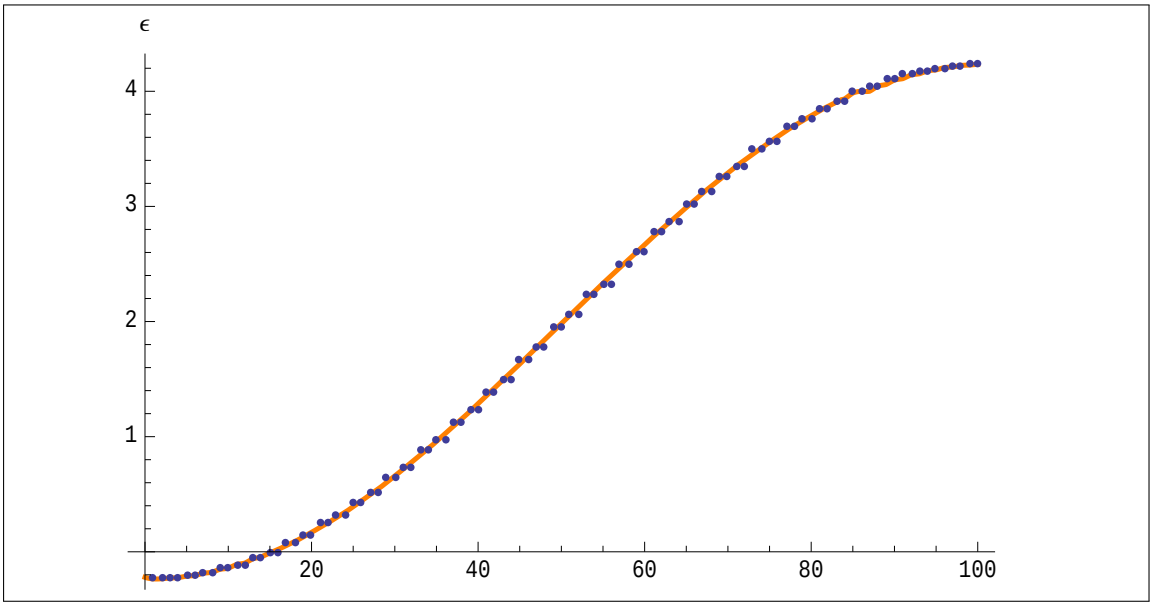

Figure 4.2: The eigenvalues of the Rashba Hamiltonian, blue dots, are plotted in ascending order combined with the analytical result, displayed with an orange interpolated curve.

In the last line we only took terms linear in $k \cdot a$ and we find the same behavior as in the continuum computation. Also, we check if the output of equation 4.21 corresponds to the eigenvalues of the discretized Rashba Hamiltonian. To do so we make a table of the energies of expression 4.21 for different values of momentum: $k \cdot a \in -\frac{m}{N}\pi, ..., \frac{m}{N}\pi$, where $m \in -50, ..., 50$ for $N = 100$. Subsequently, we plot the values of the table in ascending order and compare the result with a sorted list of the eigenvalues of our discretized Rashba matrix, the result is plotted in figure 4.2. We conclude, looking at the figure, that our discretization method works. Now before we apply this method to our full model, we make a energy momentum plot of the free particle, again showing the correspondence of the numerical computations with the analytical computations.

4.1.3 Finding the Real Energy-Momentum Plot

Another way to check if our discretization method works is to directly find the corresponding analytical behavior of the dispersion. In order to find such a dependence from our discretized Hamiltonian we need to introduce an impuls operator matrix and discretize it. Then we need to match each eigenvalue of the Hamiltonian with the corresponding impuls eigenvalue through a

function. We set up the (one-dimensional) impuls operator as follows

$$P_x\psi = -i\hbar\frac{\partial}{\partial x}\psi(x) = -i\hbar\frac{\psi_{n+1}-\psi_{n-1}}{2a} \Rightarrow -i\hbar \begin{pmatrix} 0 & 1 & 0 & \cdots & 0 & -1 \\ -1 & \ddots & \ddots & 0 & 0 & 0 \\ 0 & \ddots & \ddots & \ddots & 0 & \vdots \\ \vdots & 0 & \ddots & \ddots & \ddots & 0 \\ 0 & 0 & 0 & \ddots & \ddots & 1 \\ 1 & 0 & \cdots & 0 & -1 & 0 \end{pmatrix} \begin{pmatrix} \psi_1 \\ \vdots \\ \vdots \\ \vdots \\ \vdots \\ \psi_n \end{pmatrix}. \quad (4.24)$$

Subsequently, we check if the discretized impuls matrix commutes with the discretized Hamiltonian of, for example, the free particle. This holds, so we are able to link the momentum eigenvalues to the energy eigenvalues. We have the following eigenvalues and eigenfunctions

$$\mathcal{H}_{free}\left|\psi\right\rangle = \epsilon\left|\psi\right\rangle, \quad (4.25)$$

$$P_x\left|\xi\right\rangle = p\left|\xi\right\rangle. \quad (4.26)$$

We link the energy eigenvalues to the corresponding momentum eigenvalues, such that we are able to make an energy-momentum plot. The relation is as follows

$$\bar{\epsilon}_\alpha = \frac{\left\langle\xi_\alpha\right|\mathcal{H}_{free}\left|\xi_\alpha\right\rangle}{\left\langle\xi_\alpha\right|\left.\xi_\alpha\right\rangle}. \quad (4.27)$$

We now have a link between the the eigenvalues of the Hamiltonian and the eigenvalues of the impuls operator. We plot them and find the expected quadratic behavior of the dispersion. So, this is another way to check our discretization method.

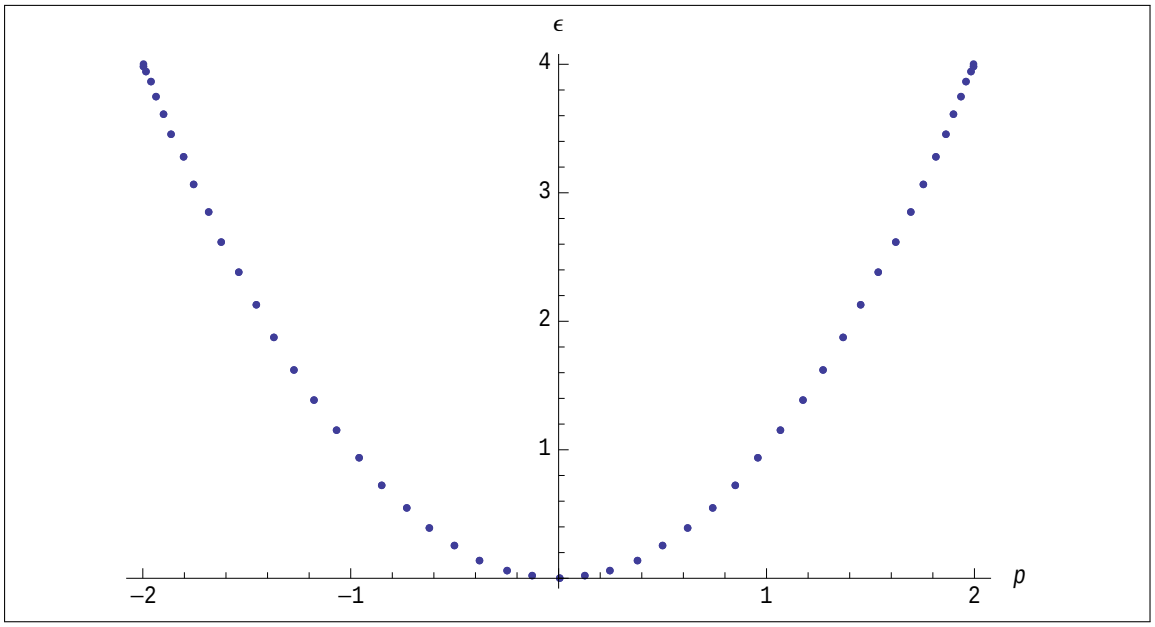

Figure 4.3: The eigenvalues of the free particle Hamiltonian are plotted against the eigenvalues of the momentum operator. We set all dimensionless variables to 1 and used a 100×100 matrix.

4.2 Solving the Schrödinger Equation

In this section we solve the Schrödinger equation for $\alpha_R \neq 0$. To do so we already introduced a discretization method and showed that it is a legit procedure. However, before we begin computing the Schrödinger equation we need to introduce Bloch's theorem, because our potential is periodic.

After giving an explanation of Bloch's theorem we turn to the computation of the total energy of the model. We split this computation up in two parts: first, we compute the total energy of the system for $\alpha_R = 0$ and compare it with the analytical result. Second, we compute the total energy of the system for $\alpha_R \neq 0$. From the total energy we deduce the term linear in q, corresponding to D. We conclude this chapter with a plot of the DM interaction as a function of the Rashba coupling for different values of the Fermi energy and the helical exchange coupling.

4.2.1 Bloch's Theorem

Bloch's theorem enters the scene since we are considering a system of electrons in a periodic exchange field. There are many ways to solve the Schrödinger equation, most of them numerical, and it can be shown that all the solutions have some underlying general properties. These underlying properties make computations easier and help to find a general understanding of the effect of the potential on the eigenfunctions or eigenvalues. For a periodic potential

$$V(\boldsymbol{x}) = V(\boldsymbol{x} + T), \tag{4.28}$$

where T is some translation, we could find the corresponding eigenfunctions $\psi_n(\boldsymbol{x})$ if we solve the Schrödinger equation. Bloch's theorem then states that all solutions have to meet. One of the ways we can write this statement is as follows

$$\psi_{n,\boldsymbol{k}}(\boldsymbol{x}) = e^{i\boldsymbol{k}\cdot\boldsymbol{x}} U_{n,\boldsymbol{k}}(\boldsymbol{x}), \tag{4.29}$$

where $U_{n,\boldsymbol{k}}(\boldsymbol{x})$ has the same periodicity as the lattice:

$$U_{n,\boldsymbol{k}}(\boldsymbol{x} + T) = U_{n,\boldsymbol{k}}(\boldsymbol{x}). \tag{4.30}$$

In this way every wave function that has this property is a Bloch wave. The impressive feature of the theorem is its scope of validity. The theorem imposes a condition on any solution of the Schrödinger equation and the theory is proven to hold. In the subscript of the bloch wave n is a general symbol for all quantum numbers, but an important thing to notice is that $\boldsymbol{k}$ is not the true momentum, it is the crystal momentum or quasi wave vector. We identify $\hbar\boldsymbol{k}$, which is a constant, as the crystal momentum. Another form of the theorem is the following

$$\psi_{n,\boldsymbol{k}}(\boldsymbol{x} + T) = e^{i\boldsymbol{k}\cdot\boldsymbol{x}} \psi_{n,\boldsymbol{k}}(\boldsymbol{x}), \tag{4.31}$$

where T again is some translation. The meaning of this statement is that the eigenfunctions obtained from the Schrödinger equation differ a phase factor $e^{i\boldsymbol{k}\cdot\boldsymbol{x}}$ between positions. From this statement we deduce that the probability of finding an electron is the same for any position in the lattice, since

$$|\psi_{n,\boldsymbol{k}}(\boldsymbol{x}+T)|^2 = |\psi_{n,\boldsymbol{k}}(\boldsymbol{x})|^2 |e^{i\boldsymbol{k}\cdot\boldsymbol{x}}|^2 = \psi_{n,\boldsymbol{k}}(\boldsymbol{x})^2. \tag{4.32}$$

We have seen two different forms of the same theory, and it can be shown that both statements are identical. Consider the first form we saw at lattice position $\boldsymbol{x}+T$ we have

$$\psi_{n,\boldsymbol{k}}(\boldsymbol{x}+T) = e^{i\boldsymbol{k}\cdot(\boldsymbol{x}+T)} U_{n,\boldsymbol{k}}(\boldsymbol{x}+T) \tag{4.33}$$

$$= e^{i\boldsymbol{k}T} e^{i\boldsymbol{k}\cdot(\boldsymbol{x})} U_{n,\boldsymbol{k}}(\boldsymbol{x}) \tag{4.34}$$

$$= \psi_{n,\boldsymbol{k}}(\boldsymbol{x}) e^{i\boldsymbol{k}\boldsymbol{x}}. \tag{4.35}$$

Finally, if the wave function is known for one value of the crystal momentum $\boldsymbol{k}$, all other wave functions are known as well, for all values of $\boldsymbol{k}$. Any wave function $\psi_{n,\boldsymbol{k}}(\boldsymbol{x})$ corresponds to a specific energy $E(\boldsymbol{k})$, and is a constant of the system. Using the first form of Bloch's theorem we deduce that any reciprocal lattice point can be used as the origin of the energy function. This means that all possible energy values are fully grasped within the first Brillouin zone. We use this in our computation of the total energy in the coming sections.

4.2.2 Proving Bloch's Theorem Using Operator Algebra

There are many ways to prove Bloch's theorem, one being more in depth then the other. It can be seen as an application of group theory using an irreducible representation. However, we will not go into group theory, but prove the theorem using operator algebra.

If two operators satisfy a commutation relation, $[H, A] = 0$, and the eigenstates of H are known, then A is block diagonal and shares the eigenvalues with H. We show this if we consider the following

$$H\,|\psi\rangle = \epsilon\,|\psi\rangle\,, \tag{4.36}$$

from the commutation relation we find $HA = AH \rightarrow HA\,|\psi\rangle = AH\,|\psi\rangle \rightarrow HA\,|\psi\rangle = A\epsilon\,|\psi\rangle\,,$

resulting in $H\,|\psi'\rangle = \epsilon\,|\psi'\rangle$, where $|\psi'\rangle = A\,|\psi\rangle\,.$

In the proof above we already choose H as an operator, which could be a Hamiltonian and is hermitian. We conclude that if the Hamiltonian commutes with an operator and if the eigenstates of that operator form a complete basis, then both operators share the same eigenstates.

Consider a translation operator $\mathcal{T}$, which translates a function on a crystal, $\mathcal{T}\psi(\boldsymbol{x}) = \psi(\boldsymbol{x}+T)$. If $[H,\mathcal{T}] = 0$. We diagonalize the translation operator and we find a complete basis, which is the plane waves basis with eigenvalues: $e^{i\boldsymbol{k}\cdot\boldsymbol{x}}$. In all generality we choose the eigenstates of the translation operator to be: $\sum_a \mathcal{C}(\boldsymbol{k}+\boldsymbol{a})e^{i(\boldsymbol{k}+\boldsymbol{a})\cdot\boldsymbol{x}}$, where $\mathcal{C}(\boldsymbol{k}+\boldsymbol{a})$ is some complex pre factor. The eigenvalue for this state is $e^{i\boldsymbol{k}\cdot T}$. We then rewrite this state as $e^{i\boldsymbol{k}\cdot\boldsymbol{x}}U_{\boldsymbol{k}}(\boldsymbol{x})$, where $U_{\boldsymbol{k}}(\boldsymbol{x}) = \sum_a \mathcal{C}(\boldsymbol{k}+\boldsymbol{a})e^{i\boldsymbol{a}\cdot\boldsymbol{x}}$. In conclusion, using the previous statement that any operator commuting with the Hamiltonian shares the same eigenstates, we can write any eigen state of the Hamiltonian in this particular form.

4.2.3 Computing the Total Energy for $\alpha_R = 0$

In order to compute the total energy of electrons coupled to a helical exchange field we first apply Bloch's theorem. The Schrödinger equation is

$$\left[\frac{\hbar^2}{2m}\nabla^2 - \Delta\frac{\boldsymbol{m}(\boldsymbol{x})}{2}\cdot\tau\right]\psi_{k,n}(\boldsymbol{x}) = \epsilon_{k,n}\psi_{k,n}(\boldsymbol{x}).$$

where, $\boldsymbol{m}(\boldsymbol{x}) = \sin qx\hat{x} + \cos qx\hat{z}$. Then applying Bloch's theorem,

$$\psi_{k,n}(\boldsymbol{x}) = e^{i\boldsymbol{k}\boldsymbol{x}}U_{k,n}(\boldsymbol{x}),$$

and using the periodicity of the potential to find the condition $U_{k,n}(\boldsymbol{x}) = U_{k,n}(\boldsymbol{x}+\frac{2\pi}{q})$. Plugging this ansatz for the wave function into the previous equation we find the equation we want to solve numerical.

$$\left[-\frac{\hbar^2}{2m}(ik+\frac{\partial}{\partial\boldsymbol{x}})^2 - \Delta\frac{\Omega(\boldsymbol{x})}{2}\cdot\tau\right]U_{k,n}.(\boldsymbol{x}) = \epsilon_{k,n}U_{k,n} \tag{4.37}$$

We need to discretize the equation as follows: $U(x) = U(x_n) = U_n$, where $x_n = x$, $x = n\cdot a$. Here n runs from $-N, -N+1, ..., N$, and has an additional subscript for either spin plus or minus. As boundary condition we have the Bloch condition and $U_{N+1} = U_{-N}$. Also, the crystal momentum goes through the first Brillouin zone: $\frac{-q}{2} < k < \frac{q}{2}$. By using this procedure the equation becomes a matrix equation and the differentials turn into difference equations. We first write (4.37) as a matrix equation,

$$\begin{pmatrix} -\frac{\hbar^2}{2m}(ik+\frac{\partial}{\partial\boldsymbol{x}})^2 - \frac{\Delta}{2}\sin(qx) & -\frac{\Delta}{2}\cos(qx) \\ -\frac{\Delta}{2}\cos(qx) & -\frac{\hbar^2}{2m}(ik+\frac{\partial}{\partial\boldsymbol{x}})^2 + \frac{\Delta}{2}\sin(qx) \end{pmatrix}\begin{pmatrix} U_{n,+} \\ U_{n,-} \end{pmatrix} = \epsilon_{k,n}\begin{pmatrix} U_{n,+} \\ U_{n,-} \end{pmatrix}. \tag{4.38}$$

We discretize as follows

$$-\frac{\hbar^2}{2m}(ik+\frac{\partial}{\partial\boldsymbol{x}})^2U_n = -\frac{\hbar^2}{2m}(-k^2+2i\boldsymbol{k}\cdot\frac{\partial}{\partial\boldsymbol{x}} + (\frac{\partial}{\partial\boldsymbol{x}})^2)U_n \tag{4.39}$$

$$\to -\frac{\hbar^2}{2m}(-k^2U_n + 2i\boldsymbol{k}\cdot\frac{U_{n+1}-U_{n-1}}{2a} + \frac{U_{n+1}+U_{n-1}-2U_n}{a^2}). \tag{4.40}$$

Using this discretization we turn equation 4.37 into a matrix equation

$$\begin{pmatrix} A_{n=1} & B & 0 & \cdots & 0 & B^* \\ B^* & A_{n=1} & \ddots & 0 & 0 & 0 \\ 0 & \ddots & \ddots & \ddots & 0 & \vdots \\ \vdots & 0 & \ddots & \ddots & \ddots & 0 \\ 0 & 0 & 0 & \ddots & A_{n=N} & B \\ B & 0 & \cdots & 0 & B^* & A_{n=N} \end{pmatrix} \begin{pmatrix} U_{1,\pm} \\ \vdots \\ \vdots \\ \vdots \\ \vdots \\ U_{n,\pm} \end{pmatrix} = \epsilon_{n,k} \begin{pmatrix} U_{1,\pm} \\ \vdots \\ \vdots \\ \vdots \\ \vdots \\ U_{n,\pm} \end{pmatrix},$$

where the 2×2 block matrices A and B have the following form,

$$A_{n=N} = \begin{pmatrix} 2 + a^2k^2 - \frac{\Delta}{2J}\cos(qaN) & -\frac{\Delta}{2J}\sin(qaN) \\ -\frac{\Delta}{2J}\sin(qaN) & 2 + a^2k^2 + \frac{\Delta}{2J}\cos(qaN) \end{pmatrix}, \tag{4.41}$$

$$B = \begin{pmatrix} -1 - \frac{iak}{2} & 0 \\ 0 & -1 - \frac{iak}{2} \end{pmatrix}. \tag{4.42}$$

In the above expressions we divided every term by J, to end up with only one dimensionless parameter, $\frac{\Delta}{J}$, aside from the crystal momentum $k \cdot a$ and $q \cdot a$. Also, B^* is the complex conjugate transpose of B. We see that the total matrix is hermitian, since $H = (H^*)^T$.

Now we compute the total energy of this discretized Hamiltonian. Since for each value of $q \cdot a$, $k \cdot a$ takes on values from $-\frac{q \cdot a}{2}$,..., $\frac{q \cdot a}{2}$, the first Brillouin zone. To compute the total energy we add all the eigenvalues of each value of $k \cdot a$ below some value for the Fermi Energy. We have to define either a constant step size or constant number of steps with which we go through the first Brillouin zone. We chose a constant number of steps. The total energy function depends on: the Fermi energy, the size of the system (matrix), $q \cdot a$, $\frac{\Delta}{J}$, $k \cdot a$. The output of the function is a total energy divided by J. By adjusting the number of steps we go through the first Brillouin zone we can adjust the precision of the computation.

The total energy of the system for $\alpha_R = 0$ is plotted in figure 4.4. We expect from theory that $D = 0$. The numerical result is $D = 0.00001$. However, this converges to zero if we make the system more precise.

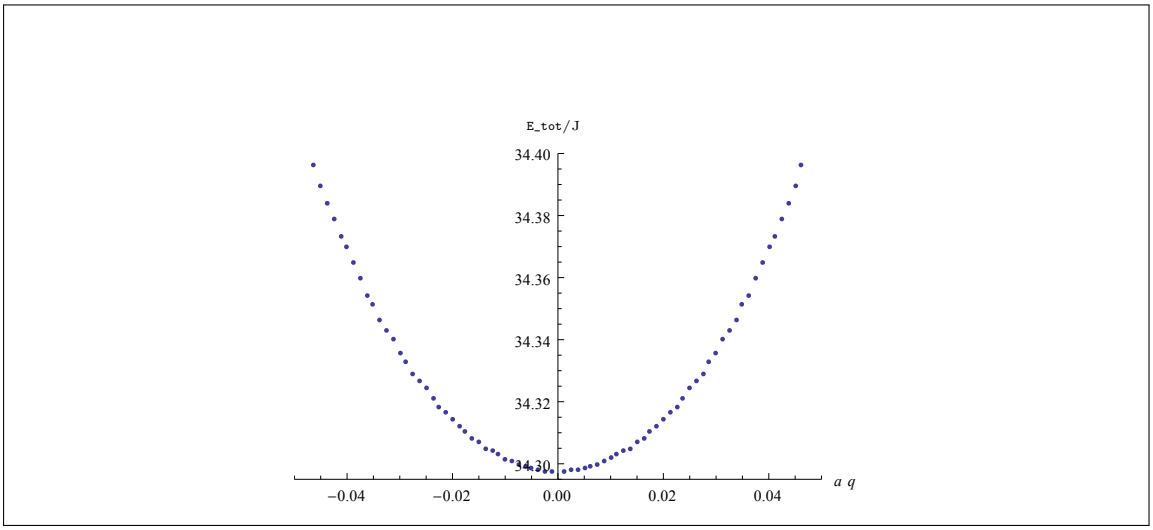

Figure 4.4: A plot of the total energy of the model for $\alpha_R = 0$, depending on $q \cdot a$. The theoretical expectation of D is zero, the numerical value is $D = 0.00001$.

4.2.4 Computing the Total Energy for $\alpha_R \neq 0$

After the preparatory work we now solve the the model where electrons are coupled to a helical exchange field and a Rashba coupling: $\alpha_R \neq 0$. We follow the same procedure as before, writing the down the Schrödinger equation in matrix form, discretizing it and finally computing the total energy of the system. The continuum Hamiltonian of this model is

$$\mathcal{H} = -\frac{\hbar^2}{2m}\nabla^2 - \frac{\boldsymbol{m}(\boldsymbol{x})}{2}\cdot\tau - \frac{\alpha_R}{\hbar}(\boldsymbol{\tau}\times\boldsymbol{p})\cdot\hat{z}.$$

Again we apply Bloch's theorem and plug the wave ansatz into the Schrödinger equation and obtain

$$\left[-\frac{\hbar^2}{2m}(ik+\frac{\partial}{\partial\boldsymbol{x}})^2\mathbb{I} - \frac{\Omega(\boldsymbol{x})}{2}\cdot\tau - i\alpha_R\tau^y(\frac{\partial}{\partial x}+ik_x)\right]U_{k,n}(\boldsymbol{x}) = \epsilon_{k,n}U_{k,n}. \tag{4.43}$$

We write the Hamiltonian as a matrix equation as follows, however we only consider one dimension,

$$\begin{pmatrix} -\frac{\hbar^2}{2m}(ik+\frac{\partial}{\partial\boldsymbol{x}})^2 - \frac{\Delta}{2}\sin(qx) & -\frac{\Delta}{2}\cos(qx) + \alpha_R(-\frac{\partial}{\partial x} - ik_x) \\ -\frac{\Delta}{2}\cos(qx) + \alpha_R(\frac{\partial}{\partial x}+ik_x) & -\frac{\hbar^2}{2m}(ik+\frac{\partial}{\partial\boldsymbol{x}})^2 + \frac{\Delta}{2}\sin(qx) \end{pmatrix}\begin{pmatrix} U_{n,+} \\ U_{n,-}\end{pmatrix} = \epsilon_{k,n}\begin{pmatrix} U_{n,+} \\ U_{n,-}\end{pmatrix}. \tag{4.44}$$

We discretize each term using the same procedure as before,

$$-i\alpha_R\tau_y(\frac{\partial}{\partial x}+ik_x)U_n = -i\alpha_R\tau_y(\frac{U_{n+1}-U_{n-1}}{2a}+ik_xU_n). \tag{4.45}$$

Imposing boundary conditions, we find the same structure as before, but the block matrices are

different. Writing equation 4.43 as a matrix equation,

$$\begin{pmatrix} A_{n=1} & B & 0 & \cdots & 0 & B^* \\ B^* & A_{n=1} & \ddots & 0 & 0 & 0 \\ 0 & \ddots & \ddots & \ddots & 0 & \vdots \\ \vdots & 0 & \ddots & \ddots & \ddots & 0 \\ 0 & 0 & 0 & \ddots & A_{n=N} & B \\ B & 0 & \cdots & 0 & B^* & A_{n=N} \end{pmatrix} \begin{pmatrix} U_{1,\pm} \\ \vdots \\ \vdots \\ \vdots \\ \vdots \\ U_{N,\pm} \end{pmatrix} = \epsilon_{n,k} \begin{pmatrix} U_{1,\pm} \\ \vdots \\ \vdots \\ \vdots \\ \vdots \\ U_{N,\pm} \end{pmatrix},$$

where the 2×2 block matrices A and B have the following form,

$$A_{n=N} = \begin{pmatrix} 2 + a^2k^2 - \frac{\Delta}{2J}\cos(qaN) & -\frac{ik\alpha_R}{J} - \frac{\Delta}{2J}\sin(qaN) \\ \frac{ik\alpha_R}{J} - \frac{\Delta}{2J}\sin(qaN) & 2 + a^2k^2 + \frac{\Delta}{2J}\cos(qaN) \end{pmatrix}, \tag{4.46}$$

$$B = \begin{pmatrix} -1 - \frac{iak}{2} & -\frac{\alpha_R}{2aJ} \\ \frac{\alpha_R}{2aJ} & -1 - \frac{iak}{2} \end{pmatrix}. \tag{4.47}$$

In the above expressions we divided every term again by J, to end up with only two dimensionless parameters, $\frac{\alpha_R}{Ja}$ and $\frac{\Delta}{J}$, aside from the crystal momentum $k \cdot a$ and $q \cdot a$. Also B^* again is the complex conjugate transpose of B. We see that the total matrix is hermitian, since $H = (H^*)^T$.

We compute the total energy of this system, along the same lines as we did previously. We construct a function that adds all eigenvalues for each configuration through the Brillouin zone, until we hit some Fermi energy.

In order to construct a plot of the DM interaction depending on spin orbit coupling we want to make different plots of the total energy of this system for different values of α_R. We analyze the linear order in q of these graphs, since this corresponds to the value of the DM interaction. In figure 4.5 we see a typical plot of the total energy for $\alpha_R \neq 0$. Notice the small displacement of the parabola, indicating the presence of a linear term.

In figure 4.6, the result is shown of the DM interaction depending on Rashba spin-orbit coupling. Although more measurements need to be done, it shows linear behavior for small values of spin-orbit coupling. This is what we expected based on our analytical computations. Also, for higher values of spin-orbit coupling we see asymptotic behavior to some value of D. This value still needs to be established. In conclusion, to give a full explanation of the physics behind this plot more measurements need to be done.

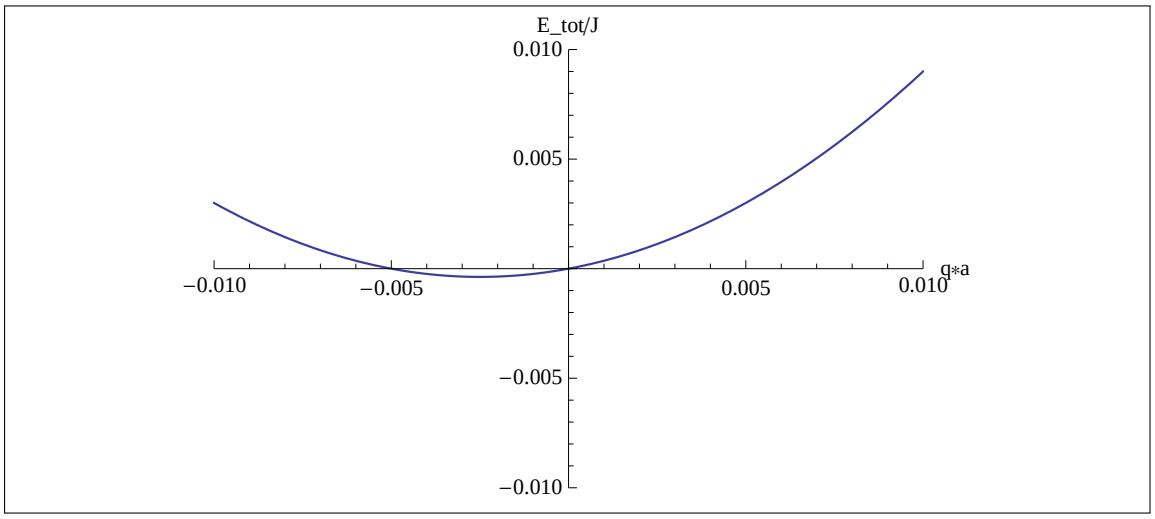

Figure 4.5: A plot of the total energy of the model for $\alpha_R \neq 0$, depending $q \cdot a$.

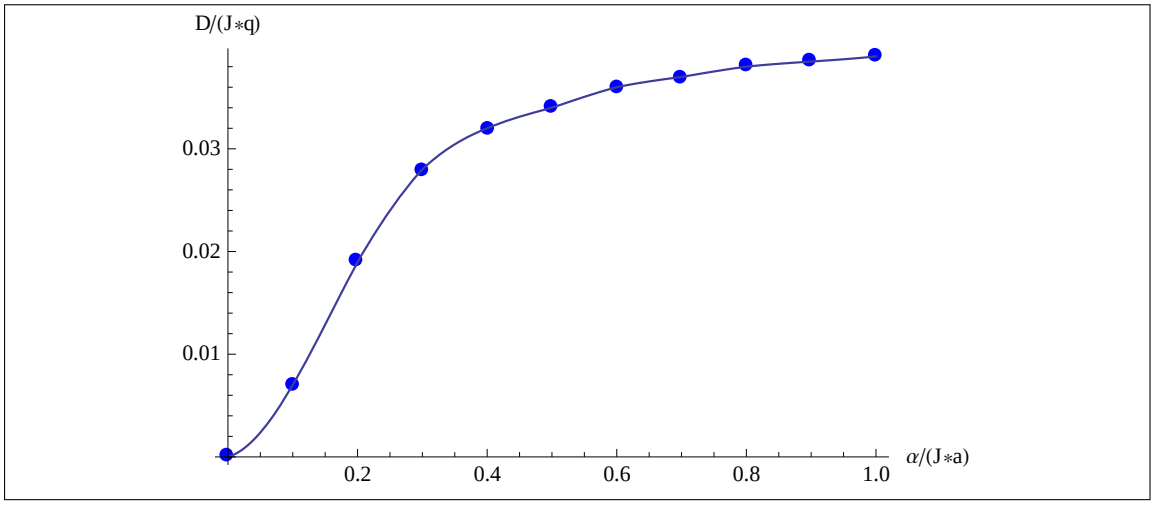

Figure 4.6: A plot of the the DM interaction as a function of spin-orbit coupling.

Chapter 5

Conclusion

In this chapter we summarize the research done in this thesis. Subsequently, we discuss possible future research on skyrmions and give an option to verify our biggest assumption.

5.1 Summary

We started this thesis with the notion that a skyrmion is a topological soliton. Although there are many types of skyrmions, we focussed on chiral skyrmions. In the introduction we asked the following question: What is the full behaviour, considering both small spin-orbit coupling and large spin orbit coupling, of the Dzyalosinskii-Moriya interaction in a chiral magnet? We set out to give context to this question in the first chapter.

In Chapter 1 we explained that chiral skyrmions are topologically and physically stable magnetization structures appearing in chiral magnets. Chirality of a compound emerges from the fact that the atomic structure lacks inversion symmetry in some direction. Then, the lack of inversion symmetry in combination with a strong spin-orbit coupling, induces a Dzyalosinskii-Moriya interaction. This, in turn, is responsible for several chiral phases, e.g. skyrmion magnetization. We analytically described the magnetization profile of a skyrmion with a phenomenological model.

In the following chapter the model to describe skyrmions was explained and the typical magnetization profile that is characteristic for a skyrmion was reproduced. This magnetization profile then led to a graphical vector representation of the skyrmion structure. This model was the basis for this thesis. We used a two-layered system, a ferromagnet on top of a non-magnet in order to break inversion symmetry in the $\hat{z}$-direction. We then assumed that the origin of the spin-orbit coupling on the surface between those two layers is described with a Rashba model. Using this toy model we computed the dependence of the DM interaction on spin-orbit coupling.

Chapter 3 consists of several computations, all aimed to reproduce the previously established result of the DM interaction. We considered two cases: $\alpha_R = 0$ and $\alpha_R \neq 0$, where α_R is the Rashba coupling constant. In the former case we used field theory and an integration over the filled Fermi

sea to compute the total energy of the system. In the latter case we used perturbation theory, and again integrated over the filled Fermi sea to find the total energy. Combining these results we concluded the chapter and verified that for small spin-orbit coupling the DM interaction depends linearly on α_R. However, the aim of this thesis is to expand this result.

This quest brought us to the final chapter, where we set out to compute the DM interaction up to all orders of α_R. This can only be done using numerics. We thus solved the Schrödinger equation of our system by discretizing the Hamiltonian such that we were able to compute the total energy. Using the total energy we found the DM interaction dependence on spin-orbit coupling. In order to match our analytical established result, the numerical result has to be linear for small values of α_R. Our result seemed to indicate such a linear behavior. We thus answered the question we asked in the beginning of the thesis in the form of a plot of the DM interaction depending on spin-orbit coupling. However, more work needs to be done on the interpretation of these plots.

In the appendix a first attempt towards a field-theoretical computation of the DM interaction is given.

5.2 Discussion

The physics behind the DM interaction dependence on α_R needs to be further explored. We have to find out if and in what way the DM interaction depends on the Fermi energy and how it behaves for larger values of α_R. Only then we can conclude what the full behavior of the DM interaction is. This is work in progress. Nevertheless, if we reflect on the validity of this research we need to question our assumptions.

In order to compute the DM interaction in a chiral magnet we used a toy model in this thesis. We set up a two-layered system, a ferromagnet on top of a non-magnet, such that inversion symmetry is broken. However, we also need a strong spin-orbit coupling to induce a DM interaction. A spin-orbit coupling can be induced by several mechanisms, but we assumed a Rashba model describing the interface of the two layers. This needs to be verified.

One possibility of verifying if a Rashba model is used to describe the interface correctly, is checking whether all mechanisms depending on spin-orbit coupling form a coherent system. We computed the dependence of the DM interaction on α_R, but there are more mechanisms depending on spin-orbit coupling. An example are current induced torques: $\frac{\partial \boldsymbol{m}}{\partial t}|_{current}$ [26]. Without going into details, it is possible to write down the symmetry-allowed torques for our system. Among these allowed terms there are ones depending on higher orders of α_R, due to intrinsic spin-orbit couplings. Since we computed the full behavior of the DM interaction for all order in α_R, this

might be of help in computing the prefactors of all torques.

Several mechanisms all depend on spin-orbit coupling induced by a Rashba model. If theoretical predictions for the mechanisms depending on α_R are in agreement, we should be able to produce results that can be checked empirically. Based on experiments it might be shown that the theoretical model works and thus establish that for certain two-layered compounds one can describe the interface with a Rashba model.

Bibliography

[1] J Scott Russell. Report on waves. In *14th meeting of the British Association for the Advancement of Science*, volume 311, page 390, 1844.

[2] Tony Hilton Royle Skyrme. A unified field theory of mesons and baryons. *Nuclear Physics*, 31:556–569, 1962.

[3] S Mühlbauer, B Binz, F Jonietz, C Pfleiderer, A Rosch, A Neubauer, R Georgii, and P Böni. Skyrmion lattice in a chiral magnet. *Science*, 323(5916):915–919, 2009.

[4] Karin Everschor. Current-induced dynamics of chiral magnetic structures. Inaugural-Dissertation zur Erlangung des Doktorgrades, Universität zu Köln.

[5] Kyoung-Whan Kim, Hyun-Woo Lee, Kyung-Jin Lee, and MD Stiles. Chirality from interfacial spin-orbit coupling effects in magnetic bilayers. *Physical review letters*, 111(21):216601, 2013.

[6] Naoto Nagaosa and Yoshinori Tokura. Topological properties and dynamics of magnetic skyrmions. *Nature nanotechnology*, 8(12):899–911, 2013.

[7] YS Lin, PJ Grundy, and EA Giess. Bubble domains in magnetostatically coupled garnet films. *Applied Physics Letters*, 23(8):485–487, 1973.

[8] AP Malozemoff and JC Slonczewski. Magnetic domain walls in bubble materials. 1979.

[9] SD Bader. Colloquium: Opportunities in nanomagnetism. *Reviews of modern physics*, 78(1):1, 2006.

[10] Achim Rosch. Extra twist in magnetic bubbles. *Proceedings of the National Academy of Sciences*, 109(23):8793–8794, 2012.

[11] Tsuyoshi Okubo, Sungki Chung, and Hikaru Kawamura. Multiple-q states and the skyrmion lattice of the triangular-lattice heisenberg antiferromagnet under magnetic fields. *Physical review letters*, 108(1):017206, 2012.

[12] Stefan Heinze, Kirsten von Bergmann, Matthias Menzel, Jens Brede, André Kubetzka, Roland Wiesendanger, Gustav Bihlmayer, and Stefan Blügel. Spontaneous atomic-scale magnetic skyrmion lattice in two dimensions. *Nature Physics*, 7(9):713–718, 2011.

[13] IE Dzyaloshinskii. On the magneto-electrical effect in antiferromagnets, 1960.

[14] Tôru Moriya. Anisotropic superexchange interaction and weak ferromagnetism. *Physical Review*, 120(1):91, 1960.

[15] Albert Fert, Vincent Cros, and João Sampaio. Skyrmions on the track. *Nature nanotechnology*, 8(3):152–156, 2013.

[16] A Neubauer, C Pfleiderer, B Binz, A Rosch, R Ritz, PG Niklowitz, and P Böni. Topological hall effect in the a phase of mnsi. *Physical review letters*, 102(18):186602, 2009.

[17] C Thessieu, C Pfleiderer, AN Stepanov, and J Flouquet. Field dependence of the magnetic quantum phase transition in mnsi. *Journal of Physics: Condensed Matter*, 9(31):6677, 1997.

[18] W Münzer, A Neubauer, T Adams, S Mühlbauer, C Franz, F Jonietz, R Georgii, P Böni, B Pedersen, M Schmidt, et al. Skyrmion lattice in the doped semiconductor fe 1- x co x si. *Physical Review B*, 81(4):041203, 2010.

[19] C Pfleiderer, T Adams, A Bauer, W Biberacher, B Binz, F Birkelbach, P Böni, C Franz, R Georgii, M Janoschek, et al. Skyrmion lattices in metallic and semiconducting b20 transition metal compounds. *Journal of Physics: Condensed Matter*, 22(16):164207, 2010.

[20] P Milde, D Köhler, J Seidel, LM Eng, A Bauer, A Chacon, J Kindervater, S Mühlbauer, C Pfleiderer, S Buhrandt, et al. Unwinding of a skyrmion lattice by magnetic monopoles. *Science*, 340(6136):1076–1080, 2013.

[21] Minhyea Lee, W Kang, Y Onose, Y Tokura, and NP Ong. Unusual hall effect anomaly in mnsi under pressure. *Physical review letters*, 102(18):186601, 2009.

[22] XZ Yu, Y Onose, N Kanazawa, JH Park, JH Han, Y Matsui, N Nagaosa, and Y Tokura. Real-space observation of a two-dimensional skyrmion crystal. *Nature*, 465(7300):901–904, 2010.

[23] F Jonietz, S Mühlbauer, C Pfleiderer, A Neubauer, W Münzer, A Bauer, T Adams, R Georgii, P Böni, RA Duine, et al. Spin transfer torques in mnsi at ultralow current densities. *Science*, 330(6011):1648–1651, 2010.

[24] Junichi Iwasaki, Masahito Mochizuki, and Naoto Nagaosa. Universal current-velocity relation of skyrmion motion in chiral magnets. *Nature communications*, 4:1463, 2013.

[25] Achim Rosch. Skyrmions: moving with the current. *Nature nanotechnology*, 8(3):160–161, 2013.

[26] ME Knoester, Jairo Sinova, and RA Duine. Phenomenology of current-skyrmion interactions in thin films with perpendicular magnetic anisotropy. *Physical Review B*, 89(6):064425, 2014.

[27] ME Knoester. Skyrmions driven by the spin hall effect, 2013. Bachelor Thesis, Utrecht University.

[28] Miguel Calvo. Quantum theory of neutrons in helical magnetic fields. *Physical Review B*, 18(9):5073, 1978.

[29] NS Kiselev, AN Bogdanov, R Schäfer, and UK Rößler. Chiral skyrmions in thin magnetic films: new objects for magnetic storage technologies? *Journal of Physics D: Applied Physics*, 44(39):392001, 2011.

[30] Stuart SP Parkin, Masamitsu Hayashi, and Luc Thomas. Magnetic domain-wall racetrack memory. *Science*, 320(5873):190–194, 2008.

[31] Kyoung-Whan Kim, Hyun-Woo Lee, Kyung-Jin Lee, and MD Stiles. Supplemental material to chirality from interfacial spin-orbit coupling effects in magnetic bilayers. `http://journals.aps.org/prl/supplemental/10.1103/PhysRevLett.111.216601/Supplementary_Information_20131013_.pdf`.

[32] UK Rößler, AN Bogdanov, and C Pfleiderer. Spontaneous skyrmion ground states in magnetic metals. *Nature*, 442(7104):797–801, 2006.

[33] A Fert and Peter M Levy. Role of anisotropic exchange interactions in determining the properties of spin-glasses. *Physical Review Letters*, 44(23):1538, 1980.

[34] A Thiaville, Y Nakatani, J Miltat, and Y Suzuki. Micromagnetic understanding of current-driven domain wall motion in patterned nanowires. *EPL (Europhysics Letters)*, 69(6):990, 2005.

[35] XZ Yu, N Kanazawa, Y Onose, K Kimoto, WZ Zhang, S Ishiwata, Y Matsui, and Y Tokura. Near room-temperature formation of a skyrmion crystal in thin-films of the helimagnet fege. *Nature materials*, 10(2):106–109, 2011.

Appendices

Appendix A

Towards a Field-Theoretic Computation of the DM Interaction

A.1 Introduction

The coming sections are a draft of the field theoretical approach to compute the DM interaction in a toy model. The procedure is as follows. We set up an effective action, where a Hubbard-Stratonovich transformation already has taken place. We then try to compute:

$$\mathcal{Z} = \int d[\boldsymbol{m}] e^{\frac{-1}{\hbar} S_{eff(\boldsymbol{m})}} \simeq \int d[\boldsymbol{m}] e^{-\beta E[\boldsymbol{m}]}, \tag{A.1}$$

where we consider only time-independent configurations as we are interested in the energy of the system. If we were to compute the effective action S, we can relate the terms to the total energy of the system. From this equality we should be able to read of the DM interaction term. Recall from the introduction of the phenomenological model of a chiral magnet that the DM interaction has a first order derivative. From this fact, we deduce that in our action we should be looking for a non-local function, i.e. a function depending on $(\boldsymbol{x} - \boldsymbol{x}')$. Also, since we will be working in momentum space, we are after terms linear in k. If we then transform back to real space, this k becomes a first order derivative. Below we sketch the procedure beginning with the structure of S

$$S = \int d\tau \int d\tau' \int d\boldsymbol{x} \int \boldsymbol{x}' \delta m(\boldsymbol{x}, \tau) \Pi(\boldsymbol{x} - \boldsymbol{x}', \tau - \tau') \delta m(\boldsymbol{x}', \tau), \tag{A.2}$$

where $\delta m(\boldsymbol{x}, \tau)$ is the magnetization and Π is a function depending on Green's functions. We then minimize and Fourier transform the action, to obtain

$$\frac{\delta S}{\delta m(\boldsymbol{x},\tau)} = \int d\tau' \int \boldsymbol{x}' \Pi(\boldsymbol{x}-\boldsymbol{x}',\tau-\tau')\delta m(\boldsymbol{x}',\tau) \tag{A.3}$$

$$= \sum_{\boldsymbol{k},n} \Pi(\boldsymbol{k},i\omega_n)\delta m(\boldsymbol{k},i\omega_n). \tag{A.4}$$

Next we use a Taylor approximation to find

$$\frac{\delta S}{\delta m(\boldsymbol{x},\tau)} = \sum_{\boldsymbol{k},n} \left[\tilde{\Pi}(\boldsymbol{0},0) + \tilde{\Pi}'_{\alpha}(\boldsymbol{0},0)k_{\alpha} + ...\right]. \tag{A.5}$$

If we transform back to real space we obtain

$$\left[\Pi(\boldsymbol{0},0) + \frac{1}{i}\Pi_{\alpha}(\boldsymbol{0},0)\frac{\partial}{\partial x_{\alpha}} + ...\right]. \tag{A.6}$$

The term with a first order derivative corresponds to the DM interaction. However, the Π-function involves traces over several Green's functions and has a non-trivial spin structure which makes the computation of the function difficult. In the next section we aim to compute the Π-function. This part is for future reference, since the computation is not fully completed yet. It should be read as a draft computation.

A.2 Phenomenological Dzyaloshinskii-Moriya Term

The phenomenological energy of a chiral magnet, including the Dzyalosinskii-Moriya term, has the following form

$$E[\boldsymbol{m}] = t_{FM}\int d\boldsymbol{x}[-\frac{J_s}{2}\boldsymbol{m}\cdot\nabla^2\boldsymbol{m} + K(1-\boldsymbol{m}_z^2) + \frac{c}{2}\left(\hat{y}\cdot(\boldsymbol{m}\times\frac{\partial\boldsymbol{m}}{\partial x}) - \hat{x}\cdot(\boldsymbol{m}\times\frac{\partial\boldsymbol{m}}{\partial y})\right) + \mu_0 HM(1-\boldsymbol{m}_z) - \mu_0 M\boldsymbol{m}\cdot\boldsymbol{H}_d]. \tag{A.7}$$

The first term in the formulation of the energy corresponds to the exchange energy with coupling J_s and the second term to anisotropy, where K is a constant. The Dzyaloshinskii-Moriya term is the third term and is determined by the constant c. We are investigating the form of the constant in the following paragraphs. The last two terms correspond to an external field H and a dipolar field $\boldsymbol{H}_d$, with μ_0 the permeability of vacuum and M the saturation magnetization.

We linearize the magnetization, $\boldsymbol{m} = (\delta m_x, \delta m_y, 1 - \frac{\delta m_x^2}{2} - \frac{\delta m_y^2}{2})$, and find the terms linear in δm for the third term of the energy. The difference between linear terms or higher order terms come from either taking the $\hat{z}$ component to be 1, or taking the $\hat{z}$ component to be quadratic in the magnetization.

$$\text{Linear terms} = \frac{c}{2}(-\frac{\partial\delta m_x}{\partial x} + \frac{\partial\delta m_y}{\partial y}). \tag{A.8}$$

The terms δm_x and δm_y are zero, since we integrate them out in the energy expression.

$$\text{Higher order terms} = \frac{c}{2}(\delta m_x - \frac{\partial \delta m_x}{\partial x} - \delta m_y + \frac{\partial \delta m_y}{\partial y})(1 - \frac{\delta m_x^2}{2} - \frac{\delta m_y^2}{2}). \tag{A.9}$$

A.3 Eigenvalues and Eigenfunctions

From the Rashba Hamiltonian with the added $J\boldsymbol{\tau} \cdot \boldsymbol{m}$ term, we try to find the corresponding eigenvalues and eigenvectors.

$$\mathcal{H} = \frac{p_x^2 + p_y^2}{2m} + \frac{\alpha_R}{\hbar}(\boldsymbol{\tau} \times \boldsymbol{p}) \cdot \hat{z} - J\tau^z m^z. \tag{A.10}$$

Rewriting this in matrix form, and noting that $p_{x_i} = -i\hbar\frac{\partial}{\partial x_i}$we obtain the following:

$$\mathcal{H} = \begin{pmatrix} \frac{\hbar^2}{2m}(k_x^2 + k_y^2) + J & \alpha_R(k_y + ik_x) \\ \alpha_R(k_y - ik_x) & \frac{\hbar^2}{2m}(k_x^2 + k_y^2) - J \end{pmatrix}. \tag{A.11}$$

In this last equation we expressed the Hamiltonian in the wave numbers k_x, k_y, this is allowed since the Hamiltonian commutes with the (two dimensional) momentum operator. From the Hamiltonian we find the energy spectrum, by computing its eigenvalues. This gives two eigenvalues: $E_{k,\delta} = \epsilon_k + \delta\sqrt{J^2 + \alpha_R^2 k^2}$ for $\delta \in [\pm]$. When $J = 0$ we find the energy of the Rashba model: $\frac{\hbar^2 k^2}{2m} + \delta\alpha_R k$. The eigenfunctions of this model are not as elegant as in the Rashba model. We find for the two eigenvectors

$$\chi_\delta(\boldsymbol{k}) = \frac{1}{\sqrt{2}} \frac{1}{\sqrt{J^2 - J\delta\sqrt{\alpha_R^2 k^2 + J^2} + \alpha_R^2 k^2}} \begin{pmatrix} \alpha_R(k_y + ik_x) \\ -J + \delta\sqrt{J^2 + \alpha_R^2 k^2} \end{pmatrix}, \tag{A.12}$$

where $\delta \in [\pm]$. The pre factor comes from demanding that the vector is orthonormal.

A.4 Field Theory Approach

We have an idea what terms we need to find now, namely, linear terms. Consider the partition function

$$\mathcal{Z} = \int d[\phi_\alpha^*] d[\phi_{\alpha'}] d[\boldsymbol{m}] e^{\frac{-1}{\hbar} S[\phi_\alpha^*, \phi_{\alpha'}, \boldsymbol{m}]}, \tag{A.13}$$

where S_E is given by the following

$$S = \int_0^{\hbar\beta} d\tau \int d\boldsymbol{x} \sum_{\sigma,\sigma'} \phi_\sigma(\boldsymbol{x}, \tau)^* \left[(\hbar\frac{\partial}{\partial\tau} - \frac{\hbar^2\nabla^2}{2m} - \mu)\delta_{\sigma,\sigma'} + J\boldsymbol{\tau}_{\sigma,\sigma'} \cdot \boldsymbol{m} + \frac{\alpha_R}{\hbar}\boldsymbol{\tau}_{\sigma,\sigma'}(-i\hbar\nabla \times \hat{z}) \right] \phi_{\sigma'}(\boldsymbol{x}, \tau). \tag{A.14}$$

The $\boldsymbol{\tau}$ are the well known Pauli matrices and here we investigate the linearized form of magnetization. We rewrite this using the Green's function

$$S = \int_0^{\hbar\beta} d\tau \int_0^{\hbar\beta} d\tau' \int d\boldsymbol{x} \int \boldsymbol{x}' \sum_{\sigma,\sigma'} \phi^*(\boldsymbol{x},\tau) \left[-\hbar G^{-1}_{\sigma,\sigma'}(\boldsymbol{x},\tau;\boldsymbol{x}',\tau') \right], \tag{A.15}$$

with

$$G^{-1}_{\sigma,\sigma'}(\boldsymbol{x},\tau;\boldsymbol{x'},\tau') = \frac{-1}{\hbar}\left[(\hbar\frac{\partial}{\partial\tau} - \frac{\hbar^2\nabla^2}{2m} - \mu)\delta_{\sigma,\sigma'} + \frac{\alpha_R}{\hbar}\boldsymbol{\tau}_{\sigma,\sigma'}(-i\hbar\nabla\times\hat{z}) + J\boldsymbol{\tau}_{\sigma,\sigma'}\boldsymbol{m} \right] \delta(\boldsymbol{x}-\boldsymbol{x'})\delta(\tau-\tau'). \tag{A.16}$$

The inverse Green's function is defined as: $G^{-1}_{\sigma,\sigma'}(\boldsymbol{x},\tau;\boldsymbol{x'},\tau') = G_0^{-1}(\boldsymbol{x},\tau;\boldsymbol{x'},\tau) - \Sigma_{\sigma,\sigma'}(\boldsymbol{x},\tau;\boldsymbol{x'},\tau)$. Next, we want to integrate out the fields from equation (A.13) and try to find the effective action

$$\mathcal{Z} = \int d[\boldsymbol{m}] e^{\frac{-1}{\hbar}S^{eff}[\boldsymbol{m}]}. \tag{A.17}$$

In the above equation the fields have been integrated out using $\int d[\phi^*]d[\phi]\exp(-\phi^* M\phi) = \exp(\mathrm{Tr}\ln M)$ resulting in

$$S^{eff}[\boldsymbol{m}] = -\hbar\,\mathrm{Tr}\ln(-G^{-1}). \tag{A.18}$$

Subsequently, we perform a Taylor Series for the trace and find for the effective action

$$S_{eff}[\boldsymbol{m}] = \int d\boldsymbol{m} \exp\left(\frac{-1}{\hbar}\int_0^{\hbar\beta} d\tau \int d\boldsymbol{x}(-\hbar\,\mathrm{Tr}\ln(G_0^{-1}) + \hbar\,\mathrm{Tr}(G_0\Sigma) + \frac{\hbar}{2}\,\mathrm{Tr}(G_0\Sigma G_0\Sigma)) \right). \tag{A.19}$$

The linear terms in $\boldsymbol{m}$ come from the second trace in the previous equation and the quadratic terms in $\boldsymbol{m}$ come from the last trace. From linearizing $\boldsymbol{m}$ in the phenomenological model, only linear terms in $\boldsymbol{m}$ appeared for the DM interaction. Therefore, we compute the only term that gives us those linear terms, namely $\hbar\,\mathrm{Tr}(G_0\Sigma)$. Before we compute this trace, we have to compute the Green's function from the equation

$$\left[\hbar\frac{\partial}{\partial\tau} - \frac{\hbar^2\nabla^2}{2m} - \mu + \frac{\alpha_R}{\hbar}\boldsymbol{\tau}_{\sigma,\sigma'}(-i\hbar\nabla\times\hat{z}) + J\tau^z m^z \right] (G_0)_{\sigma,\sigma'}(\boldsymbol{x},\tau;\boldsymbol{x'},\tau') = -\hbar\delta(\boldsymbol{x}-\boldsymbol{x'})\delta(\tau-\tau'). \tag{A.20}$$

The solution to this equation is given by

$$(G_0)_{\sigma,\sigma'} = \sum_{n,\alpha}\int d\boldsymbol{k} \frac{-\hbar}{-i\hbar\omega_n + \epsilon_\alpha - \mu}\chi_\alpha(k)\chi^\dagger_\alpha(k)e^{ik(\boldsymbol{x}-\boldsymbol{x'})}\frac{e^{-i\omega_n(\tau-\tau')}}{\hbar\beta}, \tag{A.21}$$

where the χ's are our previously found orthonormal spin vectors. Now we are ready to compute $\hbar\,\mathrm{Tr}(G_0\Sigma)$, and find the linear term in $\boldsymbol{m}$ corresponding to the earlier found Dzyaloshinski-Moriya interaction in the phenomenological model. We compute

$$\mathrm{Tr}\left[\int d\boldsymbol{k} \sum_{n,\alpha,b\in[x,y]} \frac{-\hbar}{-i\hbar\omega_n + \epsilon_\alpha - \mu}\chi_\alpha(k)\chi^\dagger_\alpha(k)e^{ik(\boldsymbol{x}-\boldsymbol{x'})}\frac{e^{-\omega_n(\tau-\tau')}}{\hbar\beta} J\boldsymbol{\tau}^b\boldsymbol{m}^b(\boldsymbol{x},\tau)\delta(\boldsymbol{x}-\boldsymbol{x'})\delta(\tau-\tau') \right]. \tag{A.22}$$

We have used as the self-energy

$$\Sigma(\boldsymbol{x},\tau;\boldsymbol{x}',\tau')_{\alpha,\alpha'} = J(\delta m_x, \delta m_y, -\frac{\delta m_x^2}{2} - \frac{\delta m_y^2}{2})\boldsymbol{\tau}_{\alpha,\alpha'}\delta(\tau-\tau')\delta(\boldsymbol{x}-\boldsymbol{x}'). \tag{A.23}$$

We excluded the 1 in the z-direction of the magnetization, since this contribution is already captured in the energy, ϵ_α. The higher order terms we also neglected in our computation of the trace, since we are merely interested up to linear order. This can be seen from only letting $b \in [x, y]$. The trace in the expression is taken over spin-space, space and time. Next we transform $\boldsymbol{m}(\boldsymbol{x},\tau)$ to fourier space, which is helpful in the computation.

$$\int d\boldsymbol{x}\int d\boldsymbol{x'}\int d\tau\int d\tau'\int d\boldsymbol{k}\int d\boldsymbol{k'}\int d\boldsymbol{k''}\sum_\alpha\sum_{n,n',n''}\mathrm{Tr}[\frac{-\hbar}{-i\hbar\omega_n+\epsilon_\alpha-\mu}\chi_\alpha(k)\chi_\alpha^\dagger(k)$$
$$e^{ik'(\boldsymbol{x}-\boldsymbol{x'})}\frac{e^{-\omega_n(\tau-\tau')}}{\hbar\beta}e^{ik(\boldsymbol{x}-\boldsymbol{x'})}\frac{e^{-i\omega_{n'}(\tau-\tau')}}{\hbar\beta}e^{ik''\boldsymbol{x}}e^{-i\omega_{n''}\tau}J\boldsymbol{\tau}^b\boldsymbol{m}_{n''}^b(k'')]. \tag{A.24}$$

Such that $k''=0$ and $n''=0$, resulting in a trace over spin space

$$\sum_{\alpha,n,b\in[x,y]}\int d\boldsymbol{k}\frac{-\hbar}{-i\hbar\omega_n+\epsilon_\alpha-\mu}\,\mathrm{Tr}[\chi_\alpha(k)\chi_\alpha^\dagger(k)J\boldsymbol{\tau}^b\boldsymbol{m}_0^b(0)]. \tag{A.25}$$

We perform the sum over the spins such that our expression becomes

$$\sum_n\int d\boldsymbol{k}\,\mathrm{Tr}[(\frac{-\hbar}{-i\hbar\omega_n+\epsilon_k+\sqrt{J^2+\alpha_R k^2}-\mu}\chi_+(k)\chi_+^\dagger(k)+\frac{-\hbar}{-i\hbar\omega_n+\epsilon_k-\sqrt{J^2+\alpha_R k^2}-\mu}\chi_-(k)\chi_-^\dagger(k))$$
$$\times\begin{pmatrix}0 & \delta m_x-i\delta m_y\\ \delta m_x+i\delta m_y & 0\end{pmatrix}]. \tag{A.26}$$

Notice that by performing the sum over the spins, in the denominator there now appears a ϵ_k, which is the free electron dispersion relation. Subsequently, we plug the expressions for the spin vectors in and perform the trace explicitly.

$$\chi_+(k)\chi_+^\dagger(k) = \frac{1}{2(J^2-J\sqrt{\alpha_R^2k^2+\alpha_R^2k^2})}$$
$$\times\begin{pmatrix}\alpha_R^2k^2 & \alpha_R(k_y+ik_x)(-J+\sqrt{J^2+\alpha_R^2k^2})\\ (-J+\sqrt{J^2+\alpha_R^2k^2})\alpha_R(k_y-ik_x) & (2J^2-2J\sqrt{J^2+\alpha_R^2k^2}+\alpha_R^2k^2)\end{pmatrix}, \tag{A.27}$$

$$\chi_-(k)\chi_-^\dagger(k) = \frac{1}{2(J^2+J\sqrt{\alpha_R^2k^2+\alpha_R^2k^2})}$$
$$\times\begin{pmatrix}\alpha_R^2k^2 & \alpha_R(k_y+ik_x)(-J-\sqrt{J^2+\alpha_R^2k^2})\\ (-J-\sqrt{J^2+\alpha_R^2k^2})\alpha_R(k_y-ik_x) & (2J^2+2J\sqrt{J^2+\alpha_R^2k^2}+\alpha_R^2k^2)\end{pmatrix}. \tag{A.28}$$

We split up the trace and perform both traces separately, each with the different prefactor coming from the propagator, so for the first trace we find

$$\frac{-\hbar}{-i\hbar\omega_n+\epsilon_k+\sqrt{J^2+\alpha_R k^2}-\mu}\,\mathrm{Tr}[\chi_+(k)\chi_+^\dagger(k)\begin{pmatrix}0 & \delta m_x-i\delta m_y\\ \delta m_x+i\delta m_y & 0\end{pmatrix}] \tag{A.29}$$

$$= \frac{-\hbar}{-i\hbar\omega_n + \epsilon_k + \sqrt{J^2 + \alpha_R k^2} - \mu} \frac{1}{2} \frac{1}{J^2 - J\sqrt{\alpha_R^2 k^2 + J^2} + \alpha_R^2 k^2} (-J + \sqrt{J^2 + \alpha_R^2 k^2})(2\alpha_R)(k_y \delta m_x - k_x \delta m_y). \tag{A.30}$$

Similarly, for the second trace we find

$$\frac{-\hbar}{-i\hbar\omega_n + \epsilon_k - \sqrt{J^2 + \alpha_R k^2} - \mu} \operatorname{Tr}[\chi_-(k)\chi_-^\dagger(k) \begin{pmatrix} 0 & \delta m_x - i\delta m_y \\ \delta m_x + i\delta m_y & 0 \end{pmatrix}] \tag{A.31}$$

$$= \frac{-\hbar}{-i\hbar\omega_n + \epsilon_k - \sqrt{J^2 + \alpha_R k^2} - \mu} \frac{1}{2} \frac{1}{J^2 + J\sqrt{\alpha_R^2 k^2 + J^2} + \alpha_R^2 k^2} (-J - \sqrt{J^2 + \alpha_R^2 k^2})(2\alpha_R)(k_y \delta m_x - k_x \delta m_y). \tag{A.32}$$

Next, we perform the sum over n, the Matsubara expansions, such that we have

$$\int d\boldsymbol{k}\ \alpha_R [N(\epsilon_k - \mu + \sqrt{J^2 + \alpha_R^2 k^2}) \frac{(-J + \sqrt{J^2 + \alpha_R^2 k^2})}{J^2 - J\sqrt{\alpha_R^2 k^2 + J^2} + \alpha_R^2 k^2} - N(\epsilon_k - \mu - \sqrt{J^2 + \alpha_R^2 k^2}) \frac{(-J - \sqrt{J^2 + \alpha_R^2 k^2})}{J^2 + J\sqrt{\alpha_R^2 k^2 + J^2} + \alpha_R^2 k^2}](k_y \delta m_x - k_x \delta m_y), \tag{A.33}$$

where $N(x)$ is the Fermi-Dirac distribution.

A.4.1 Higher Order Terms in the Magnetization

To compute higher order terms in the magnetization we need to perform $\operatorname{Tr}[G_0 \Sigma G_0 \Sigma]$, where both the Green's function and the self energy are known

$$\operatorname{Tr}[G_0 \Sigma G_0 \Sigma] = \int d\boldsymbol{x} \int d\boldsymbol{x}' \int d\boldsymbol{x}'' \int d\boldsymbol{x}''' \int d\tau \int d\tau' \int d\tau'' \int d\tau'''$$
$$\times \operatorname{Tr}[\sum_{n,\alpha} \int d\boldsymbol{k} \frac{-\hbar}{-i\omega_n + \epsilon_\alpha - \mu} \chi_\alpha(\boldsymbol{k}) \chi_\alpha^\dagger(\boldsymbol{k}) e^{ik(\boldsymbol{x} - \boldsymbol{x}')} \frac{e^{-i\omega_n(\tau - \tau')}}{\hbar\beta} J\boldsymbol{m}(\boldsymbol{x}', \tau') \cdot \boldsymbol{\tau} \delta(\boldsymbol{x} - \boldsymbol{x}') \delta(\tau - \tau')$$
$$\times \sum_{n',\alpha'} \int d\boldsymbol{k}' \frac{-\hbar}{-i\omega_n' + \epsilon_{\alpha'} - \mu} \chi_{\alpha'}(\boldsymbol{k}') \chi_{\alpha'}^\dagger(\boldsymbol{k}') e^{ik'(\boldsymbol{x}'' - \boldsymbol{x}''')} \frac{e^{-i\omega_{n'}(\tau'' - \tau''')}}{\hbar\beta} J\boldsymbol{m}(\boldsymbol{x}''', \tau''') \cdot \boldsymbol{\tau} \delta(\boldsymbol{x}''' - \boldsymbol{x}) \delta(\tau''' - \tau)]. \tag{A.34}$$

We immediately integrate over $\boldsymbol{x}''$, $\boldsymbol{x}'''$, τ'' and τ''', implying the following: $\boldsymbol{x}''' \to \boldsymbol{x}$, $\boldsymbol{x}'' \to \boldsymbol{x}'$, $\tau''' \to \tau$ and $\tau'' \to \tau$,

$$\int d\boldsymbol{x} \int d\boldsymbol{x}' \int d\tau \int d\tau' \operatorname{Tr}[\sum_{n,\alpha} \int d\boldsymbol{k} \frac{-\hbar}{-i\omega_n + \epsilon_\alpha - \mu} \chi_\alpha(\boldsymbol{k}) \chi_\alpha^\dagger(\boldsymbol{k}) e^{ik(\boldsymbol{x} - \boldsymbol{x}')} \frac{e^{-i\omega_n(\tau - \tau')}}{\hbar\beta} J\boldsymbol{m}(\boldsymbol{x}', \tau') \cdot \boldsymbol{\tau}$$
$$\times \sum_{n',\alpha'} \int d\boldsymbol{k}' \frac{-\hbar}{-i\omega_n' + \epsilon_{\alpha'} - \mu} \chi_{\alpha'}(\boldsymbol{k}') \chi_{\alpha'}^\dagger(\boldsymbol{k}') e^{ik'(\boldsymbol{x}' - \boldsymbol{x})} \frac{e^{-i\omega_{n'}(\tau' - \tau)}}{\hbar\beta} J\boldsymbol{m}(\boldsymbol{x}, \tau) \cdot \boldsymbol{\tau}]. \tag{A.35}$$

Just as before we Fourier transform the magnetization, resulting in

$$\int d\boldsymbol{x}\int d\boldsymbol{x}'\int d\tau\int d\tau'\,\mathrm{Tr}[\sum_{n,\alpha}\int d\boldsymbol{k}\frac{-\hbar}{-i\omega_n+\epsilon_\alpha-\mu}\chi_\alpha(\boldsymbol{k})\chi_\alpha^\dagger(\boldsymbol{k})e^{ik(\boldsymbol{x}-\boldsymbol{x}')}\frac{e^{-i\omega_n(\tau-\tau')}}{\hbar\beta}$$
$$\times J\sum_{n'}\int d\boldsymbol{k}'\boldsymbol{m}_{n'}(\boldsymbol{k}')e^{i\boldsymbol{k}'\boldsymbol{x}'}e^{i\omega_{n'}\tau'}\cdot\boldsymbol{\tau}$$
$$\sum_{n'',\alpha'}\int d\boldsymbol{k}''\frac{-\hbar}{-i\omega_n''+\epsilon_{\alpha'}-\mu}\chi_{\alpha'}(\boldsymbol{k}'')\chi_{\alpha'}^\dagger(\boldsymbol{k}'')e^{ik''(\boldsymbol{x}'-\boldsymbol{x})}\frac{e^{-i\omega_{n''}(\tau'-\tau)}}{\hbar\beta}$$
$$\times J\sum_{n'''}\int d\boldsymbol{k}'''\boldsymbol{m}_{n'''}(\boldsymbol{k}''')e^{i\boldsymbol{k}'''\boldsymbol{x}}e^{-i\omega_{n'''}\tau}\cdot\boldsymbol{\tau}]. \quad \text{(A.36)}$$

By integrating over $\boldsymbol{x}$, $\boldsymbol{x}'$, τ and τ', we find four delta functions in our expression

$$\int d\boldsymbol{k}\int d\boldsymbol{k}'\int d\boldsymbol{k}''\int d\boldsymbol{k}'''\sum_{n,n',n'',n''''}\mathrm{Tr}[\sum_{\alpha,\alpha'}\hbar^2J^2\frac{1}{-i\omega_n\hbar+\epsilon_\alpha-\mu}\chi_\alpha(\boldsymbol{k})\chi_\alpha^\dagger(\boldsymbol{k})\boldsymbol{m}_{n'}(\boldsymbol{k}')\cdot\boldsymbol{\tau}$$
$$\times\frac{1}{-i\omega_{n''}\hbar+\epsilon_{\alpha'}-\mu}\chi_\alpha(\boldsymbol{k}'')\chi_\alpha^\dagger(\boldsymbol{k}'')\boldsymbol{m}_{n'''}(\boldsymbol{k}''')\cdot\boldsymbol{\tau}$$
$$\times\delta(\boldsymbol{k}-\boldsymbol{k}''+\boldsymbol{k}''')\delta(-\boldsymbol{k}+\boldsymbol{k}'+\boldsymbol{k}'')\delta(-\omega_n+\omega_{n''}-\omega_{n'''})\delta(\omega_n-\omega_{n'}-\omega_{n''})], \quad \text{(A.37)}$$

subsequently, this reduces the equation to the following if we integrate over $\boldsymbol{k}'$, $\boldsymbol{k}''$[1], $\omega_{n'}$ and $\omega_{n'''}$:

$$\int d\boldsymbol{k}\int d\boldsymbol{k}''\sum_{n,n'}\hbar^2J^2\,\mathrm{Tr}[\frac{1}{-i\omega_n\hbar+\epsilon_\alpha-\mu}\chi_\alpha(\boldsymbol{k})\chi_\alpha^\dagger(\boldsymbol{k})\boldsymbol{m}_{n-n''}(\boldsymbol{k}-\boldsymbol{k}'')\cdot\boldsymbol{\tau}$$
$$\times\frac{1}{-i\omega_{n''}\hbar+\epsilon_{\alpha'}-\mu}\chi_\alpha(\boldsymbol{k}'')\chi_\alpha^\dagger(\boldsymbol{k}'')\boldsymbol{m}_{n''-n}(\boldsymbol{k}''-\boldsymbol{k})\cdot\boldsymbol{\tau}]. \quad \text{(A.38)}$$

Next we make the integral symmetric in the eigenvectors by letting $\boldsymbol{k}\to\boldsymbol{k}+\boldsymbol{k}''$ and $\omega_n\to\omega_n+\omega_{n''}$, such that we find

$$\int d\boldsymbol{k}\int d\boldsymbol{k}''\sum_{n,n'}\hbar^2J^2\,\mathrm{Tr}[\frac{1}{-i\omega_{n+n''}\hbar+\epsilon_\alpha-\mu}\chi_\alpha(\boldsymbol{k}+\boldsymbol{k}'')\chi_\alpha^\dagger(\boldsymbol{k}+\boldsymbol{k}'')\boldsymbol{m}_n(\boldsymbol{k})\cdot\boldsymbol{\tau}$$
$$\times\frac{1}{-i\omega_{n''}\hbar+\epsilon_{\alpha'}-\mu}\chi_\alpha(\boldsymbol{k}'')\chi_\alpha^\dagger(\boldsymbol{k}'')\boldsymbol{m}_{-n}(-\boldsymbol{k})\cdot\boldsymbol{\tau}]. \quad \text{(A.39)}$$

We then set $\boldsymbol{k}''=\boldsymbol{q}$, $n''\to n$ and introduce a new function $\Pi_{a,b}$ to rewrite our result as

$$\mathrm{Tr}[G_0\Sigma G_0\Sigma]=\int d\boldsymbol{k}\sum_n\sum_{a,b\in x,y}m_n^a(\boldsymbol{k})\Pi_{a,b}(\boldsymbol{k},\omega_n)m_{-n}^b(-\boldsymbol{k}). \quad \text{(A.40)}$$

In this equation $\Pi_{a,b}$ is

$$\Pi_{a,b}=\int d\boldsymbol{q}\sum_{n'}\hbar^2J^2\,\mathrm{Tr}[\frac{1}{-i\omega_{n+n'}\hbar+\epsilon_\alpha-\mu}\chi_\alpha(\boldsymbol{k}+\boldsymbol{q})\chi_\alpha^\dagger(\boldsymbol{k}+\boldsymbol{q})\tau_a\frac{1}{-i\omega_{n'}\hbar+\epsilon_{\alpha'}-\mu}\chi_{\alpha'}(\boldsymbol{q})\chi_{\alpha'}^\dagger(\boldsymbol{q})\tau_b]. \quad \text{(A.41)}$$

[1]We choose these momenta since the eigenvectors do not depend on them.

The next step is to compute $\Pi_{a,b}$ by first splitting the fraction and subsequently performing the Matsubara sum, such that we obtain

$$\Pi_{a,b}(\boldsymbol{k},\omega_n) = \sum_{\alpha,\alpha'} \hbar^2 J^2 \int d\boldsymbol{q} \frac{N_{FD}(\epsilon_\alpha(\boldsymbol{k}+\boldsymbol{q})-\mu) - N_{FD}(\epsilon_{\alpha'}(\boldsymbol{q})-\mu)}{\epsilon_{\alpha'}(\boldsymbol{q}) - \epsilon_\alpha(\boldsymbol{k}+\boldsymbol{q}) - i\omega_n} \operatorname{Tr}[\chi_\alpha(\boldsymbol{k}+\boldsymbol{q})\chi_\alpha^\dagger(\boldsymbol{k}+\boldsymbol{q})\tau_a\chi_{\alpha'}(\boldsymbol{q})\chi_{\alpha'}^\dagger(\boldsymbol{q})\tau_b]. \tag{A.42}$$

Or, when we symmetrize the integral by letting $\boldsymbol{q} \to \boldsymbol{q} - \boldsymbol{k}/2$, we find

$$\Pi_{a,b}(\boldsymbol{k},0) = \sum_{\alpha,\alpha'} \hbar^2 J^2 \int d\boldsymbol{q} \frac{N_{FD}(\epsilon_\alpha(\boldsymbol{k}/2+\boldsymbol{q})-\mu) - N_{FD}(\epsilon_{\alpha'}(\boldsymbol{q}-\boldsymbol{k}/2)-\mu)}{\epsilon_{\alpha'}(\boldsymbol{q}-\boldsymbol{k}/2) - \epsilon_\alpha(\boldsymbol{k}/2+\boldsymbol{q})}$$
$$\operatorname{Tr}[\chi_\alpha(\boldsymbol{k}/2+\boldsymbol{q})\chi_\alpha^\dagger(\boldsymbol{k}/2+\boldsymbol{q})\tau_a\chi_{\alpha'}(\boldsymbol{q}-\boldsymbol{k}/2)\chi_{\alpha'}^\dagger(\boldsymbol{q}-\boldsymbol{k}/2)\tau_b], \tag{A.43}$$

where we also have set $\omega = 0$.

We now let $k \to -k$ and see what relation we find

$$\Pi_{a,b}(-\boldsymbol{k},0) = \sum_{\alpha,\alpha'} \hbar^2 J^2 \int d\boldsymbol{q} \frac{N_{FD}(\epsilon_\alpha(-\boldsymbol{k}/2+\boldsymbol{q})-\mu) - N_{FD}(\epsilon_{\alpha'}(\boldsymbol{q}+\boldsymbol{k}/2)-\mu)}{\epsilon_{\alpha'}(\boldsymbol{q}+\boldsymbol{k}/2) - \epsilon_\alpha(-\boldsymbol{k}/2+\boldsymbol{q})}$$
$$\operatorname{Tr}[\chi_\alpha(-\boldsymbol{k}/2+\boldsymbol{q})\chi_\alpha^\dagger(-\boldsymbol{k}/2+\boldsymbol{q})\tau_a\chi_{\alpha'}(\boldsymbol{q}+\boldsymbol{k}/2)\chi_{\alpha'}^\dagger(\boldsymbol{q}+\boldsymbol{k}/2)\tau_b]. \tag{A.44}$$

The factor in front of the trace is obviously invariant under the transformation. The trace part can be rewritten using the cyclic properties of the trace, and we find

$$\Pi_{a,b}(-\boldsymbol{k},0) = \Pi_{b,a}(\boldsymbol{k},0). \tag{A.45}$$

A.5 Comparing Terms

Before we explicitly compute this last integral, we first formally express the DM interaction. This is nice since we are able to see where the terms we need for the DM interaction interaction come from. So, we start by varying the energy of the system and subsequently linearizing this expression.

$$E[\boldsymbol{m}+\delta\boldsymbol{m}] = t_{FM} \int d\boldsymbol{x}[-\frac{J_s}{2}(\boldsymbol{m}+\delta\boldsymbol{m})\cdot\nabla^2(\boldsymbol{m}+\delta\boldsymbol{m}) + K(1-(\boldsymbol{m}+\delta\boldsymbol{m})_z^2)$$
$$+ \frac{c}{2}\left(\hat{y}\cdot((\boldsymbol{m}+\delta\boldsymbol{m})\times\frac{\partial(\boldsymbol{m}+\delta\boldsymbol{m})}{\partial x}) - \hat{x}\cdot((\boldsymbol{m}+\delta\boldsymbol{m})\times\frac{\partial(\boldsymbol{m}+\delta\boldsymbol{m})}{\partial y})\right)$$
$$+ \mu_0 HM(1-(\boldsymbol{m}+\delta\boldsymbol{m})_z) - \mu_0 M(\boldsymbol{m}+\delta\boldsymbol{m})\cdot\boldsymbol{H}_d]. \tag{A.46}$$

Only taking terms linear in $\delta\boldsymbol{m}$ into account, and using partial integration to find

$$\frac{\delta E[\boldsymbol{m}]}{\delta \boldsymbol{m}_\alpha} = -J_s\nabla^2\boldsymbol{m}_\alpha - 2Km_\alpha + C\left(\epsilon_{y\beta\alpha}\frac{\partial \boldsymbol{m}_\beta}{\partial x} - \epsilon_{x\beta\alpha}\frac{\partial \boldsymbol{m}_\beta}{\partial y}\right) - \mu_0 HM - \mu_0 M\boldsymbol{H}_\alpha. \tag{A.47}$$

Recall the partition function can be expressed as a function depending on the effective action, and also as a function depending on the energy. We use this to find a formal expression for the DM

interaction term. After the fields have been integrated out, we write the partition function as

$$\mathcal{Z} = \int d[\boldsymbol{m}] e^{\frac{-1}{\hbar} S_{eff(\boldsymbol{m})}} = \int d[\boldsymbol{m}] e^{-\beta E[\boldsymbol{m}]}. \tag{A.48}$$

We already computed the linear and higher order terms of the effective action separately, recall

$$S_{eff}[\boldsymbol{m}] = \left(\frac{-1}{\hbar} \int_0^{\hbar\beta} d\tau \int d\boldsymbol{x} (-\hbar \operatorname{Tr} \ln(G_0^{-1}) + \hbar \operatorname{Tr}(G_0 \Sigma) + \frac{\hbar}{2} \operatorname{Tr}(G_0 \Sigma G_0 \Sigma)) \right). \tag{A.49}$$

However, since we are interested in the DM interaction interaction, and this interaction has derivatives in it we suspect that the only place where these derivatives can reside is in the non-local Π function, coming from the $\mathrm{Tr}[G_0 \Sigma G_0 \Sigma]$ part of the action. Now we compare the terms

$$\frac{-1}{\hbar} \frac{\delta S_{eff}[\boldsymbol{m}]}{\delta \boldsymbol{m}^a} = -\beta \frac{\delta E[\boldsymbol{m}]}{\delta \boldsymbol{m}}. \tag{A.50}$$

From this equation we get the following equality, only considering the terms first order in k

$$\frac{-1}{\hbar} \left(\frac{\hbar}{2} \int d\boldsymbol{k} \sum_{n,a,b \in [x,y]} \Pi_{a,b}(\boldsymbol{k}, \omega_n) \boldsymbol{m}^b_{-n}(-\boldsymbol{k}) \right) = -\beta C \left(\epsilon_{y\beta\alpha} \frac{\partial \boldsymbol{m}_\beta}{\partial x} - \epsilon_{x\beta\alpha} \frac{\partial \boldsymbol{m}_\beta}{\partial y} \right). \tag{A.51}$$

Thus we want to find the terms linear in k for our Π function. This is done using an expansion around 0,

$$\Pi(\boldsymbol{k}, i\omega_n) \simeq \Pi(0,0) + \frac{\partial \Pi(\boldsymbol{k}, 0)}{\partial k_\alpha}|_{k_\alpha = 0} \, k_\alpha + ... \tag{A.52}$$

We write the DM interaction formally by putting the linear term of the expansion of Π in and transforming back to real space, to find

$$\frac{i}{\hbar} \sum_{a,b \in [x,y]} \left(\frac{\partial \Pi_{a,b}(\boldsymbol{k}, 0)}{\partial k_\alpha}|_{k_\alpha = 0} \right) \frac{\partial}{\partial x_\alpha} \boldsymbol{m}^b(\boldsymbol{x}) = -\beta C \left(\epsilon_{y\beta\alpha} \frac{\partial \boldsymbol{m}_\beta}{\partial x} - \epsilon_{x\beta\alpha} \frac{\partial \boldsymbol{m}_\beta}{\partial y} \right). \tag{A.53}$$

We write the terms as

$$\epsilon_{y\beta\alpha} \frac{\partial \boldsymbol{m}_\beta}{\partial x} = \hat{y} \times \frac{\partial \boldsymbol{m}}{\partial x}|_\alpha, \tag{A.54}$$

$$\epsilon_{x\beta\alpha} \frac{\partial \boldsymbol{m}_\beta}{\partial y} = \hat{x} \times \frac{\partial \boldsymbol{m}}{\partial y}|_\alpha, \tag{A.55}$$

$$\sum_{a,b \in [a,b]} \Pi^{a,b}_\alpha \frac{\partial}{\partial x_\alpha} \boldsymbol{m}^b(\boldsymbol{x}) = \Pi^{xx}_\alpha \frac{\partial}{\partial x_\alpha} m^x(x) + \Pi^{yx}_\alpha \frac{\partial}{\partial x_\alpha} m^x(x) + \Pi^{xy}_\alpha \frac{\partial}{\partial x_\alpha} m^y(x) + \Pi^{yy}_\alpha \frac{\partial}{\partial x_\alpha} m^y(x), \tag{A.56}$$

where $\Pi_\alpha = \frac{\partial \Pi_{a,b}(\boldsymbol{k},0)}{\partial k_\alpha}|_{k_\alpha = 0}$. We are free to choose α, either as x or y, the equation should hold for both.

In addition to a linear order in k, we assume a linear order in α_R. For this reason we first linearize our eigenvectors in α_R

$$\chi_+(\boldsymbol{k}) \simeq \begin{pmatrix} \frac{k_y + i k_x}{\boldsymbol{k}} \\ \frac{\alpha_R \boldsymbol{k}}{2J} \end{pmatrix} + \mathcal{O}(\alpha_R^2), \tag{A.57}$$

$$\chi_-(\boldsymbol{k}) \simeq \begin{pmatrix} \frac{\alpha_R}{2J}(k_y + ik_x) \\ 1 \end{pmatrix} + \mathcal{O}(\alpha_R^2). \tag{A.58}$$

Recall equation (A.42), where we are now able to perform the traces and only keep terms linear in α_R. We immediately include the sums over α, α', which yields

$$\Pi_{a,b}(\boldsymbol{k}, 0) = \hbar^2 J^2 \int d\boldsymbol{q} \frac{N_{FD}(\epsilon_-(\boldsymbol{k}+\boldsymbol{q}) - \mu) - N_{FD}(\epsilon_+(\boldsymbol{q}) - \mu)}{\epsilon_+(\boldsymbol{q}) - \epsilon_-(\boldsymbol{k}+\boldsymbol{q})} \frac{(q_x - q_y)(q_x + q_y)}{\boldsymbol{q}^2} \begin{pmatrix} 1 & i \\ -i & 1 \end{pmatrix}_{a,b}$$
$$- \frac{N_{FD}(\epsilon_+(\boldsymbol{k}+\boldsymbol{q}) - \mu) - N_{FD}(\epsilon_-(\boldsymbol{q}) - \mu)}{\epsilon_-(\boldsymbol{q}) - \epsilon_+(\boldsymbol{k}+\boldsymbol{q})} \frac{(k_x^2 - (k_y - q_x + q_y)(k_y + q_x + q_y))}{(\boldsymbol{k}+\boldsymbol{q})^2} \begin{pmatrix} 1 & i \\ -i & 1 \end{pmatrix}_{a,b}. \tag{A.59}$$

The next step is to introduce cylindrical coordinates and explicitly evaluate the integrals over the angle. This is done easily, since the Fermi distributions do not depend on the angles and the terms coming from the trace do.

After the integrations over the angles have been performed we still need to linearize the Fermi distributions in α_R and then find the terms linear in k of Π to see what the coefficient of the DM interaction is.